1995

Fatigue resistant design of cantivelered sign, signal, and luminaire support structures

James Peter Van Dien
Lehigh University

Van Dien,
James Peter

Fatigue Resistant Design of Cantilevered Sign, Signal, and Luminaire Support Structures

January 14, 1995

FATIGUE RESISTANT DESIGN OF CANTILEVERED SIGN, SIGNAL, AND LUMINAIRE SUPPORT STRUCTURES

by

James Peter Van Dien

A Thesis

Presented to the Graduate and Research Committee

of Lehigh University

in Candidacy for the Degree of

Master of Science

in

Civil Engineering

Lehigh University

December 1995

CERTIFICATE OF APPROVAL

Approved and recommended for acceptance as a thesis in partial fulfillment of the requirements for the degree of Master of Science in Civil Engineering:

Dec. 7, 1995
Date

John W. Fisher, Ph.D., P.E.
Joseph T. Stuart Professor
of Civil Engineering

Le-Wu Lu, Ph.D.
Professor and Chairman of
the Department of Civil and
Environmental Engineering

ACKNOWLEDGEMENTS

The research reported herein was performed under National Cooperative Highway Research Program (NCHRP) Project 10-38 at the Center for Advanced Technology for Large Structural Systems (ATLSS) at Lehigh University. The wind tunnel experimental program was conducted at the Wright Brothers Memorial Wind Tunnel Facility at the Massachusetts Institute of Technology (MIT).

The author is grateful for the support and direction provided by Mr. Mark R. Kaczinski, Research Engineer, and Dr. Robert J. Dexter, Senior Research Engineer, of the ATLSS Center. Messrs. Kaczinski and Dexter served as principle investigators for this project and directed the work reported herein. In addition, the author would like to thank Dr. John W. Fisher, Joseph T. Stuart Professor of Civil Engineering and Director of the ATLSS Center, for providing invaluable guidance over the course of the research program. The author also wishes to recognize Dr. Eric J. Kaufmann, Research Engineer at the ATLSS Center, for assisting with the anchor bolt fatigue test program.

The author would also like to acknowledge Dr. Eugene E. Covert, Professor of Aeronautics and Astronautics at MIT. The wind tunnel experimental program was conducted under the direction of Dr. Covert, with the assistance of Mr. Frank H. Durgin, Research Engineer, and Mr. Philip Cali, Research Assistant.

Finally, the author would like to thank Annette Pieroni for her assistance with the preparation of the figures and tables contained in this report.

TABLE OF CONTENTS

LIST OF TABLES

LIST OF FIGURES

ABSTRACT

Experimental and analytical research was performed to develop guidelines for the fatigue design of cantilevered sign, signal, and luminaire support structures due to galloping and/or vortex shedding. Aerodynamic and aeroelastic wind tunnel tests were performed at the Massachusetts Institute of Technology on one-eighth and one-half scale models to characterize the dynamic response of cantilevered sign and signal support structures to the galloping and vortex shedding phenomena. Dynamic finite-element analyses were performed in this study to: 1) simulate the wind-tunnel experiments and identify the amplitude of the across-wind loads on the sign and signal attachments which correspond to the measured base moment amplitudes during galloping and vortex shedding; 2) model the full-scale prototype structures represented by the wind-tunnel test specimens to verify scaling laws; and, 3) model full-scale cantilevered support structures that were observed galloping in the field and identify the amplitude of the across-wind loads on the sign and signal attachments which correspond to the observed displacement amplitudes. The analyses showed that the loads experienced by the structures in the field were reasonably consistent with the loads determined from the wind-tunnel tests. An equivalent static across-wind (vertical) traction range (1 kPa) is proposed for the design of cantilevered support structures for galloping-induced fatigue. The traction range is to be applied vertically (like a shear force) to the area of signal and sign attachments projected on a vertical plane. The stress ranges resulting from this applied traction range must be lower than the constant amplitude fatigue limit (CAFL) for the various details of the structures, ensuring essentially infinite life. Typical cantilevered support structure connection details were categorized according to the existing AASHTO/AWS fatigue design curves. Because of a lack of data near the fatigue limit, fatigue tests were performed on

snug- and fully-tightened anchor bolts. A CAFL corresponding to the AASHTO Category D fatigue limit (i.e. 48 MPa) should be used in the design of both snug- and fully-tightened anchor bolts in the regime of infinite life (e.g. greater than two million cycles).

Chapter One

INTRODUCTION

1.1 STATEMENT OF THE PROBLEM

Cantilevered sign, signal, and luminaire support structures are used extensively on major interstate highways and at local intersections for the purposes of traffic control and roadway illumination. The fact that cantilevered support structures are supported by a single vertical support as opposed to two supports for a traditional overhead support structure increases motorist safety by minimizing the probability of vehicle collision. The span of these cantilevers has been increasing over the years as they are used on roads with more lanes and as the setback distance of the column from the roadway has increased for safety reasons. It is not unusual for the cantilever to span more than 12 meters. These structures have low mass and stiffness, and associated low resonant frequencies of about 1 Hz. The damping is extremely low, typically less than one percent of the critical damping. These conditions make cantilevered support structures particularly susceptible to vibration due to wind-loading.

Cantilevered sign, signal, and luminaire support structures are designed in accordance with the AASHTO Standard Specifications for Structural Supports for Highway Signs, Luminaires, and Traffic Signals [4]. Historically, the performance of a majority of the structures designed with these specifications has been satisfactory. However, the results of a state department of transportation survey conducted in conjunction with this research indicated that approximately one-half of the 36 states which responded to the survey experience problems with wind-induced vibration of cantilevered support structures [27]. Several states reported occurrences of horizontal mast-arm vibration amplitudes in excess of 600 mm under steady-state winds with velocities in

the range of 5 m/s to 15 m/s [27]. Generally, the reported vibrations were observed to occur in the plane of the structure (i.e. vertical-plane vibrations of the horizontal mast arm) in a direction normal to the direction of wind flow.

The large-amplitude, across-wind vibrations observed in cantilevered support structures can be attributed to galloping and/or vortex shedding. Each of these phenomena are aeroelastic instabilities characterized by large-amplitude, resonant vibrations which occur normal to the direction of wind flow. In some cases, the stress ranges resulting from these vibrations are relatively small. In these cases, the vibration is only a serviceability problem; i.e. motorists cannot clearly see the signals or signs or are afraid to drive under the vibrating structures. Because of the excessive number of complaints that are generated, this large-amplitude vibration is deemed unacceptable.

In many cases, however, the magnitudes of the stress ranges induced in critical connection details result in the initiation and propagation of fatigue cracks. The 36 state departments of transportation which responded to the survey reported a total of 80 occurrences of fatigue damage in cantilevered support structures resulting from wind-loading [27]. All of the occurrences of fatigue damage were reported at either the mast-arm-to-column connection, column-to-base-plate connection, or anchor bolts [27]. The propagation of these cracks has resulted in the collapse of several cantilevered support structures [22].

The provisions of the AASHTO Standard Specifications for Structural Supports for Highway Signs, Luminaires, and Traffic Signals [4] are vague and insufficient with respect to the design of structures for vibration and fatigue. Furthermore, the commentary to the specifications does not contain adequate guidance for the application of the current provisions. The reported problems with the performance of cantilevered support structures underscore the need for

improvements in the current specifications with respect to the provisions pertaining to vibration and fatigue.

1.2 OBJECTIVES

Research was conducted to form a basis for guidelines for preventing excessive vibration and fatigue of cantilevered sign, signal, and luminaire support structures. The specific objectives of the research were as follows:

- Identify and characterize the susceptibility of cantilevered support structures to the galloping and vortex shedding phenomena.

- Develop equivalent static load models which reasonably represent the magnitude of the fluctuating pressures to which cantilevered support structures are subjected during galloping- and vortex-induced vibrations.

- Identify fatigue-sensitive cantilevered support structure connection details and categorize those details according to the AASHTO [3] and/or AWS [6] fatigue design curves.

- Determine the fatigue strength of axially-loaded, snug- and fully-tightened anchor bolts.

1.3 SUMMARY OF APPROACH

The approach to this research was as follows:

- A literature review and survey of state departments of transportation were performed to determine the nature and extent of fatigue damage in cantilevered support structures and to identify the conditions under which cantilevered support structures have been observed to oscillate in the field. These tasks resulted in the identification of galloping and vortex shedding as the most critical fatigue-loading mechanisms.

- Aerodynamic wind tunnel tests were performed to evaluate the susceptibility of cantilevered support structures to galloping phenomenon. Aeroelastic wind tunnel tests were performed to investigate the characteristics of the dynamic response of cantilevered support structures subjected to galloping- and vortex-induced vibrations. The data obtained from the aeroelastic tests (lift moment amplitudes at the base of the vertical support) were incorporated into a series of dynamic finite-element simulations to estimate the magnitude of the across-wind pressure fluctuations associated with galloping and vortex shedding.

- Dynamic finite-element analyses of the full-scale prototype structures represented by the wind-tunnel test specimens was used to verify scaling laws. Then, full-scale cantilevered support structures that were observed galloping in the field were modeled to determine the amplitude of the across-wind loads on the sign and signal attachments which correspond to the observed displacement amplitudes. The results

of the dynamic finite-element analyses were used to develop an equivalent static load model to be used in the design of cantilevered support structures for fatigue.

- Fatigue-sensitive cantilevered support structure connection details were identified through a review of state department of transportation standard drawings of cantilevered support structures. Existing knowledge of the fatigue of weldments was used to categorize the fatigue strengths of these details according to the AASHTO [3] and/or AWS [6] fatigue design curves.

- Full-scale fatigue tests were performed to determine lower-bound estimates of the fatigue strength of axially-loaded, snug- and fully-tightened anchor bolts in the regimes of finite and infinite life.

1.4 SCOPE OF REPORT

Chapter Two provides background information related to the galloping and vortex shedding phenomena. Included in this chapter is a review of previous research programs which were performed to evaluate the performance of cantilevered support structures subjected to galloping- and vortex-induced vibrations.

Chapter Three summarizes the wind tunnel experimental test program. A description of the experiments and summary of the results is provided in this chapter. Chapter Four describes the dynamic finite-element analyses and summarizes the development of the equivalent static load models for the galloping and vortex shedding phenomena.

Chapter Five discusses the categorization of typical cantilevered connection details to the AASHTO [3] and/or AWS [6] fatigue design curves. The actual categorization of connection details is contained in an appendix to this report.

Chapter Six summarizes the anchor bolt fatigue test program. A description of the experiments, summary of the results, and recommendations for the design of anchor bolts for fatigue is presented in this chapter.

Chapter Seven presents the conclusions and synthesizes the results of this research in a series of guidelines which can be used in the design of cantilevered support structures for vibration and fatigue resulting from galloping and vortex shedding. In addition, recommendations for future research are presented.

Chapter Two

AEROELASTIC WIND EFFECTS ON CANTILEVERED SUPPORT STRUCTURES

2.1 INTRODUCTION

Cantilevered sign, signal, and luminaire support structures are susceptible to two types of wind-loading which are critical with respect to the design for vibration and fatigue: (1) galloping and (2) vortex shedding. Galloping and vortex shedding are aeroelastic phenomena caused by a coupling between the aerodynamic forces which act on a structure (caused by the action of wind) and the structural vibrations. Aeroelastic instability, commonly referred to as self-excited motion, results when the motion of a structure, induced by initial aerodynamic forces caused by the action of wind, causes variations in those forces which cause successively larger oscillations.

Cantilevered support structure vibrations resulting from galloping and vortex shedding are particularly critical with respect to fatigue. The characteristic dynamic response of a cantilevered support structure to either of these aeroelastic phenomena is a large-amplitude, across-wind, resonant vibration. The magnitude of the stress ranges induced in the connection details of cantilevered support structures subjected to galloping- and vortex-induced vibrations is generally quite large, thus the initiation and propagation of fatigue cracks is highly probable. As a result, the research reported herein was oriented towards the development of fatigue design criteria which address the behavior of cantilevered support structures subjected to galloping- and vortex-induced vibrations.

Chapter Two provides a summary of the galloping and vortex shedding phenomena as they relate to the performance of cantilevered sign, signal, and luminaire support structures. Section 2.2 discusses the galloping phenomenon while Section 2.3 is devoted to a discussion of the vortex shedding phenomenon. Each section contains a brief summary of the mechanics of the phenomenon, an evaluation of the susceptibility of cantilevered support structures to the phenomenon, a summary of the methods to mitigate vibrations resulting from the phenomenon, and a review of current design specifications which contain provisions for the design of cantilevered support structures for the phenomenon.

2.2 GALLOPING

2.2.1 General

Galloping is a form of aeroelastic instability characterized by large-amplitude, resonant oscillations which occur in a single, uncoupled mode of vibration [33] normal to the direction of wind flow. Galloping-induced oscillations primarily occur in flexible, lightly-damped structures and, as will be discussed below, are limited to those structures with non-symmetrical cross-sections (i.e. circular cylinders are not susceptible to galloping-induced vibrations). The phenomenon has been extensively studied in a variety of structures such as square and rectangular prismatic members and ice-coated transmission conductors.

Galloping-induced oscillations are caused by aerodynamic forces which act on a structural element as it is subjected to periodic variations in the angle of attack of the wind flow. The periodically varying angle of attack is generated by across-wind oscillation of the structure. If the aerodynamic forces are aligned with the direction of across-wind motion, successively larger amplitudes of oscillation, and thus galloping, result.

The derivation of the conditions under which galloping-induced oscillations occur is significantly simplified through the use of a quasi-steady approach, i.e. the aerodynamic forces to which a structure is subjected under a periodically varying angle of attack of the wind flow are assumed to be identical to the forces to which the structure would be subjected under static variations in the angle of attack. The quasi-steady assumption has been adopted in the following derivation of the conditions under which galloping-induced oscillations occur. Additional discussion pertaining to the mechanics of the galloping phenomenon can be found in References 8, 14, 29, and 38.

Consider, as depicted in Figure 2.1, a sign or signal attachment (which is assumed to be a single-degree-of-freedom system) subjected to motion $\dot{y}$ in a direction normal to the direction of the free-stream, steady-state flow, V. The relative movement of the structure with respect to the steady-state flow results in a relative velocity, V_{rel}. The orientation of the relative velocity vector, V_{rel}, with respect to the steady-state flow velocity vector, V, is defined as the angle of attack, α:

$$\alpha = \arctan\frac{\dot{y}}{V} \tag{2.1}$$

Positive values of the angle of attack are defined as is shown in Figure 2.1.

The aerodynamic drag and lift forces per unit length, F_D and F_L, respectively, imposed upon the structure with respect to the relative velocity are given by:

$$F_D = \frac{1}{2}\rho V_{rel}^2 D C_D \tag{2.2}$$

$$F_L = \frac{1}{2}\rho V_{rel}^2 D C_L \tag{2.3}$$

where ρ is the density of air, D is the across-wind dimension of the element, C_D is the drag force coefficient, C_L is the lift force coefficient, and the remaining variables are as previously defined. For a given structure, the aerodynamic lift and drag forces can be predicted by standard aerodynamic theory or measured in wind tunnel tests.

The component of the aerodynamic lift and drag forces in the y-direction yields the aerodynamic lift force per unit length, $F_y(\alpha)$, acting normal to the free-stream velocity, V:

$$F_y(\alpha) = -F_D \sin\alpha - F_L \cos\alpha \tag{2.4}$$

Equation 2.4 can be rewritten as:

$$F_y(\alpha) = \frac{1}{2}\rho V^2 D C_{Fy}(\alpha) \tag{2.5}$$

where $C_{Fy}(\alpha)$ is the lift force coefficient of the aerodynamic force per unit length acting normal to the free-stream velocity. The free-stream velocity, V, is related to the relative velocity, V_{rel}, by the following:

$$V = V_{rel}\cos\alpha \tag{2.6}$$

It follows from Equations 2.2 through 2.6 that the lift force coefficient, $C_{Fy}(\alpha)$, is given by:

$$C_{Fy}(\alpha) = -[C_L(\alpha) + C_D(\alpha)\tan\alpha]\sec\alpha \tag{2.7}$$

For the equilibrium position (i.e. zero displacement), the angle of attack, α, is equal to zero and the aerodynamic force per unit length normal to the free-stream velocity is approximated by:

$$F_y(\alpha=0) \approx \frac{\partial F_y(\alpha)}{\partial \alpha}\Big|_{\alpha=0} \alpha \tag{2.8}$$

Differentiating Equation 2.5, evaluating at $\alpha = 0$, and substituting the approximation $\alpha \approx \dot{y}/V$ (valid for small α) yields the following expression for the aerodynamic force per unit length normal to the free-stream velocity, $F_y(\alpha = 0)$:

$$F_y(\alpha=0) = \frac{1}{2}\rho VD\left(\frac{dC_{Fy}}{d\alpha}\right)\Big|_{\alpha=0} \dot{y} \tag{2.9}$$

Substituting Equation 2.9 into the standard equation of motion for a single-degree-of-freedom system yields:

$$m[\ddot{y} + 2\xi\omega\dot{y} + \omega^2 y] = \frac{1}{2}\rho VD\left(\frac{dC_{Fy}}{d\alpha}\right)\Big|_{\alpha=0} \dot{y} \tag{2.10}$$

where m is the mass per unit length, ξ is the damping ratio, and ω is the circular natural frequency of the structure. Differentiating Equation 2.7 yields:

$$\frac{dC_{Fy}}{d\alpha} = -\left(\frac{dC_L}{d\alpha} + C_D\right) \tag{2.11}$$

Substituting Equation 2.11 into Equation 2.10 yields:

$$m[\ddot{y} + 2\xi\omega\dot{y} + \omega^2 y] = -\frac{1}{2}\rho VD\left(\frac{dC_L}{d\alpha} + C_D\right)\Big|_{\alpha=0} \dot{y} \tag{2.12}$$

Examination of the right side of Equation 2.12 indicates that the aerodynamic force normal to the free-stream velocity is coupled to the velocity, $\dot{y}$. As a result, the right side of the equation is termed aerodynamic damping. The aerodynamic damping contributes to the mechanical damping (i.e. the term $2m\xi\omega$) possessed by the structural system. Combining the aerodynamic and mechanical damping terms yields an effective damping given by d_e:

$$d_e = 2m\xi\omega + \frac{1}{2}\rho VD\left(\frac{dC_L}{d\alpha} + C_D\right)\Big|_{\alpha=0} \tag{2.13}$$

If the effective damping is greater than zero, the system is stable and galloping from the equilibrium position will not occur. However, if the effective damping is less than zero, the system is unstable and galloping-induced oscillations from the equilibrium position will result. Since the mechanical damping possessed by the structural system is always positive, galloping-induced oscillations from the equilibrium position result when the following inequality is satisfied:

$$\frac{dC_{Fy}}{d\alpha} = -\left(\frac{dC_L}{d\alpha} + C_D\right)\Big|_{\alpha=0} > \frac{4m\xi\omega}{\rho VD} \tag{2.14}$$

Equation 2.14 is an exact condition for evaluating the susceptibility of a structure to galloping from the equilibrium position. Generally, however, the mechanical damping term is neglected [31], and the potential susceptibility of a structure to galloping from the equilibrium position is evaluated using the following inequality:

$$\left(\frac{dC_{Fy}}{d\alpha}\right)\Big|_{\alpha=0} = -\left(\frac{dC_L}{d\alpha} + C_D\right)\Big|_{\alpha=0} > 0 \tag{2.15}$$

Equation 2.15 is referred to as the Den Hartog stability criterion [15]. The Den Hartog stability criterion states that "a section is dynamically unstable if the negative slope of the lift curve is greater than the ordinate of the drag curve [15]." As is evident from Equation 2.15, this condition is satisfied when the slope of the lift force coefficient normal to the free-stream velocity, $dC_{Fy}/d\alpha$, is positive (in other words, when the term $dC_L/d\alpha + C_D$ is negative). When the Den Hartog stability criterion is satisfied, a structure possesses aerodynamic characteristics which result in negative aerodynamic damping. Thus, the Den Hartog stability criterion defines one of the

primary conditions (i.e. negative aerodynamic damping) necessary for the occurrence of galloping from the equilibrium position.

As was discussed above, however, galloping from the equilibrium position can only occur if the magnitude of the negative aerodynamic damping is greater than the magnitude of the positive mechanical damping possessed by the structure (i.e. galloping can only occur if the effective damping is less than zero). As is evident in Equation 2.13, the magnitude of the negative aerodynamic damping is a function of the free-stream flow velocity. Rearranging Equation 2.14, the minimum wind velocity, V_0, necessary for negative effective damping is given by:

$$V_0 = \frac{4m\xi\omega}{\rho D \frac{dC_{Fy}}{d\alpha}} \tag{2.16}$$

Thus, two conditions are necessary for a structure to gallop from the equilibrium position: (1) the Den Hartog stability criterion must be satisfied (which defines the condition of negative aerodynamic damping), and (2) the structure must be subjected to a minimum onset wind velocity at which the negative aerodynamic damping exceeds the positive mechanical damping possessed by the structure.

Inspection of Equation 2.16 indicates that the magnitude of the onset wind velocity necessary for galloping is a function of the dynamic and aerodynamic characteristics of the structure. The onset wind velocity is directly proportional to the mechanical damping possessed by the structure [34] and is also proportional to the mass and stiffness of the structure. Furthermore, the onset wind velocity is inversely related to the slope of the lift force coefficient curve, C_{Fy}. Thus, a highly flexible structure with low damping (such as a typical cantilevered support structure) will be susceptible to galloping-induced oscillations at relatively low wind velocities provided, of course, that the Den Hartog stability criterion is satisfied.

Once galloping is initiated, the characteristics of the dynamic response in the across-wind direction are dictated by energy considerations. At wind velocities exceeding the onset velocity, the energy inputed to the structure by the flow exceeds the energy dissipated by structural damping. Since the energy inputed to the structure is a function of flow velocity, the amplitudes of vibration associated with the galloping phenomenon increase with flow velocity. The amplitude of the across-wind oscillation at any particular flow velocity is limited by nonlinearities in the fluid force or by nonlinearities in the structure [8].

Several researchers have proposed various analytical models to predict the dynamic characteristics of structures subjected to galloping [33, 34, 36]. The models are based upon quasi-steady theory in which it is assumed that aerodynamic data can be can be used to describe and predict the dynamic behavior of a structure during galloping. One of the most comprehensive analytical models currently available was developed by Novak [34]. The model has been used to predict the behavior of structural members composed of square and rectangular cross-section with acceptable accuracy. In addition, the model has been extended to predict the response of multi-degree-of-freedom systems to the galloping phenomenon. The accuracy of these analyses, however, is dependent upon an accurate representation of the variation in the aerodynamic lift force coefficient, C_{Fy}, with angle of attack. For complicated geometrical configurations, aerodynamic wind tunnel tests must be performed to obtain this relationship. Furthermore, the analysis is quite tedious and computationally intensive for multi-degree-of-freedom systems. Thus, current analytical models which attempt to predict the dynamic response of structures to the galloping phenomenon are not well-suited for inclusion in a design specification.

It should be noted that the results of previous research indicate that structures may also be susceptible to galloping-induced oscillations under conditions in which the Den Hartog stability criterion is not satisfied (i.e. $dC_{Fy}/d\alpha \leq 0$). Novak [34] found that two criteria must be satisfied

in order for galloping to occur under such conditions: (1) the structure must be subjected to an initial disturbance in the across-wind direction, the magnitude of which must be approximately equal to the amplitude of the galloping response, and (2) the structure must be subjected to a minimum onset wind velocity. It was found that the magnitude of the initial, across-wind disturbance and onset wind velocity are proportional to the level of damping possessed by the structure. Furthermore, it was also found that the magnitude of the minimum onset wind velocities required to initiate galloping in structures which did not satisfy the Den Hartog stability criterion was significantly greater than the magnitude of the minimum onset wind velocity required to initiate galloping in structures which did satisfy the criterion. The implication of this research with respect to the performance of cantilevered support structures is that these structures may be susceptible to galloping-induced oscillations even when configured with attachments which possess aerodynamic characteristics that do not satisfy the Den Hartog stability criterion. Sources of the initial, across-wind displacement required to initiate galloping under such conditions include natural-wind gusts, truck-induced wind gusts, and vortex shedding.

In summary, a structure will be subject to galloping-induced oscillations from the equilibrium condition when two conditions are satisfied: (1) the structure possesses aerodynamic characteristics which satisfy the Den Hartog stability criterion and (2) the structure is subjected to a certain minimum onset wind velocity. The Den Hartog stability criterion establishes whether the aerodynamic characteristics of the structure are such that negative aerodynamic damping is possible (i.e. the criterion establishes the condition under which the across-wind force, F_y, will be oriented in the same direction as the across-wind motion). The minimum onset wind velocity establishes the condition for which the magnitude of the negative aerodynamic damping will be greater than the magnitude of the positive mechanical damping possessed by the structure. When both of the above conditions are satisfied, the structure is unstable and large-amplitude, across-

wind oscillations result. The amplitudes of the oscillations are proportional to the wind velocity and occur at the natural frequency of the structure.

2.2.2 Evaluation of the Susceptibility to Galloping

As was discussed in Chapter One, the oscillations observed in cantilevered support structures in the field are consistent with the characteristics of the galloping phenomenon. These characteristics include the sudden onset of large-amplitude, across-wind vibrations which increase with wind velocity and occur at the natural frequency of the structure. Based upon existing knowledge of the galloping phenomenon, it is known that the observed vibrations of cantilevered support structures in the field are not the result of galloping of the support members. A majority of cantilevered support structures are composed of structural elements consisting of circular cross-sections. As was previously discussed, elements with circular cross-section are not susceptible to galloping-induced vibrations. The symmetry of a circular cylinder lends to the development of a pure drag force when subjected to a periodically varying angle of attack of the wind flow. As a result, the aerodynamic force which develops normal to the free-stream velocity is always oriented opposite to the direction of across-wind motion (i.e. circular cylinders always experience positive aerodynamic damping). Thus, circular cylinders are not susceptible to the galloping instability. This fact is important because it indicates that the across-wind vibrations observed in the cantilevered support structures in the field are the result of the aerodynamic characteristics possessed by the attachments to these structures (i.e. signs/signals).

This fact was confirmed by McDonald et al. [32] in a research program which was recently conducted to evaluate the susceptibility of cantilevered signal support structures to the galloping phenomenon. McDonald et al. [32] performed tow tank tests to measure the aerodynamic forces acting on horizontally-mounted signal attachments (i.e. signals mounted

parallel to the horizontal mast-arm) composed of various geometrical configurations under flow directions from the front and the rear. The results of these tests indicated that the configuration of the signal attachments and the direction of flow significantly influence the susceptibility for galloping. Signal attachments configured with backplates and subjected to flow from the rear were found to be most susceptible to galloping (i.e. the slope of the lift force coefficient curve, C_{Fy}, was greatest for this configuration and flow direction). Conversely, signal attachments configured without backplates were found not to be susceptible to galloping for flow from both the front and the rear (i.e. the slope of the lift force coefficient curve, C_{Fy}, indicated positive aerodynamic damping).

McDonald et al. [32] also performed full-scale tests on two cantilevered signal support structures to evaluate the dynamic response exhibited by these structures during occurrences of galloping-induced oscillations. One of the structures tested had a horizontal support length of 12.2 m and the other had a horizontal support length of 14.6 m. Each of the structures was mounted to a rotatable foundation which permitted the structures to be oriented normal to the prevailing wind direction. Tests on the 12.2 m structure were conducted with the structure configured with signal attachments which were found to be both susceptible and not susceptible to galloping from the equilibrium position during the tow tank experiments. Tests in which the structure was mounted with signal attachments found not to be susceptible to galloping from the equilibrium position during the tow tank experiments did not exhibit galloping-induced oscillations when tested in the field. However, when configured with signal attachments found to be susceptible to galloping during the tow tank tests, the structure was observed to experience galloping oscillations with displacement amplitudes at the tip of the horizontal support estimated at between 300 to 400 mm. The results of tests on the 14.6 m structure were similar. Galloping was observed in this structure at a wind velocity equal to 4.5 m/s with a maximum measured stress range in the vertical

support (at a location 330 mm from the base) equal to approximately 34 MPa. As will be discussed in Chapter Five, fatigue cracks would be expected to form under a 34 MPa stress range for a large majority of cantilevered support structure connection details.

Thus, the results of previous research programs confirm that cantilevered signal support structures are susceptible to galloping as a result of the aerodynamic characteristics possessed by the attachments to these structures. Tow tank experiments performed by McDonald et al. [32] indicate that horizontally-mounted signal attachments configured with backplates possess aerodynamic characteristics which satisfy the Den Hartog stability criterion. Furthermore, the results of these tests indicate that the susceptibility of cantilevered signal support structures to the galloping phenomenon is dependent upon the direction of flow as well as upon the geometrical configuration of the attachment. Full-scale field tests conducted by McDonald et al. [32] illustrated that cantilevered signal support structures are susceptible to significant amplitudes of vibration due to galloping at relatively low wind velocities. Furthermore, stress measurements made during occurrences of galloping-induced vibrations indicate that, even at low wind velocities, cantilevered support structures are subject to stress ranges which are potentially damaging with respect to fatigue.

2.2.3 Mitigation of Galloping-Induced Vibrations

As was discussed in Section 2.2.1, a structure which possesses aerodynamic characteristics that satisfy the Den Hartog stability criterion will experience galloping-induced vibrations at a certain onset wind velocity, defined previously as V_0. The magnitude of the wind velocity at which galloping vibrations will initiate is dependent upon the dynamic properties of the structure (i.e. mass, damping, and stiffness). As a result, two primary means exist by which to mitigate galloping-induced oscillations in cantilevered support structures: (1) changing the dynamic

characteristics of the structure such that the magnitude of the onset wind velocity is greater than the wind velocity for which steady-state flows are typically maintained, or (2) changing the aerodynamic characteristics of the attachments such that the structure will be experience positive aerodynamic damping when subjected to a periodically varying angle of attack of the wind flow.

The dynamic properties of a cantilevered support structure can be altered by changing either the structure's mass, stiffness, and/or damping. Increasing any of the three dynamic properties increases the magnitude of the onset wind velocity required to initiate galloping vibrations. Increases in stiffness and mass can be obtained by increasing the sizes of the structural supports. Increases in damping can be obtained by mounting a variety of external damping devices to the structure. McDonald et al. [32] evaluated the effectiveness of two types of external damping devices for mitigating galloping-induced vibrations in cantilevered signal support structures: (1) a tuned-mass damper and (2) a liquid-tuned damper. The tuned-mass damper was dismissed as a potential mitigation measure following an evaluation which indicated that the installation of such a device to the horizontal mast-arm of a cantilevered support structure would be impractical. The liquid-tuned damper, which consisted of a 914 mm long PVC pipe filled with water and inserted into the end of the horizontal mast-arm of a full-scale signal support structure, was found to be ineffective in mitigating galloping-induced vibrations.

The aerodynamic properties of the attachments to cantilevered support structures can be altered in one of two ways: (1) the geometric configuration of the attachment can be changed to either minimize or eliminate the characteristics which result in negative aerodynamic damping or (2) a device which is known to provide positive aerodynamic damping can be mounted to the structure. With respect to the first method, the simplest method by which to reduce the susceptibility of a signal attachment to negative aerodynamic damping would be to remove the backplate. Based upon the results of tow tank tests conducted by McDonald et al. [32], signals

configured without a backplate did not possess aerodynamic characteristics which satisfied the Den Hartog stability criterion (i.e. signal without backplates were found to possess positive aerodynamic damping). As a result, removal of the backplates from signals would eliminate the condition which creates the galloping instability. With respect to the second method, McDonald et al. [32] evaluated the effectiveness of a damping plate mounted to the horizontal support of a cantilevered signal support structure. The damping plate consisted of a sign blank measuring 410 mm x 1680 mounted horizontally (i.e. parallel to the horizon) directly above the signal attachment located closest to the tip of the horizontal mast-arm. The results of full-scale tests indicated that the damping plate provided enough positive aerodynamic damping to effectively mitigate galloping-induced vibrations. It was noted, however, that smaller damping plates did not effectively mitigate the vibrations. In addition, damping plates mounted at locations other than directly above the outermost signal were also not effective at mitigating the galloping-induced vibrations.

2.2.4 Review of Design Specifications

Current specifications used for the design cantilevered support structures for vibration and fatigue [4, 35] do not recognize or contain provisions pertaining to the galloping phenomenon. As a result, designers are provided no guidance regarding the design of cantilevered support structures for galloping-induced vibrations.

2.3 VORTEX SHEDDING

2.3.1 General

Vortex shedding is a wake-induced aerodynamic phenomenon which typically develops during steady, uniform flows, and produces resonant oscillations in a plane normal to the direction of flow. Unlike galloping, which results from a periodic variation in the angle of attack of the wind flow, vortex shedding is caused by the shedding of vortices in a regular, alternating pattern in the wake of a structural element. The phenomenon has been studied in a wide-range of structures, some of which include bridge decks, hyperbolic cooling towers, antenna masts, and pipelines.

When a structural element is exposed to a steady, uniform flow, vortices are shed in the wake behind the element in an alternating pattern commonly referred to as a von Karman vortex street (Figure 2.2). The frequency at which vortices are shed from the element, f_s, is given by the Strouhal relation:

$$f_s = \frac{SV}{D} \tag{2.17}$$

where S is the Strouhal number, D is the across-wind dimension of the element, and V is the free-stream wind velocity. As is indicated by Equation 2.17, the frequency at which vortices are shed is primarily dependent upon the velocity of the flow, the across-wind dimension of the element, and the shape of the element (as defined by the magnitude of the Strouhal number). Table 2.1 summarizes the magnitude of the Strouhal number for typical cantilevered support structure attachments and structural members. A brief discussion of each is provided in the following paragraphs.

For circular cylinders, the magnitude of the Strouhal number is dependent upon the characteristics of the flow as defined by the Reynolds number, R:

$$R = \frac{VD}{\nu} \tag{2.18}$$

where V is the free-stream flow velocity, D is the across-wind dimension of the element, and ν is the kinematic viscosity of air. In the regime of subcritical flow, defined by Reynolds numbers less than approximately 3×10^5, the Strouhal number is equal to 0.18. Vortex formation in the subcritical regime is coherent and centered around one well-defined frequency. In the regime of critical flow, defined by Reynolds number between approximately 3×10^5 and 3.5×10^6, the Strouhal number increases sharply. Vortex formation in this flow regime is highly disorganized and occurs over a broad range of frequencies. In the regime of supercritical flow, defined by Reynolds numbers greater than approximately 3.5×10^6, vortex formation again becomes centered around one well-defined frequency with a Strouhal number equal to approximately 0.25. Figure 2.3 summarizes the relationship between Strouhal number and Reynolds number for flow around a circular cylinder.

Vortex formation in the wake of a sign or signal is approximately independent of Reynolds number and occurs in a regular, coherent manner at well-defined frequencies for all velocities for which uniform, steady-state flow is maintained. The value of the Strouhal number for a flat plate, such as a sign, is equal to 0.14. For a signal, the value of the Strouhal number is dependent upon the geometrical configuration and orientation of the signal with respect to the flow. McDonald et al. [32] found that the Strouhal number for a signal varies between 0.13 and 0.28, with an average value of approximately 0.20.

Vortex shedding is an aerodynamic phenomenon if the frequency of vortex shedding, as predicted by the Strouhal relation, does not match one of the natural frequencies of the structure. In these cases, the shedding of vortices in the wake of a structure will elicit only a nominal periodic response. However, when the frequency of vortex shedding approaches one of the natural

frequencies of a flexible, lightly-damped structure, significant amplitudes of vibration can result. The primary implication of this large-amplitude, across-wind, resonant vibration is that it has a strong organizing effect on the pattern with which vortices are shed. The result is an increase in vortex strength, an increase in the spanwise correlation of the vortex shedding forces, and a tendency for the vortex shedding frequency to become coupled to the natural frequency of the structure.

The tendency for the vortex shedding frequency to become coupled to the natural frequency of a structure is termed lock-in. The critical wind velocity, V_{cr}, at which lock-in occurs is given by the Strouhal relation:

$$V_{cr} = \frac{f_n D}{S} \tag{2.19}$$

where f_n is the natural frequency of the structure, D is the across-wind dimension of the element, and S is the Strouhal number. Figure 2.4 illustrates a schematic of the lock-in phenomenon. As predicted by the Strouhal relation, the frequency at which vortices are shed from a structure is linearly related to the flow velocity. However, as the frequency of vortex shedding, f_s, approaches one of the natural frequencies of a structure, f_n, lock-in occurs and the frequency of vortex shedding becomes dependent solely on the natural frequency of the structure. The result is a condition of resonant vibration that persists over a range of wind velocities.

The amplitudes of vibration associated with the lock-in phenomenon are generally limited by the ability of vortices to be shed from the structure in a symmetric pattern. Large amplitudes of vibration tend to interfere with the symmetric pattern of vortex formation. Previous research indicates the maximum amplitudes of displacements associated with the lock-in phenomenon rarely exceed approximately 1 to 1.5 times the across-wind dimension of the structural element from which vortices are shed [8, 29].

2.3.2 Evaluation of the Susceptibility to Vortex Shedding

Current knowledge concerning wind characteristics can be used to generally bound the velocities under which structures will be subject to vortex-induced vibrations. For example, one basic assumption for the formation of vortices in the wake of any element is that the element is subjected to uniform, steady-state flow. Natural turbulence tends to interfere with the symmetric formation of periodic vortices in the wake of a structure by reducing the length over which the vortex shedding forces remain correlated. As a result, natural turbulence creates an upper-bound on the maximum wind velocity for which periodic vortex shedding can occur. Previous research indicates the level of turbulence associated with wind velocities above approximately 15 to 20 m/s limits the symmetric formation of periodic vortices [29]. At the opposite end of the spectrum, vortex formation at wind velocities below approximately 5 m/s generates forces with magnitudes insufficient to excite even lightly-damped structures [29]. Based upon this knowledge, structures can be reasonably assumed to be susceptible to vortex-induced vibrations in the range of wind velocities between approximately 5 and 15 m/s.

The range of wind velocities for which vortex-induced vibrations can be expected to occur provides a convenient criterion by which to evaluate the potential susceptibility of cantilevered sign, signal, and luminaire support structures to this wind-loading phenomenon. The following paragraphs provide a brief discussion of the critical wind velocities for which lock-in will occur for the range of member and attachment dimensions typically used in cantilevered support structures. A comparison of these critical wind velocities with the range of wind velocities for which vortex-induced vibrations can be expected to occur suggests that the susceptibility of cantilevered support structures to vortex shedding lock-in is generally quite limited.

Figure 2.5 depicts the wind velocities required to initiate vortex-induced vibrations due to the shedding of vortices from the circular supports of cantilevered support structures in the supercritical flow regime. The results are based upon the Reynolds number relationship:

$$V_{supercritical} = \frac{R_{supercritical}\nu}{D} \tag{2.20}$$

where $V_{supercritical}$ is the wind velocity required to enter the supercritical flow regime, $R_{supercritical}$ is the Reynolds number corresponding to the supercritical flow regime (3.5×10^6), ν is the kinematic viscosity of air (14.6 mm^2/s), and D is the across-wind dimension (i.e. diameter) of the circular support. As is evident from Figure 2.5, the diameters selected are representative of the range of diameters typically used in cantilevered support structures. The results of the calculations shown in Figure 2.5 indicate that the wind velocities required to initiate vortex shedding in the supercritical flow regime are well above the maximum velocity for which uniform, steady-state flows are typically maintained (i.e. 20 m/s). As a result, only the subcritical flow regime need be considered when evaluating the susceptibility of cantilevered support structures to vortex-induced vibration caused by the shedding of vortices from the supports.

Figure 2.6 depicts the critical wind velocities required to initiate lock-in due to the shedding of vortices from the circular supports of cantilevered support structures in the subcritical flow regime. The results are based upon the Strouhal relation:

$$V_{cr} = \frac{f_n D}{S} \tag{2.21}$$

where f_n is the natural frequency of the structure (assumed to be 1 Hz, which is a typical value for the first mode of vibration of a cantilevered support structure in the vertical plane), D is the across-wind dimension (i.e. diameter) of the circular support, and S is the Strouhal number (0.18 for subcritical flow). Again, the diameters selected are representative of the range of diameters

typically used in cantilevered support structures. The results of the calculations shown in Figure 2.6 indicate that the wind velocities for which vortices will be shed from the circular supports of cantilevered support structures fall below the minimum wind velocity of 5 m/s required to initiate vibration in even lightly-damped structures. Thus, cantilevered support structures are generally not expected to be susceptible to vortex-induced vibrations due to the shedding of vortices from the supports.

Based upon the above calculations, it can also be assumed that tapered circular support members will not be susceptible to vortex-induced vibrations due to the shedding of vortices from the supports. Vortex shedding lock-in in a tapered element occurs at multiple critical wind velocities as a result of the variation in diameter along the length of the tapered element:

$$V_{cr}(x) = \frac{f_n D(x)}{S} \qquad (2.22)$$

where $V_{cr}(x)$ is the critical wind velocity corresponding to the across-wind dimension D(x), f_n is the natural frequency of the structure, D(x) is the across-wind dimension (i.e. diameter) at a distance x along the tapered element, and S is the Strouhal number. At low critical wind velocities, vortices are shed from the tip of the tapered element at frequencies which correspond to the natural frequency of the structure. As the wind velocity increases, the location at which vortices are shed at frequencies which correspond to the natural frequency of the structure moves from the tip towards the base of the tapered element (i.e. from the smallest diameter to the largest diameter). Thus, vortex shedding lock-in in a tapered structural element is a condition of localized resonance in which the vortex shedding forces remain correlated over a limited length of the element at each discrete increment in critical wind velocity. Since the diameters of tapered elements used in cantilevered support structures fall within the diameters indicated in Figure 2.6, it is evident that the range in critical wind velocities associated with lock-in of tapered elements

will also fall below the minimum velocity required to initiate vortex-induced vibrations (i.e. 5 m/s).

The critical wind velocities for which lock-in would occur due to the shedding of vortices from sign attachments are shown in Figure 2.7. The results depicted in Figure 2.7 were calculated using Equation 2.21 with a natural frequency equal to 1 Hz and a Strouhal number equal to 0.14. Examination of these critical wind velocities indicates that vortex-induced vibrations would be expected for sign depths ranging from approximately 800 mm to 2800 mm. The critical wind velocities for sign attachments with depths greater than approximately 2800 mm are above the velocity for which steady, uniform flows are expected. Thus, cantilevered support structures mounted with sign attachments greater than approximately 2800 mm in depth are not expected to be susceptible to vortex-induced vibrations.

The critical wind velocities for which lock-in would occur due to the shedding of vortices from signal attachments are shown in Figure 2.8. The results depicted in Figure 2.8 were calculated using Equation 2.21 with a natural frequency equal to 1 Hz and a Strouhal number equal to 0.20. Examination of these critical wind velocities indicates that vortex-induced vibrations would be expected for signal depths greater than approximately 1000 mm. Thus, horizontally-mounted signal attachments (i.e. mounted with the directional lights oriented parallel to the horizontal mast-arm), with typical depths ranging from approximately 300 mm to 500 mm, would not be expected to experience vortex-induced vibrations. Vertically-mounted signal attachments (i.e. mounted with the directional lights oriented perpendicular to the horizontal mast-arm), however, with depths ranging from approximately 900 mm to 1300 mm, would be expected to be susceptible to vortex-induced vibrations.

The preceding observations related to the susceptibility of cantilevered support structures to vortex-induced vibrations are supported by the results of previous researchers. McDonald et

al. [32] conducted a series of water table and tow tank experiments to evaluate the potential susceptibility of cantilevered support structure signal attachments and support members to the vortex shedding phenomenon. Much like a wind tunnel test, the water table experiments were conducted on scale models to measure the frequencies at which vortices would be shed from various structural members and attachments. Flow velocities equivalent to 4.5 m/s and 9 m/s were considered. A partial summary of the results is provided in Table 2.2. As is evident from the data tabulated in Table 2.2, the frequencies at which vortices were shed from circular and octagonal supports at the two flow velocities considered were well above the natural frequency of 1 Hz possessed by a majority of cantilevered support structures. The results of the water table experiments, therefore, support the preceding conclusions that cantilevered support structures are generally not susceptible to vibrations due to the shedding of vortices from the supports.

As is shown in Table 2.2, the frequencies at which vortices were shed from signal attachments configured with a backplate, however, can be observed to fall significantly closer to the typical natural frequency of 1 Hz possessed by a majority of cantilevered support structures. Based upon the results of these tests, it appears that vortex-induced vibrations resulting from the shedding of vortices from signal attachments is a possibility.

The results of the water table tests conducted by McDonald et al. [32], however, did not consider the three-dimensional characteristics associated with flow around signal attachments. Full-scale flow-visualization tests were conducted by McDonald et al. [32] using a tow tank to evaluate these effects. The results indicated that the three-dimensional characteristics of signal attachments interfered with the formation of a regular pattern of vortices at a well-defined frequency. The frequency at which vortices were shed was observed to be highly random. In addition, the vortices shed in the wake of the attachments were disorganized. As a result, it was concluded that cantilevered signal support structures were unlikely to experience significant

amplitudes of across-wind oscillation due to the shedding of vortices from the signal attachments. Thus, even though the calculated critical flow velocities for a majority of signal attachments fall in the range for which vortex shedding would be expected, the occurrence of significant amplitudes of vibration are unlikely due to the incoherent, random characteristics of the vortex street in the wake of a signal attachment.

Based upon the above discussion concerning the susceptibility of cantilevered support structures to vortex-induced vibrations, the following general observations can be made:

- A large majority of cantilevered support structures will not be susceptible to vortex-induced vibrations due to the shedding of vortices from the supports. For typical member dimensions, the critical wind velocities necessary for lock-in fall below the minimum velocity required to initiate vortex-induced vibrations (5 m/s). Only those support structures with the largest member dimensions will be potentially susceptible to vortex-induced vibrations resulting from the shedding of vortices from the supports.

- Cantilevered signal support structures will not be susceptible to significant amplitudes of across-wind vibration resulting from the shedding of vortices from the attachments to these structures. Although the critical wind velocities generally fall within the range of velocities for which vortex-induced vibrations would be expected, the three-dimensional characteristics of flow around signal attachments interferes with the formation of a coherent pattern of vortices at one well-defined frequency.

- Cantilevered sign support structures mounted with sign attachments with relatively small depths (i.e. less than approximately 2800 mm) will be susceptible to vortex-

induced vibrations when considering the range of wind velocities for which vortex shedding would be expected.

It should be noted that the preceding statements are generalized conclusions based upon the typical characteristics of natural wind. As with any natural phenomenon, variations from what is considered "typical" can occur. For example, vortex-induced vibrations of bridge structures have been observed during uniform, steady-state wind flows exceeding 27 m/s. As a result, the preceding conclusions represent qualitative generalities regarding the potential susceptibility of cantilevered support structures to the vortex shedding phenomenon. The conclusions are intended to indicate that the large-amplitude, across-wind vibrations observed in the majority of cantilevered support structures in the field are due to the galloping phenomenon. It is recognized, however, that cantilevered support structures may be susceptible to vortex-induced vibrations under conditions outside of the bounds presented above.

2.3.3 Mitigation of Vortex-Induced Vibrations

Similar to the mitigation of galloping-induced vibrations, the effects of vortex shedding can be mitigated by one of two methods: (1) altering the dynamic properties of the structure (i.e. mass, stiffness, and/or damping) or (2) altering the aerodynamic characteristics of the structure.

Significant amplitudes of vibration associated with vortex shedding can be avoided by ensuring that the critical wind velocity associated with lock-in falls outside of the range of wind velocities for which vortex shedding would be expected (i.e. 5 m/s to 20 m/s). This can be achieved by either increasing or decreasing the natural frequency of the structure (through variations in the mass and stiffness). Of course, decreasing the natural frequency such that the critical wind velocity is less than the lower limit for vortex shedding (i.e. 5 m/s) is generally not

feasible for a majority of cantilevered support structures. Existing cantilevered support structures are already quite flexible and additional reductions in stiffness may increase the susceptibility for galloping-induced oscillations. Increasing the natural frequency, however, could readily be achieved through increased member dimensions so that the critical wind velocity falls above the upper-bound velocity for which uniform, steady-state flows are typically maintained (i.e. 20 m/s). The increased levels of stiffness associated with increases in natural frequency would also be beneficial in limiting the susceptibility of cantilevered support structures to the galloping phenomenon.

The dynamic properties of cantilevered support structures can also be altered through the use of external damping devices such as tuned-mass and impact dampers. As was discussed in Section 2.2.3, however, the results of research conducted by McDonald et al. [32] indicate that the use of tuned-mass dampers in cantilevered support structures is impractical. Furthermore, previous experience [26] obtained with the use of impact dampers to reduce cantilevered support structure vibrations indicates that such damping devices are not effective for structures with natural frequencies of vibration below approximately 1 Hz.

Vortex-induced vibrations can also be minimized by altering the aerodynamic characteristics of the element from which vortices are shed. This is achieved by altering the cross-section of the element such that the formation of a coherent pattern of vortices at one well-defined frequency is prevented. With respect to the shedding of vortices from members with circular cross-sections, helical strakes, shrouds, and rectangular plates installed at intervals along the members have proven to be an effective method by which to mitigate vibrations in structures such as stacks and chimneys [8, 31]. Although the use of such devices has proven effective in a variety of structures, their effectiveness for preventing vortex-induced vibrations in cantilevered support structures has been questioned by Edwards et al. [17]. The results of wind tunnel tests

conducted by Edwards et al. [17] suggest that the installation of strakes to the support members of cantilevered support structures do not significantly reduce the response of these structures to vortex shedding.

2.3.4 Review of Design Specifications

Several design specifications [4, 35] contain provisions for the design of structures for vortex-induced vibrations. The following paragraphs summarize the provisions contained within two specifications and compare the magnitudes of the across-wind forces specified in each.

The current AASHTO Specifications [4] for the design of cantilevered sign, signal, and luminaire support structures contain provisions for the design of simple cantilever poles for vortex shedding. The provisions are based upon research conducted by Brockenbrough [10]. The methodology of the AASHTO design provisions are as follows: The natural frequency is estimated using an analytical solution for the natural frequency corresponding to the first mode of vibration of a simple pole. The critical wind velocity, V_{cr}, associated with vortex-shedding lock-in is computed using the Strouhal relation (i.e. Equation 2.19). The transverse pressure, P_t, acting on the pole is given by:

$$P_t = \frac{P}{2\beta} \tag{2.23}$$

where:

$$P = 0.0473 V_{cr}^2 C_d C_h \tag{2.24}$$

where β is the damping ratio (conservatively estimated in the Specifications as 0.005), $1/2\beta$ is the dynamic magnification factor for a single-degree-of-freedom-system (conservatively estimated in the Specifications as 100), C_d is the drag force coefficient (determined based upon the shape of the element), and C_h is the height coefficient (used to account for the variation in wind velocity

with height above ground). The transverse pressure, P_t, is then used to compute stresses for the design of the pole for fatigue.

Tapered poles are accounted for in the Specifications in a similar manner. Equations are provided to compute equivalent lengths and diameters for estimation of the natural frequencies of tapered poles. The critical wind velocity is computed using the Strouhal relation (i.e. Equation 2.19), evaluated using the diameter of the pole at a distance 3L/4 (where L is the length of the pole) from the base. The transverse pressure, P_t, acting on the pole is then given by Equations 2.23 and 2.24.

As mentioned above, the provisions contained in the current Specifications for vortex shedding are based upon research conducted on simple cantilever poles. Thus, the applicability of these provisions to the design of cantilevered support structures for vortex shedding is questionable. Furthermore, the provisions do not contain adequate guidance concerning application of the transverse loading. Specifically, the provisions do not specify whether the transverse loading, P_t, represents a pressure range or a pressure amplitude.

The Ontario Highway Bridge Design Code, Third Edition [35] also contains provisions for the design of support structures for vortex shedding. The provisions require that a structure be designed based upon the results of a dynamic modal analysis to solve for the amplitude of the steady-state response due to an applied force per unit length in the transverse direction, $F_s(x,t)$, defined as:

$$F_s(x,t) = \frac{1}{2}\rho V_{cr}^2 C_s D \sin[2\pi n_e t] \qquad (2.25)$$

where ρ is the density of air, V_{cr} is the critical wind velocity computed from the Strouhal relation (Equation 2.19), C_s is the transverse force coefficient, D is the across-wind dimension of the structural element, n_e is the natural frequency of the structure, x is the coordinate describing the

length or height along the structure, and t is time. For circular elements subjected to flow in the subcritical flow regime, the transverse force coefficient C_s is specified as 0.71. Furthermore, the loading is an amplitude applied to the structure in accordance with mode shape being considered in the analysis and is assumed to act in phase along the entire length of the element.

The design of tapered elements is accounted for in the Ontario Code [35] in a manner similar to that described above. As was previously discussed, however, vortex shedding lock-in in a tapered structural element is a condition of localized resonance in which the vortex shedding forces remain correlated over a limited length of the element at each discrete increment in critical wind velocity. The Ontario Code specifies that, in a tapered element, the across-wind load, $F_s(x,t)$, be assumed to act over a length equal to ±10 percent of the diameter D(x) at which the critical wind velocity is calculated. The length of the structural element over which the transverse load is applied represents a conservative estimate of the length over which the vortex shedding forces remain perfectly correlated. As a result, the design of structures with tapered elements requires a series of modal analyses in which the transverse load is incrementally moved along the tapered member to solve for the maximum amplitude of the steady-state response of the structure. At each increment, the load is assumed to act in the direction of the natural mode of vibration at the location being considered.

For the design of simple cantilever poles for vortex shedding, the Ontario Code [35] permits the use of a simplified analysis using an equivalent static load per unit length, F_s, applied transverse to the direction of the free-stream wind velocity to estimate the amplitude of the steady-state, dynamic response:

$$F_s = \frac{0.3}{\xi} C_s D V_{cr}^2 \qquad (2.26)$$

where ξ is the damping ratio (assumed to equal 0.0075 for steel and aluminum poles), C_s is the transverse force coefficient, D is the across-wind dimension of the element, and V_{cr} is the critical wind velocity computed in accordance with the Strouhal relation (Equation 2.19).

Comparison of the AASHTO Specifications [4] and Ontario Code [35] indicates that the provisions for the design of simple cantilevered poles are approximately equivalent. Consider, for example, a simple prismatic cantilever pole with a diameter equal to 305 mm and a natural frequency equal to 5 Hz. Using the Strouhal relation (with a Strouhal number equal to 0.18, which is specified in each of the design codes), the critical wind velocity, V_{cr}, for lock-in is equal to 8.5 m/s (30.6 km/hr).

Based upon the AASHTO Specifications, the equivalent static transverse pressure would be given by: (assuming a drag force coefficient equal to 1.10 and a height coefficient equal to 1.00):

$$\frac{P}{2\beta} = \frac{0.0473 V_{cr}^2 C_d C_h}{2\beta} = \frac{(0.0473)(30.6 km/hr)^2 (1.10)(1.00)}{2(0.005)}$$

$$= 4870\ Pa \qquad (2.27)$$

The equivalent transverse force per unit length, F_t, would therefore be given by:

$$F_t = \frac{P}{2\beta}(D) = (4870Pa)(0.305m)$$

$$= 1490\ \frac{N}{m} \tag{2.28}$$

Based upon the provisions of the Ontario Code, the amplitude of the equivalent static transverse load per unit length is given by:

$$F_s = \frac{0.3}{\xi} C_s D V_{cr}^2 = \frac{0.3}{0.0075}(0.71)(0.305m)(8.5m/s)^2$$

$$= 630\ \frac{N}{m} \tag{2.29}$$

Thus, the AASHTO Specifications [4] and the Ontario Code [35] specify approximately the same equivalent static transverse load per unit length (assuming the equivalent static pressure specified in the AASHTO Specifications is a pressure range and not a pressure amplitude) for the design of a simple cantilever poles for vortex-induced vibrations.

Geometry	Flow Regime	Strouhal Number
Circular Cylinder	Subcritical	0.18
	Critical	NA
	Supercritical	0.25
Sign	NA	0.14
Signal	NA	0.13 - 0.28

NA = not applicable

Table 2.1 - Strouhal Number for Circular Supports, Sign Attachments, and Signal Attachments.

Configuration	Vortex Shedding Frequency (Hz) for Wind of	
	4.5 m/s	9.0 m/s
Octagonal Cylinder	3.8	7.7
Circular Cylinder	4.5	8.9
Signal with Backplate	1.3	2.7

Table 2.2 - Summary of Water Table Test Results Obtained by McDonald et al. [32].

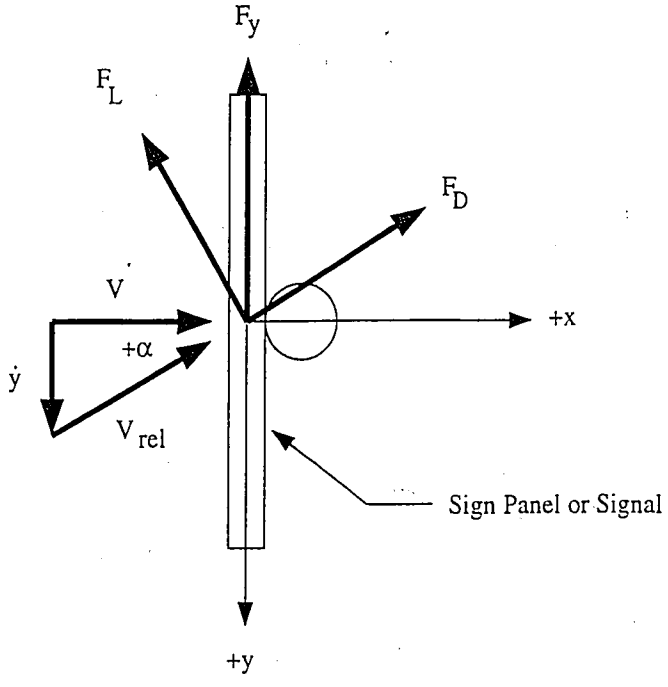

Figure 2.1 - Schematic of the Galloping Phenomenon.

Figure 2.2 - Schematic of a von Karman Vortex Street in the Wake of a Circular Cylinder.

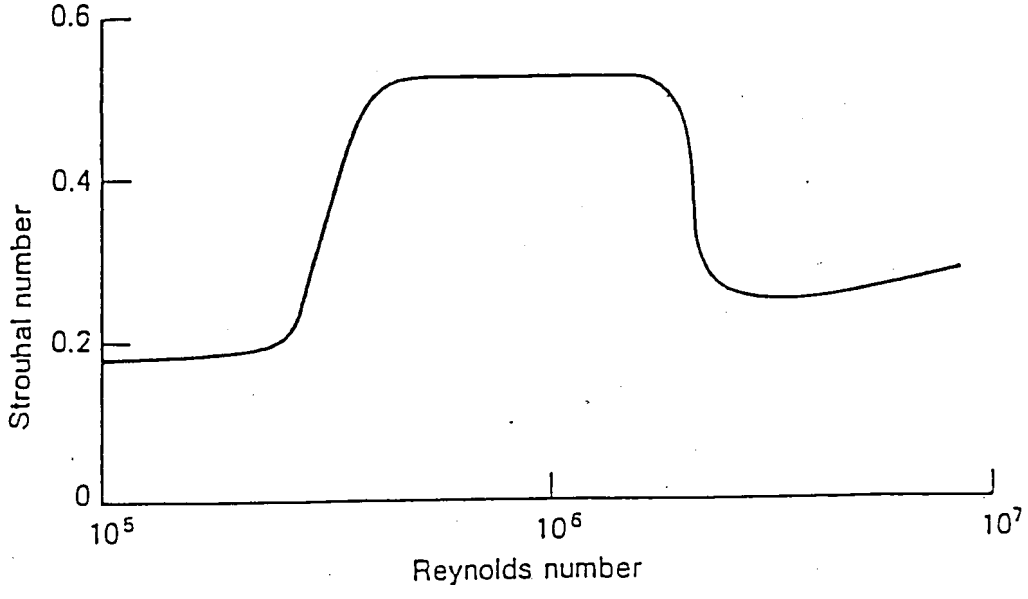

Figure 2.3 - Relationship Between Strouhal Number and Reynolds Number for a Circular Cylinder.

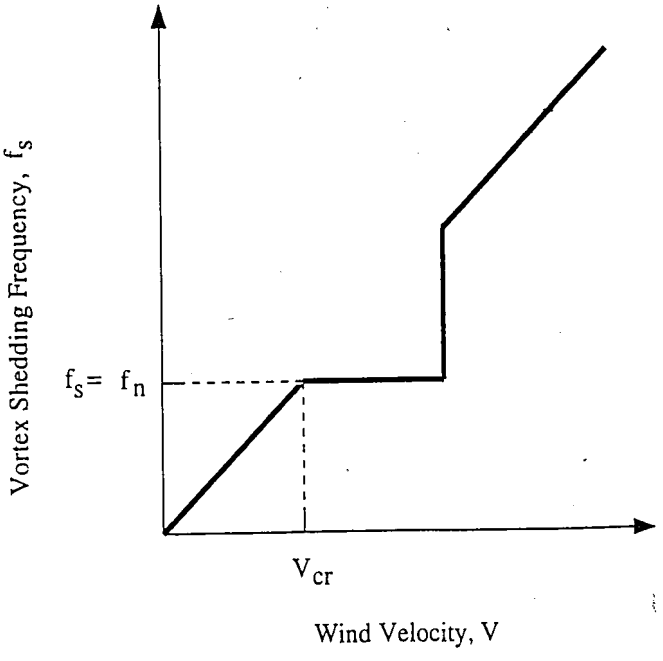

Figure 2.4 - Schematic of Vortex Shedding Lock-In.

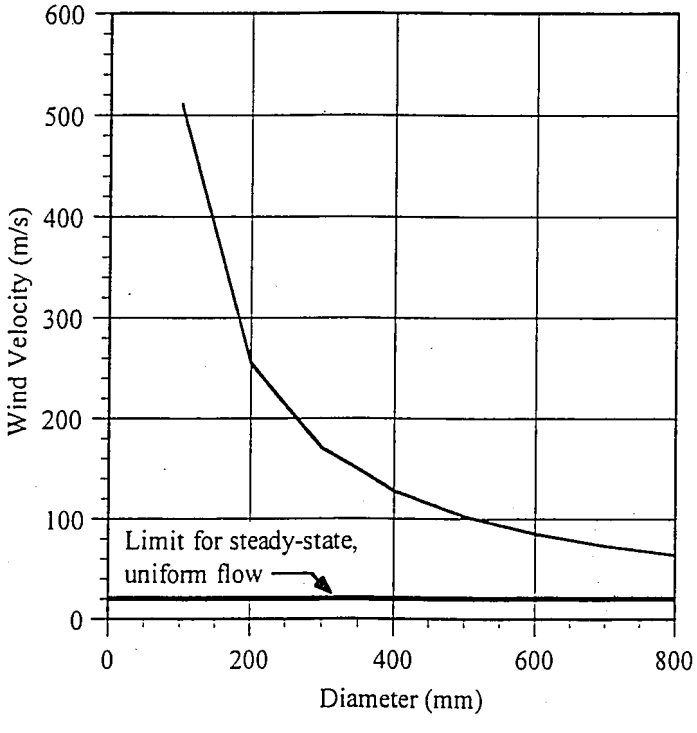

Figure 2.5 - Wind Velocities Required to Enter Supercritical Flow Regime for Flow Around a Circular Support.

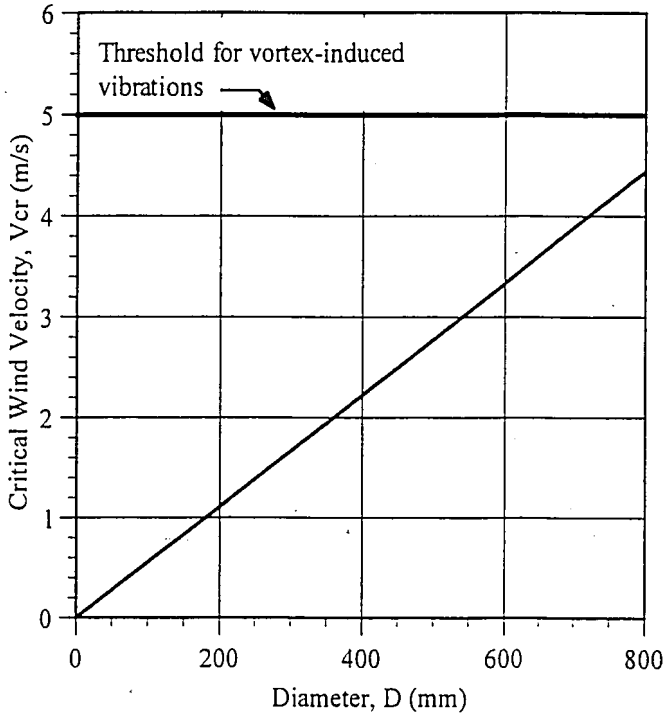

Figure 2.6 - Critical Wind Velocities Required For Vortex Shedding Lock-In For Circular Supports.

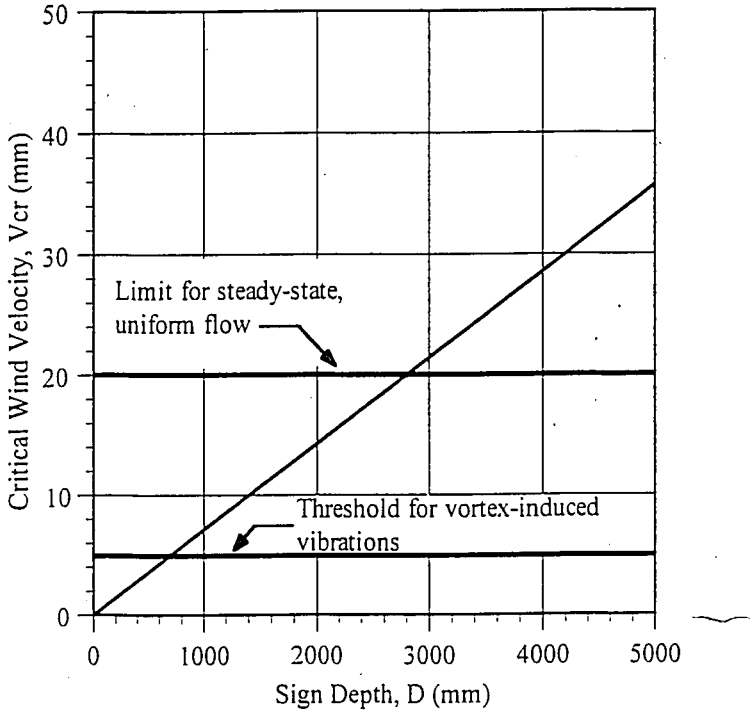

Figure 2.7 - Critical Wind Velocities Required For Vortex Shedding Lock-In For Sign Attachments.

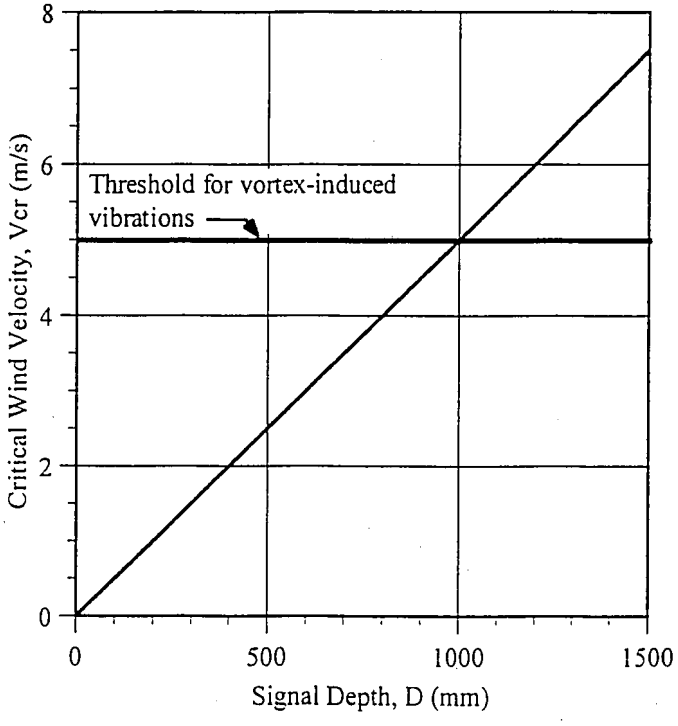

Figure 2.8 - Critical Wind Velocities Required For Vortex Shedding Lock-In For Signal Attachments.

Chapter Three

WIND TUNNEL TESTS

3.1 INTRODUCTION

This Chapter summarizes the results of wind tunnel tests which were performed to evaluate galloping on scale-models of cantilevered support structures. The wind tunnel tests were conducted in two phases. The first phase consisted of a series of aerodynamic tests (i.e. not including the effects of structural interaction) to determine the relative susceptibility of various cantilevered support structure attachments (i.e. signs and signals) to the galloping phenomenon. The susceptibility for galloping was evaluated by applying the Den Hartog stability criterion to the measured aerodynamic lift and drag forces exerted on each of the test specimens under steady-state flow conditions. The second phase consisted of a series of aeroelastic tests (i.e. including the effects of structural interaction) to study the dynamic behavior of cantilevered sign and signal support structures subjected to galloping- and vortex-induced vibrations. These tests were simulated using dynamic finite-element analyses (described in Chapter Four) to estimate the magnitude of the dynamic loads to which the wind tunnel models were subjected during galloping- and vortex-induced vibrations. This was accomplished by correlating the results of the finite-element analyses to the magnitudes of the base moments measured during the wind tunnel tests.

The wind tunnel tests were conducted at the Wright Brothers Memorial Wind Tunnel at the Massachusetts Institute of Technology (MIT). The wind tunnel at the MIT facility is a closed, single return test system capable of wind velocities up to 76 m/s. The elliptical test area measures 2290 mm high x 3050 mm wide x 4570 mm long.

As is the case with most wind tunnel tests, the limited size of the test area at the MIT facility required that testing be conducted on scale models. Selection of a model scale was based primarily upon the level of wind tunnel blockage below which two-dimensional flow conditions could be maintained (i.e. three percent blockage). For the prototype dimensions of the cantilevered support structures considered in the aeroelastic test program, a three percent blockage required that the aeroelastic model specimens be fabricated to one-eighth scale. In order to maintain consistency between the aeroelastic and aerodynamic test programs, the aerodynamic test models were also fabricated to one-eighth scale. However, as will be discussed in Section 3.2, tests on one of the aerodynamic test specimens were duplicated using a specimen fabricated to one-half scale in order to investigate possible scale effects. Tests on the one-half scale aerodynamic specimen verified that scale effects were not excessive, and therefore the one-eighth scale aerodynamic and aeroelastic test results are expected to be representative of the behavior exhibited by full-scale cantilevered support structures.

This Chapter is organized into two basic sections. Section 3.2 summarizes the specimen details, experimental procedures, and results related to the aerodynamic test program while Section 3.3 summarizes the specimen details, experimental procedures, and results related to the aeroelastic test program. The reader is referred to Reference 13 for additional details of the wind tunnel test program.

3.2 AERODYNAMIC TEST PROGRAM

3.2.1 Objectives

As was discussed in Chapter Two, a structure is potentially susceptible to galloping-induced oscillations when a periodically varying angle of attack of the wind flow produces aerodynamic forces which are aligned with the across-wind motion of the structure. The

alignment of these forces with the across-wind motion of the structure generates negative aerodynamic damping. If the total damping possessed by the structure (mechanical damping plus aerodynamic damping) is less than zero, the structure becomes unstable and large-amplitude, across-wind galloping oscillations occur. Thus, one of the primary factors (besides the level of mechanical damping) which drives the galloping phenomenon is the aerodynamic characteristics of the structure (i.e. the relation between the aerodynamic lift and drag forces under varying angles of attack of the wind flow). These aerodynamic forces can be measured in the wind tunnel under static conditions to evaluate the potential susceptibility for galloping-induced oscillations.

For example, recent research conducted by McDonald et al. [32] has established that cantilevered signal support structures possess aerodynamic characteristics which make these structures susceptible to galloping. This research indicates that the galloping-induced vibrations observed in cantilevered signal support structures in the field are generated by the aerodynamic lift and drag forces exerted on the attachments (i.e. signals). The scope of this previous work, however, was limited to horizontally-mounted signal attachments (i.e. signals which are mounted parallel to the horizontal mast arm) and also did not consider the possibility of galloping-induced oscillations in cantilevered sign support structures.

The aerodynamic test program reported herein was conducted to evaluate the aerodynamic characteristics of various cantilevered support structure attachments (which were not considered within the scope of previous research programs) to determine their susceptibility to the galloping phenomenon. Specifically, tests were conducted on two types of attachments: (1) a vertically-mounted signal (i.e. mounted perpendicular to the horizontal mast-arm) configured with and without a backplate, and (2) a sign. The primary objective of these tests was to qualitatively evaluate the relative susceptibility of each of the attachments to the galloping phenomenon with respect to attachment geometry and flow direction.

3.2.2 Specimen Details and Test Matrix

The signal test specimens were fabricated to both one-eighth and one-half scales in order to investigate the effects of model scale. Details of the one-eighth and one-half scale signal specimens are provided in Figures 3.1 and 3.2, respectively. As is indicated in each of these figures, the signal specimens were fabricated with a removable backplate so that the effects of this geometrical variation on the susceptibility to galloping could be evaluated. For reference purposes, the dimensions of the prototype signal from which each of the test specimens was scaled are shown in boldface in each of the figures. The dimensions of the prototype signal are typical for a signal with a 305 mm lens diameter.

Two one-eighth scale sign attachments were also included in the aerodynamic test program. The aspect ratio between each of the specimens was varied by a factor of two in order to evaluate the effect of this parameter on susceptibility to galloping. Details of the two sign attachments are summarized in Figures 3.3 and 3.4, respectively. Again, the dimensions of the prototype signs from which each of the model specimens was scaled are shown in boldface in each of the figures.

The aerodynamic test matrix is shown in Table 3.1. The matrix is composed of six test series. At least two tests were conducted within each of the test series to determine the aerodynamic force coefficients for flows from the front and rear of each specimen. For several specimens, additional tests were also performed to establish repeatability of the results.

3.2.3 Aerodynamic Test Set-Up and Experimental Procedure

Schematics of the aerodynamic test set-up are provided in Figures 3.5(a) and 3.5(b). As is indicated, each of the test specimens was mounted to a steel cylinder which extended vertically from the floor of the wind tunnel. The set-up was oriented so as to simulate the flow conditions

to which an attachment detail would be subjected when mounted to the horizontal mast-arm of a cantilevered support structure. The vertical cylinder was attached to a mounting flange which in turn was bolted to a mechanical pyramidal balance located just below the floor of the wind tunnel. The balance was used to measure the aerodynamic drag and lift forces exerted on each of the specimens during testing. As is indicated in Figure 3.5(c), the orientations of the aerodynamic lift and drag forces measured by the mechanical balance were fixed with respect to a global coordinate system defined by the direction of the wind tunnel flow. The aerodynamic drag forces measured by the mechanical balance were oriented in a horizontal plane parallel to the direction of the wind tunnel flow while the aerodynamic lift forces were oriented in a horizontal plane perpendicular to the wind tunnel flow. The mounting flange could be rotated ±10 degrees to provide a twenty degree variation in the angle of attack of the wind tunnel flow with respect to the test specimen.

Each of the aerodynamic tests was conducted by subjecting the test specimen to a uniform, steady-state flow and measuring the aerodynamic lift and drag forces as the specimen was rotated in one to two degree increments through a range of twenty degrees. The aerodynamic lift and drag data were then analyzed using the procedure described in Section 3.2.4 to evaluate the susceptibility of each specimen to galloping.

3.2.4 Evaluation of the Aerodynamic Force Measurements

Static angles of attack, as were produced during the aerodynamic tests by rotating the specimens with respect to the wind tunnel flow, simulate the conditions under which signs and signals experience galloping. Figure 3.6 shows the nomenclature and sign convention for the aerodynamic test set-up rotated at an arbitrary angle of attack, α, with respect to the wind tunnel flow, V_{tunnel}. The drag and lift forces measured by the mechanical balance are shown in Figure

3.6 in accordance with the global coordinate system fixed with respect to the wind tunnel flow. As is indicated, the velocity produced by the wind tunnel, V_{tunnel}, simulates the relative velocity, V_{rel}, which was previously discussed in Chapter Two (see Figure 2.1). The vector components of the wind tunnel flow, V_x and V_y, are defined with respect to a local coordinate system that rotates with the attachment. The velocity V_x simulates the free-stream velocity, V, defined in Figure 2.1 while the velocity V_y simulates the velocity to which the attachment would be subjected under across-wind motion $\dot{y}$. The force of interest with respect to evaluating the susceptibility of a signal to galloping, F_y, is oriented in accordance with the local coordinate system defined in Figure 3.6.

The standard aeronautical sign convention is used to define the angle of attack, α. In a flow from left to right, clockwise rotations of the attachment (as is shown in Figure 3.6) result in positive angles of attack. Similarly, in a flow from left to right, counter-clockwise rotations of the attachment result in negative angles of attack. Thus, positive angles of attack (as is shown in Figure 3.6) produce a velocity V_y oriented in the negative y-direction while negative angles of attack produce a velocity V_y oriented in the positive y-direction.

For each of the aerodynamic tests, the aerodynamic forces measured by the mechanical balance were converted to force coefficients using the following relationships:

$$C_L = \frac{F_L}{\frac{1}{2}\rho V_{tunnel}^2 A} \tag{3.1}$$

$$C_D = \frac{F_D}{\frac{1}{2}\rho V_{tunnel}^2 A} \tag{3.2}$$

$$C_{D_{pole}} = \frac{F_{D_{pole}}}{\frac{1}{2}\rho V_{tunnel}^2 A_{pole}} \tag{3.3}$$

where C_L is the lift force coefficient corresponding to the aerodynamic lift force, F_L, acting on the test specimen; C_D is the drag force coefficient corresponding to the aerodynamic drag force, F_D, acting on the test specimen; C_{Dpole} is the drag force coefficient corresponding to the aerodynamic drag force, F_{Dpole} acting on the vertical cylinder to which the test specimen was mounted (measured prior to mounting the specimen); ρ is the density of air; A is the projected area of the attachment; and A_{pole} is the projected area of the vertical cylinder to which the attachment was mounted.

The relative flow velocity, V_x, is related to the wind tunnel flow velocity, V_{tunnel}, by the following:

$$V_x = V_{tunnel}\cos\alpha \tag{3.4}$$

Furthermore, it is known that the lift force normal to the relative velocity, F_y, is related to the lift and drag forces by the following:

$$F_y = -[F_L\cos\alpha + F_D\sin\alpha] \tag{3.5}$$

From Equations 3.1 through 3.5, the lift force coefficient, C_{Fy}, corresponding to the aerodynamic force normal to the free-stream flow velocity, V_x, was computed using:

$$C_{Fy} = -[C_L + (C_D - C_{Dpole})\tan\alpha]\sec\alpha \tag{3.6}$$

Note that the aerodynamic drag force acting on the vertical cylinder to which the test specimens were mounted was not included in the calculation of the lift force coefficient, C_{Fy}. The susceptibility of an attachment to galloping is based solely on the aerodynamic forces which act

on the attachment, including the effects of forces which are generated by the presence of the support (i.e. interference forces which result from flow interactions between the attachment and the cylinder). Since the aerodynamic drag force acting on the pole was measured prior to the mounting of the test specimen, the calculation of the lift force coefficient (Equation 3.6) included the effect of interference forces but did not include the effect of forces acting only on the vertical cylinder.

The susceptibility of each of the attachments to the galloping phenomenon was then evaluated in accordance with the Den Hartog stability criterion [15], i.e. the attachment is potentially susceptible to galloping if:

$$\frac{dC_{Fy}}{d\alpha} > 0 \qquad (3.7)$$

3.2.5 Aerodynamic Test Results

The aerodynamic test results for the one-half scale signal attachment configured without a backplate (Test Series III) are shown in Figures 3.7(a) and 3.7(b) for flows from the front and the rear, respectively. The results are plotted in terms of the lift force coefficient, C_{Fy}, versus angle of attack, α. As is shown in Figure 3.7(a), the slope of the lift force coefficient for flow from the front of the signal is negative in the vicinity of α equal to zero, indicating that the aerodynamic force, F_y, acting on the signal is oriented opposite to the direction of across-wind motion. As a result, the attachment is not susceptible to galloping from the equilibrium position when mounted to the horizontal mast-arm in a plane normal to the horizon (i.e. perpendicular to the roadway).

However, in the region of $-10 < \alpha < -3$, the slope of the lift force coefficient is positive, indicating that the signal could be susceptible to galloping-induced oscillations if mounted to the

horizontal mast-arm of a cantilevered support structure at angles in this range (such as might occur to improve the visibility of the signal from the roadway). Thus, for flow from the front, the signal attachment configured without a backplate will not be susceptible to galloping-induced vibrations unless it is mounted at an angle to improve the visibility of the signal from the roadway.

Figure 3.7(b) depicts the lift force coefficient computed for flow from the rear of the signal configured without a backplate. As is shown, the slope of the lift force coefficient is positive in the vicinity of α equal to zero, indicating that the signal is potentially susceptible to galloping-induced vibrations from the equilibrium position when subjected to flow from the rear.

The aerodynamic test results for the one-half scale signal attachment configured with a backplate (Test Series IV) are depicted in Figures 3.8(a) and 3.8(b) for flow from the front and the rear, respectively. As is shown in Figures 3.8(a) and (b), the slope of the lift force coefficient for flows from both the front and rear of the signal is positive in the vicinity of α equal to zero, indicating a potential susceptibility for galloping-induced oscillations from the equilibrium position regardless of the direction of flow. In addition, note the relative magnitudes of the slopes of the lift force coefficient between the two flow conditions. In the vicinity of α equal to zero, the slope of the lift force coefficient is greater (i.e. more positive) for flow from the rear, indicating a stronger potential for galloping when the signal is subjected to flow from this direction.

The effect of configuring a signal with a backplate can be evaluated by comparing Figures 3.7 and 3.8. As is shown in Figures 3.7(a) and 3.8(a), the addition of a backplate to a signal creates conditions which are favorable for galloping from the equilibrium position when the signal is subjected to flow from the front, i.e. the slope of the lift force coefficient becomes positive in the vicinity of α equal to zero with the addition of a backplate to the signal. Similarly, for flow from the rear (as is shown in Figures 3.7(b) and 3.8(b)), the addition of a backplate increases the signal's potential for galloping from the equilibrium position, i.e. the slope of the lift force

coefficient is greater (i.e. more positive) in the vicinity of α equal to zero for the signal configured with a backplate.

The results of tests on the one-eighth scale signal specimens were generally consistent with the results shown in Figures 3.7 and 3.8. Although not specifically shown, the results indicate that the scale effects were not significant. Thus, the wind tunnel tests can be considered reasonable representations of the characteristics possessed by full-scale cantilevered support structures in the field. The reader is referred to Reference 13 for additional information regarding the evaluation of the test data for scale effects.

The aerodynamic test results for the one-eighth scale "full-size" sign attachment (Test Series V) are depicted in Figures 3.9(a) and 3.9(b) for flow from the front and rear, respectively. As is shown in Figures 3.9(a) and 3.9(b), the slope of the lift coefficient is slightly positive or near zero for the angles of attack considered. Based on the strong susceptibility of the sign support structure to gallop during the aeroelastic tests (as will be discussed in Section 3.3.4), the slope of the lift coefficient in these aerodynamic tests would be expected to be more positive than was observed. The aerodynamic data obtained from tests on the "half-sized" specimen (Test Series VI) were consistent with the data shown in Figure 3.9. As a result, aspect ratio does not appear to influence the susceptibility of sign attachments to galloping-induced oscillations.

3.2.6 Summary

The results of the aerodynamic test program indicate that cantilevered sign and signal support structures are potentially susceptible to large-amplitude, across-wind vibrations resulting from the galloping phenomenon. Specifically, this susceptibility arises from the aerodynamic characteristics possessed by the attachments (i.e. signs and signals) to these structures, which is

in agreement with the results of previous research programs [32]. Furthermore, the results of the aerodynamic research program indicate that:

- signal attachments, configured with or without a backplate, are more susceptible to galloping when subjected to flow from the rear,

- signal attachments are more susceptible to galloping when configured with a backplate,

- the susceptibility of sign attachments to the galloping phenomenon is independent of aspect ratio and flow direction.

The results of the aerodynamic test program are also in agreement with the conditions under which galloping-induced oscillations have been observed in cantilevered support structures in the field. For example, a majority of cantilevered signal support structures have been observed to vibrate when the signals are configured with a backplate and the direction of flow is from the rear. Inspection of the lift coefficient data obtained from the aerodynamic tests indicates that signal attachments are most susceptible to galloping under these conditions, i.e. the slope of the lift coefficient with respect to angle of attack was greatest (most positive) for tests in which the signals were configured with a backplate and flow was from the rear. This observation serves to provide a level of confidence that the wind tunnel tests reasonably simulate the aerodynamic characteristics and dynamic behavior of full-scale support structures in the field.

3.3 AEROELASTIC TEST PROGRAM

3.3.1 Objectives

The results of the aerodynamic test program indicate that cantilevered support structure attachments (i.e. signs and signals) possess aerodynamic characteristics which are potentially favorable for the occurrence of galloping. The aerodynamic tests, however, provided no information concerning the dynamic behavior of cantilevered support structures subjected to galloping- and vortex-induced vibrations. Therefore, aeroelastic tests were performed to evaluate the magnitude of the support structure forces (in terms of moments at the base of the vertical supports of the test specimens) to which cantilevered support structures are subjected during occurrences of galloping- and vortex-induced vibrations (the magnitudes of the across-wind loads could not be directly measured). Dynamic finite-element analyses (described in Chapter Four) were then used to estimate the amplitude of the loads on the attachments which corresponded to the measured base moment amplitudes.

3.3.2 Specimen Details and Test Matrix

A total of five cantilevered-support-structure configurations (two signal supports and three sign supports) were included in the aeroelastic test program. Details of each of the specimens are summarized in Figures 3.10 to 3.14. The specimens are identified as Specimens A through E, with the prototype dimensions from which each of the models were fabricated shown in boldface. Each of the prototype structures were fabricated from steel. The material from which each of the model specimens were fabricated (steel or aluminum) is shown in the upper-left corner of each figure. As was discussed previously, all of the model specimens were fabricated to one-eighth scale.

Details of the two cantilevered signal support structures are shown in Figures 3.10 and 3.11. Specimen A, shown in Figure 3.10, was a one-eighth scale model of a signal support structure known to have experienced galloping-induced vibrations. The prototype structure from which the model was scaled was observed to experience vertical-plane, galloping-induced vibrations in the field when flow was from the rear with velocities in the range of 16 m/s. Under these flow velocities, the displacement amplitudes at the tip of the horizontal mast-arm, estimated from a videotape of the vibrating structure, were approximately 305 mm to 610 mm. As is shown in Figure 3.10, the prototype structure was composed of uniformly tapered structural elements. Due to difficulties encountered in fabrication, the model specimen was fabricated using non-uniformly tapered structural elements which approximately simulated the mass and stiffness of the prototype structure.

Specimen B, shown in Figure 3.11, was a one-eighth scale model of a signal support structure that was tested to evaluate the effects of slight variations in structural stiffness on the dynamic response to galloping and/or vortex shedding. As is shown, Specimen B was identical to Specimen A with the exception of the horizontal support being prismatic.

Details of the three cantilevered sign support structures are shown in Figures 3.12 through 3.14. Each of the model sign support structures were fabricated from aluminum (in order to facilitate fabrication of the specimens) and sized such that the mass and stiffness properties adequately simulated the properties of the prototype structures. Specimen C, shown in Figure 3.12, was a one-eighth scale model of a single-arm sign support structure composed of prismatic vertical and horizontal supports. Specimen D, shown in Figure 3.13, was a one-eighth scale model of a sign support structure with a prismatic vertical support and a two-chord truss horizontal support. Specimen E, shown in Figure 3.14, was identical to Specimen D with the exception of the vertical support being replaced with a vertical support of reduced stiffness.

As is indicated in Figures 3.10 through 3.14, each of the specimens were configured with a variety of attachment details. Specimens A and B were tested with signal attachments configured with and without backplates (details of each of these attachments are shown in Figure 3.15). Specimen C was tested with two sign attachments as shown in Figures 3.16 and 3.17. Specimen D was tested with the sign attachment shown in Figure 3.16 and Specimen E was tested with the two sign attachments shown in Figures 3.16 and 3.18. As is evident from each of these figures, the geometric dimensions of the attachment details included in the aeroelastic test program were identical to the dimensions of the attachment details included in the aerodynamic test program. The weights of each of the attachments are shown in the upper left corner of each figure. In addition, each of the specimens were also tested with no attachments.

The test matrix for the aeroelastic test program is shown in Table 3.2. Each of the specimens was tested under two basic conditions: (1) configured with attachments, and (2) configured without attachments. Tests in which the specimens were configured with attachments were performed with flows from both the front and the rear.

3.3.3 Aeroelastic Test Set-Up and Experimental Procedure

A schematic of the aeroelastic test set-up is provided in Figure 3.19. As is indicated, the specimens were mounted in the wind tunnel such that the flow was normal to the plane of the structure. The vertical support of each of the test specimens was mounted to a dynamic balance which was used to measure the moments to which each of the specimens were subjected during testing. The dynamic balance was instrumented with two pairs of strain gages located on orthogonal planes. These gages permitted the measurement of the drag and lift moments shown schematically in Figure 3.19.

The dynamic properties (i.e. natural frequency and damping) of each of the models was determined by hanging a mass from the end of the horizontal support. The string used to support the mass was cut and the resulting dynamic response recorded by the data acquisition system. The strain output (i.e. strain versus time) was used to estimate the natural frequency corresponding to the first vertical mode of vibration of each model. In addition, the level of damping possessed by the model was calculated using the log decrement method [11]. Each of the models was then subjected to discreet increments of increasing flow velocity. At each increment in velocity, uniform, steady-state flow conditions were maintained and data from each of the strain gages attached to the dynamic balance were recorded by the data acquisition system. The strain data were then processed to determine the lift and drag moment amplitudes.

3.3.4 Aeroelastic Test Results

3.3.4.1 Galloping

Figure 3.20 shows the observed dynamic response of Specimen A configured with signal attachments without backplates (Test Series I-A) under flow from the front. The data is presented in terms of the lift moment amplitude versus flow velocity. The arrows indicate the progression of the test with respect to flow velocity. As is indicated, the specimen did not exhibit significant vertical-plane oscillations when subjected to increasing flow velocities. Similar results were obtained when Specimen A was subjected to flow from the rear.

Figures 3.21(a) and 3.21(b) show the observed lift moment amplitude for Specimen A configured with signal attachments with backplates (Test Series II-A) under flow from the front and the rear, respectively. As is shown in Figure 3.21(a), the specimen exhibited no significant dynamic response in the vertical plane for flow from the front. However, for flow from the rear (Figure 3.21(b)), the specimen exhibited severe oscillations resulting from the galloping

phenomenon. The characteristics of the response observed in this test consisted of significant amplitudes of vibration perpendicular to the direction of flow (i.e. the oscillations were oriented in the vertical plane).

Figures 3.22(a) through 3.22(c) depict time histories of the dynamic response depicted in Figure 3.21(b) at three discrete flow velocities. The data is presented in terms of the root-mean-square (rms) variation in lift moment versus time. Again, note the increase in magnitude of the lift moment with respect to the drag moment for increasing flow velocities, which is characteristic of the galloping phenomenon. At low flow velocities (Figure 3.22(a)), the specimen exhibited no significant dynamic response in the vertical plane. As the flow velocity was increased, as depicted in Figures 3.22(b) and 3.22(c), the galloping instability became apparent as the range in lift moment increased in much greater proportion than the range in drag moment. At the peak flow velocity (Figure 3.22(c)), the response of the structure was oriented primarily in the vertical plane.

Several interesting characteristics can be observed with regards to the dynamic response depicted in Figure 3.21(b). First, note the persistent nature of the galloping phenomenon as the flow velocity was decreased from a peak of 18.2 m/s. Significant vertical plane oscillations continued even with decreases in the flow velocity. This type of behavior has been observed in various other types of structures which are susceptible to galloping-induced vibrations (e.g. transmission lines) [25] and suggests that once galloping-induced oscillations are initiated in a structure, damaging stress cycles may continue to occur even with reductions in the flow velocity. Second, note the reduction in the relative magnitude of the lift moment amplitude as the flow velocity was increased a second time. This is evidence of the inherent variability in the dynamic response of a structure to the galloping phenomenon and indicates the highly specific conditions which must be present in order for significant across-wind vibrations to occur. As further evidence of the dependence of galloping to specific flow conditions, the galloping response of

Specimen A shown in Figure 3.21(b) occurred only once during the aeroelastic test program. Repeated testing of Specimen A under identical flow conditions failed to reproduce the results shown in Figure 3.21(b).

Tests conducted on Specimen B (Test Series I-B and II-B) did not exhibit a significant vertical plane response when configured with either attachment TS-1D or TS-2D and subjected to flow from either the front or the rear. In general, the dynamic response of Specimen B under each of the conditions considered were similar to that shown in Figure 3.20. The lack of response in the across-wind direction could have possibly been due to the lack of very specific conditions which must be present for galloping to occur. Therefore, it cannot be concluded with certainty that the increased stiffness of the horizontal support prevented galloping-induced oscillations in this specimen.

Figures 3.23(a) and 3.23(b) illustrate the observed dynamic response of Specimen C for Test Series I-C under flow from the front and the rear, respectively. Each of the tests were conducted with the specimen configured with attachment RS-1D. As is indicated in Figure 3.23(a), the specimen exhibited a significant vertical-plane response due to galloping when subjected to flow from the front. A comparison of the characteristics of the response with those shown in Figure 3.21(b) indicate several similarities, the most notable of which are: (1) the increase in response with increasing flow velocity and (2) the persistent nature of the galloping oscillations as the flow velocity was decreased. As is shown in Figure 3.23(b), the specimen did not exhibit a significant vertical plane-response due to the galloping phenomenon when subjected to flow from the rear.

Figure 3.24(a) and 3.24(b) depict the observed dynamic response of Specimen C for Test Series II-C under flow from the front and rear, respectively. Each of the tests was conducted with the specimen configured with attachment RS-3D. Note that the projected area of attachment RS-

3D was one-half the projected area of specimen RS-1D. Again, for flow from the front, the specimen exhibited significant vertical-plane oscillations due to the galloping phenomenon. In addition, a comparison of Figures 3.23(a) and 3.24(a) indicates that, at the flow velocity corresponding to the peak vertical-plane response, the magnitude of the lift moment for attachment RS-3D was approximately one-half the magnitude of the lift moment for attachment RS-1D. This observation suggests that the forces to which a cantilevered support structure is subjected during occurrences of galloping are directly proportional to the projected area of the attachment detail. As is shown in Figure 3.24(b), Specimen C did not exhibit significant vertical-plane response when configured with attachment RS-3D and subjected to flow from the rear.

Figure 3.25 depicts the observed dynamic response of Specimen D for Test Series I-D under flow from the front. As is indicated, Specimen D did not exhibit significant vertical plane oscillations for flow from the front of the specimen. Similar results were obtained for flow from the rear. The observed dynamic response of Specimen E was similar to that of Specimen D for all of the flow conditions and attachment configurations considered (i.e. Test Series I-E and II-E). Reductions in the column stiffness (i.e. Test Series I-E) and sign mass (i.e. Test Series II-E) did not increase the susceptibility of Specimen E to galloping-induced vibrations. However, because of the sensitivity to specific conditions, it cannot be concluded that the truss structure is less susceptible to galloping than the single-arm cantilevered sign structure (i.e. Specimen C). In fact, failures of truss structures in the field have been attributed to vertical-plane vibrations which are consistent with the occurrence of galloping [22].

3.3.4.2 Vortex Shedding

Table 3.3 summarizes the predicted critical wind velocities at which each of the test specimens was expected to exhibit vortex-induced vibrations due to the shedding of vortices from

the attachments. The table consists of seven columns of data. The first two columns summarize the test specimen and attachment detail, respectively. The third column indicates the average natural frequency of the test specimen as determined from vertical-plane, free-vibration tests. The fourth column indicates the depth of the attachment. The fifth column indicates the value of the Strouhal number used to predict the critical flow velocity at which lock-in was expected. Finally, the sixth and seventh columns summarize the values of the predicted and observed critical wind velocities for each specimen. Predicted values of the critical wind velocity, V_{cr}, were calculated using the Strouhal relation:

$$V_{cr} = \frac{f_n D}{S} \tag{3.8}$$

where f_n is the average measured natural frequency corresponding to the first vertical-plane mode of vibration, D is the depth of the attachment, and S is the Strouhal number.

As is indicated in Table 3.3, none of the test specimens exhibited vortex-induced vibrations when configured with either sign or signal attachments. Inspection of the data presented in Table 3.3 indicates that the magnitudes of the predicted critical wind velocities for which lock-in of the signal support specimens (i.e. Specimens A and B) would be expected were near or below the threshold wind velocity (i.e. 5 m/s) below which the vortex shedding force is considered insufficient to excite significant amplitudes of vibration [29]. In addition, the results of research conducted by McDonald et al. [32] suggest that the three-dimensional characteristics of signal attachments disrupt the formation of coherent vortices at one-well defined frequency. As a result, vortex-induced vibration of the signal support specimens due to the shedding of vortices from the attachments would not be expected.

Inspection of the data for the cantilevered sign support specimens (i.e. Specimens C, D, and E) shows that the predicted critical wind velocities for each of the specimens is greater than

the threshold velocity of 5 m/s. Vortex-induced vibrations, however, were not observed. One possible explanation for the lack of vortex-induced vibration may be that sign attachments also possess three-dimensional characteristics which interfere with the formation of coherent vortices at one-well defined frequency.

Table 3.4 summarizes the predicted critical wind velocities at which each of the test specimens without attachments was expected to exhibit vortex-induced vibrations due to the shedding of vortices from the horizontal mast-arms. As is indicated in Table 3.4, the tapered and prismatic signal support structures (Specimens A and B) did not experience vortex-induced vibrations. Inspection of the predicted critical wind velocities for which vortex shedding lock-in would be expected in these specimens indicates that the predicted velocities fall below the threshold velocity of 5 m/s necessary for vortex-induced vibrations. As a result, vortex-induced vibrations would not be expected in these specimens.

The prismatic sign support structure (Specimen C) did exhibit a significant vortex-induced response resulting from the shedding of vortices from the horizontal mast-arm. As is indicated in Table 3.4, the predicted velocity is approximately 18 percent less than the velocity at which the peak dynamic response was observed. This result is reasonable considering that lock-in probably began at a wind velocity slightly below the velocity at which peak across-wind response was observed. Figure 3.26 depicts the dynamic response of Specimen C. As is indicated, a sharp peak in the response occurs at the critical wind velocity at which the vortex shedding frequency corresponds to the natural frequency of the specimen (i.e. lock-in). This is in contrast to the characteristic increase in across-wind response with increasing wind velocity associated with galloping (see Figure 3.23(a)). Figure 3.27 depicts a time history of the observed dynamic response at the critical wind velocity. As is indicated, the response is harmonic and dominated by the lift moment.

The contrast in behavior between the signal support specimens (Specimens A and B) and the sign support specimen (Specimen C) can be attributed to the magnitudes of the critical wind velocities at which lock-in was expected for each of these structures. The diameters of the support members for Specimens A and B resulted in critical wind velocities which were significantly less than the wind velocity of 5 m/s which previous researchers indicate as being the minimum wind velocity required to initiate significant amplitudes of wind-induced vibration [29]. The diameter of the support members for Specimen C resulted in a critical wind velocity which was very near the threshold velocity of 5 m/s. Based upon the results of these tests, it appears that the threshold wind velocity proposed by Kolousek [29] represents a reasonable estimate of the minimum wind velocity at which significant amplitudes of vibration can be expected.

3.3.5 Summary

The results of the aeroelastic test program permit several conclusions to be drawn concerning the dynamic response of cantilevered support structures to the galloping and vortex shedding phenomena. With respect to galloping:

- The galloping phenomenon was extremely difficult to reproduce in the wind tunnel experiments, even though the support structure models had extremely low levels of damping. Some models which theoretically should have been strongly susceptible to galloping did not exhibit galloping-induced vibrations. Other models which exhibited galloping-induced vibration on one occasion did not exhibit an identical response in repeated tests. The difficulties encountered in reproducing the galloping phenomenon in many of the test series can be attributed to the very specific conditions (dynamic properties of the structure, aerodynamic properties of the attachment details, and

characteristics of the flow) which must be present in order for galloping-induced oscillations to occur. This sensitivity to very specific conditions is also evident in the observed dynamic responses of cantilevered support structures in the field.

- Cantilevered signal support structures are most susceptible to galloping-induced oscillations when the signal attachments are rigidly mounted on the mast-arm and are configured with backplates. This observation is in agreement with the results of the aerodynamic test program reported in this Chapter, tow tank tests conducted by McDonald et al. [32], and full-scale field tests performed by McDonald et al. [32]. In addition, the results are consistent with the observed dynamic responses of cantilevered signal support structures in the field.

- The results suggest that, once the galloping instability is initiated, the resulting across-wind resonant vibrations persist even with reductions in the flow velocity. This fact is, of course, detrimental to the behavior of the structure with respect to fatigue, i.e. damaging stress cycles may persist in a structure subjected to galloping-induced oscillations even with reductions in the flow velocity.

- The trussed cantilevered sign support structures considered in this test program did not exhibit a susceptibility to galloping-induced vibration.

With respect to vortex shedding:

- Vortex-induced vibrations generated by the shedding of vortices from the attachments to cantilevered sign and signal support structures does not appear critical with respect to the design of these structures for vibration and fatigue.

- The Strouhal relation provides a reasonable estimate of the critical wind velocity at which resonant vortex shedding can be expected.

- Cantilevered support structures are most susceptible to vortex-induced vibrations due to the shedding of vortices from the horizontal supports, i.e. vortex shedding from the column does not appear to be significant.

- Vortex shedding need not be considered in the design of cantilevered support structures for fatigue when the critical wind velocity for lock-in (as computed by the Strouhal relation) falls significantly below 5 m/s. As a result, only those structures with horizontal supports of relatively large diameter are susceptible to vortex-induced vibration (which is in agreement with the conclusions presented in Chapter Two).

- The addition of attachments to the horizontal supports of cantilevered support structures appears to disrupt the spanwise correlation of the vortex shedding forces. As a result, vortex-induced vibrations need only be considered prior to the installation of attachments to the structure.

- Cantilevered support structures composed of tapered structural members do not appear susceptible to vortex-induced vibrations. In general, the dimensions of the tapered elements are such that the critical wind velocities will fall below the threshold wind velocity of 5 m/s necessary for a significant across-wind pressure fluctuation. Furthermore, the vortex shedding forces which develop in a tapered structural member will be correlated over a limited length of the member. As a result, the probability of generating a significant vortex shedding force in a tapered structural member is quite limited.

Test Series	Specimen	Test Number	Flow Direction
I	TS-1S	1	Front
		2	Rear
II	TS-2S	3	Front
		4	Rear
III	TS-3S	5	Front
		6	Rear
IV	TS-4S	7	Front
		8	Rear
V	RS-1S	9	Front
		10	Rear
VI	RS-2S	11	Front
		12	Rear

Table 3.1 - Aerodynamic Test Matrix.

Test Series	Support Structure	Test Number	Attachments	Flow Direction
I-A	A	1	TS-1D	Front
		2	TS-1D	Rear
		3	None	NA
II-A	A	4	TS-2D	Front
		5	TS-2D	Rear
		6	None	NA
I-B	B	7	TS-1D	Front
		8	TS-1D	Rear
		9	None	NA
II-B	B	10	TS-2D	Front
		11	TS-2D	Rear
		12	None	NA

Note: NA = not applicable

Table 3.2(a) - Aeroelastic Test Matrix (Signal Support Specimens).

Test Series	Support Structure	Test Number	Attachments	Flow Direction
I-C	C	13	RS-1D	Front
		14	RS-1D	Rear
		15	None	NA
II-C	C	16	RS-3D	Front
		17	RS-3D	Rear
		18	None	NA
I-D	D	19	RS-1D	Front
		20	RS-1D	Rear
		21	None	NA
I-E	E	22	RS-1D	Front
		23	RS-1D	Rear
II-E	E	24	RS-2D	Front
		25	RS-2D	Rear

Note: NA = not applicable

Table 3.2(b) - Aeroelastic Test Matrix (Sign Support Specimens).

Table 3.3 - Predicted and Observed Critical Wind Velocities for Vortex Shedding Lock-In Resulting From the Shedding of Vortices From the Attachments.

Specimen[1]	Attachments	Average Natural Frequency (Hz)	Depth, D (mm)	Strouhal Number	Predicted V_{cr} (m/s)	Observed V_{cr} (m/s)
A	TS-1D	7	133	0.20	4.7	-[2]
A	TS-2D	7	165	0.20	5.8	-
B	TS-1D	5.5	133	0.20	3.7	-
B	TS-2D	5.5	165	0.20	4.5	-
C	RS-1D	10	230	0.14	16.4	-
C	RS-2D	11	230	0.14	18.1	-
D	RS-1D	13.5	230	0.14	22.2	-
E	RS-1D	11.3	230	0.14	18.6	-
E	RS-3D	12.8	230	0.14	21.0	-

[1]See Figures 3.10 through 3.14 for details of each of the test specimens.
[2]Indicates vortex-induced vibrations were not observed.

Table 3.4 - Predicted and Observed Critical Wind Velocities for Vortex Shedding Lock-In Resulting From the Shedding of Vortices From the Supports.

Specimen[1]	Attachments	Average Natural Frequency (Hz)	Diameter, D (mm)	Strouhal Number	Predicted V_{cr} (m/s)	Observed V_{cr} (m/s)
A	None	8.5	18[2] 8[3]	0.18	0.9 0.4	-[4]
B	None	6.7	16	0.18	0.6	-
C	None	14.1	57	0.18	4.5	5.5

[1]See Figures 3.10 through 3.14 for details of each of the test specimens.
[2]Diameter at base of mast-arm.
[3]Diameter at tip of mast-arm.
[4]Indicates vortex-induced vibrations were not observed.

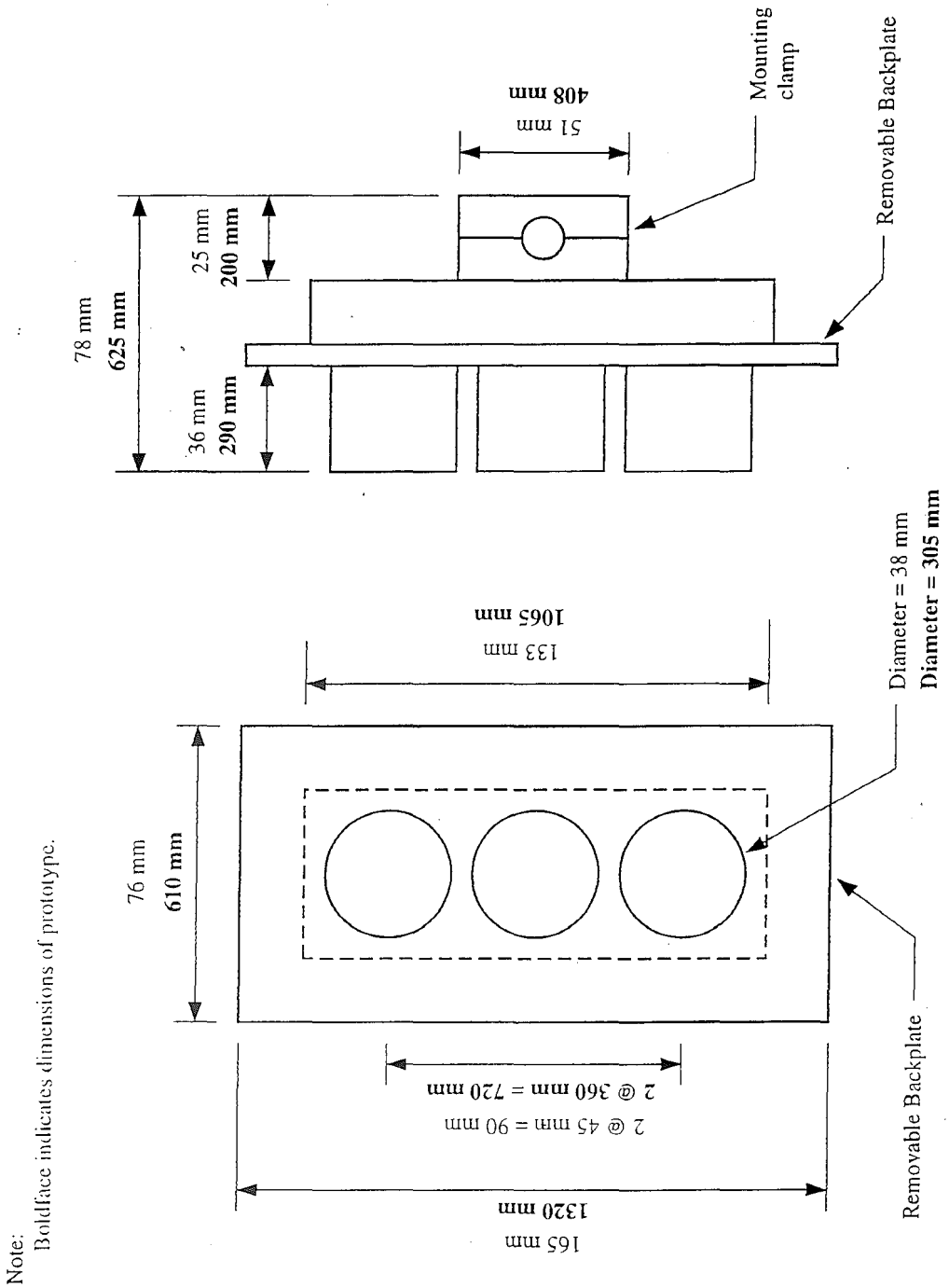

Figure 3.1 - Dimensions of the One-Eighth Scale Signal Attachment Included in the Aerodynamic Test Program. **Specimen TS-1S** Denotes the Signal Attachment Configured Without Backplate. **Specimen TS-2S** Denotes the Signal Attachment Configured With Backplate.

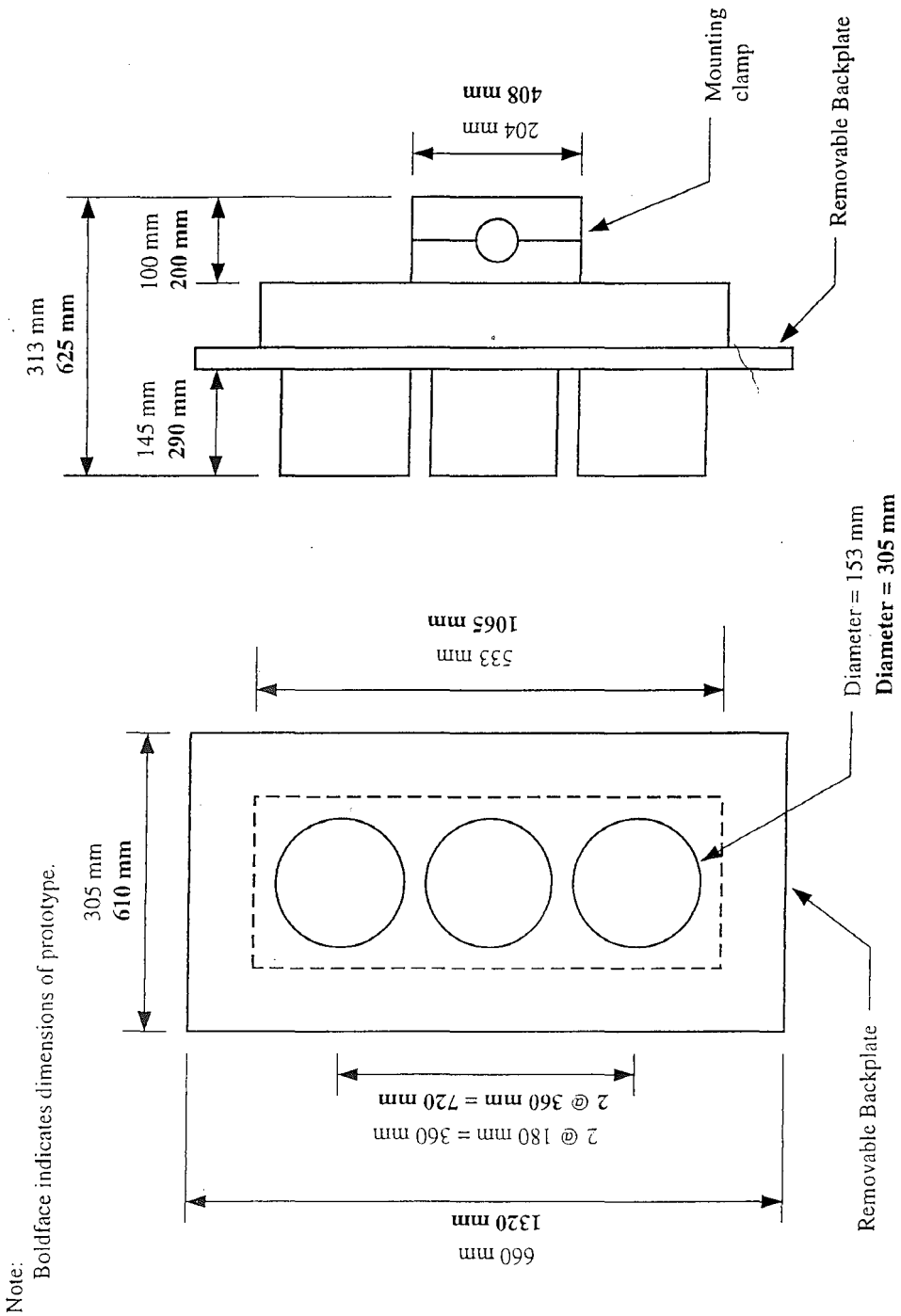

Figure 3.2 - Dimensions of the One-Half Scale Signal Attachment Included in the Aerodynamic Test Program. **Specimen TS-3S** Denotes the Signal Attachment Configured Without Backplate. **Specimen TS-4S** Denotes the Signal Attachment Configured With Backplate.

Note:
Boldface indicates dimensions of prototype.

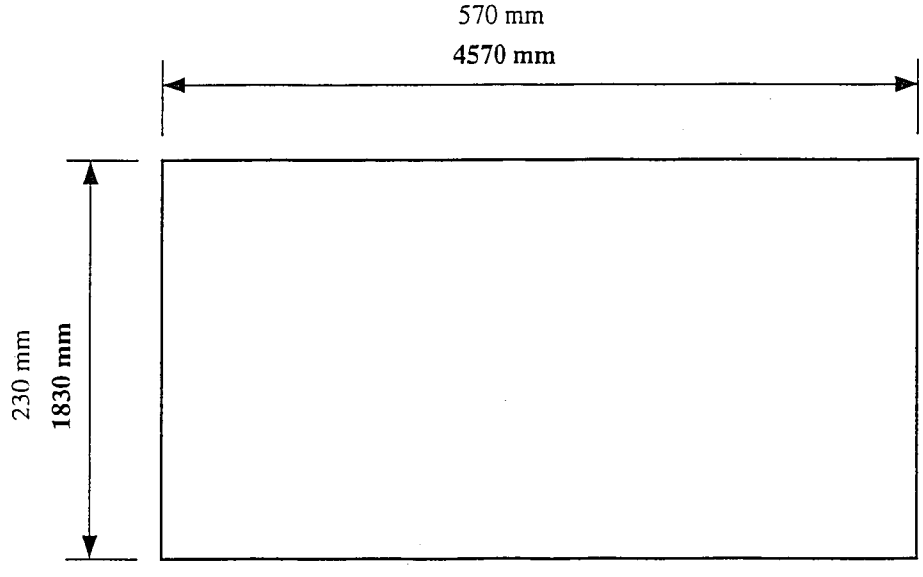

Figure 3.3 - Dimensions of the One-Eighth Scale "Full-Size" Sign Attachment (**Specimen RS-1S**) Included in the Aerodynamic Test Program.

Note:
Boldface indicates dimensions of prototype.

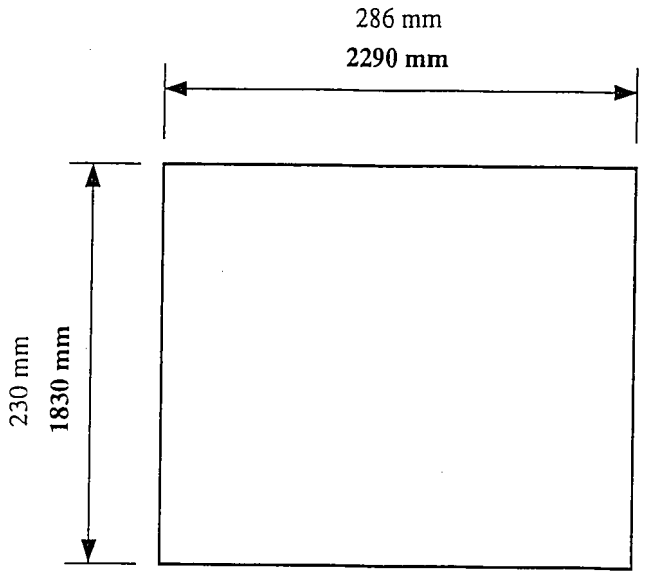

Figure 3.4 - Dimensions of the One-Eighth Scale "Half-Size" Sign Attachment (**Specimen RS-2S**) Included in the Aerodynamic Test Program.

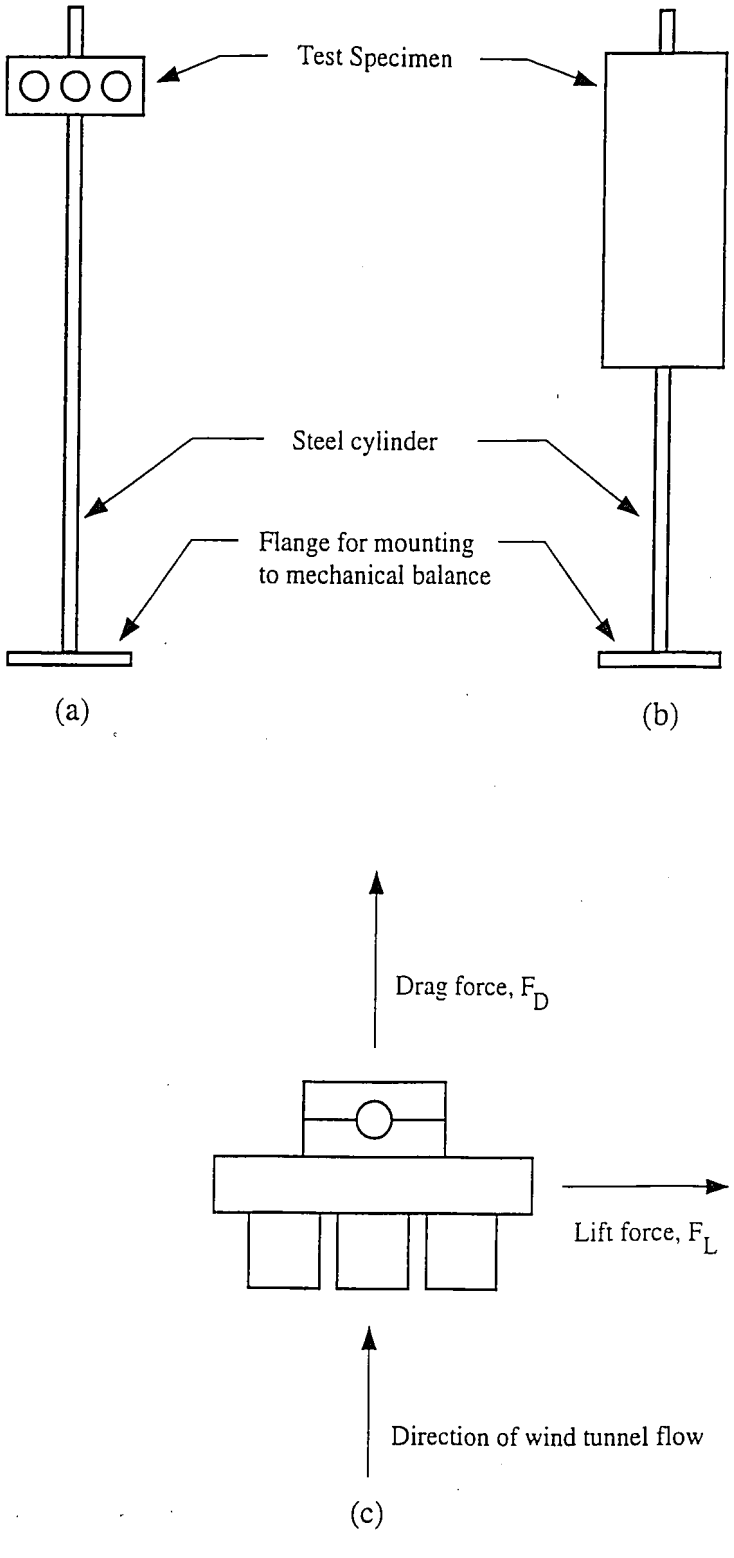

Figure 3.5 - Schematic Showing the Orientation of the (a) Signal and (b) Sign Attachments During the Aerodynamic Tests and, (c) Orientation of the Aerodynamic Forces Measured by the Mechanical Balance.

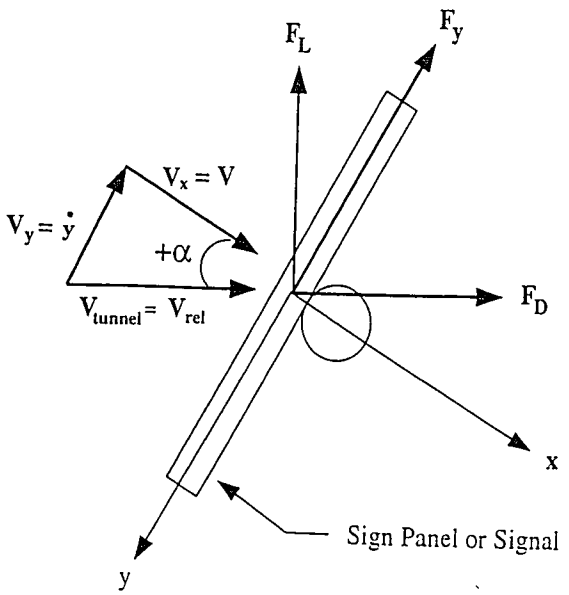

Figure 3.6 - Global and Local Reference Axes, Nomenclature, and Sign Convention for the Aerodynamic Tests.

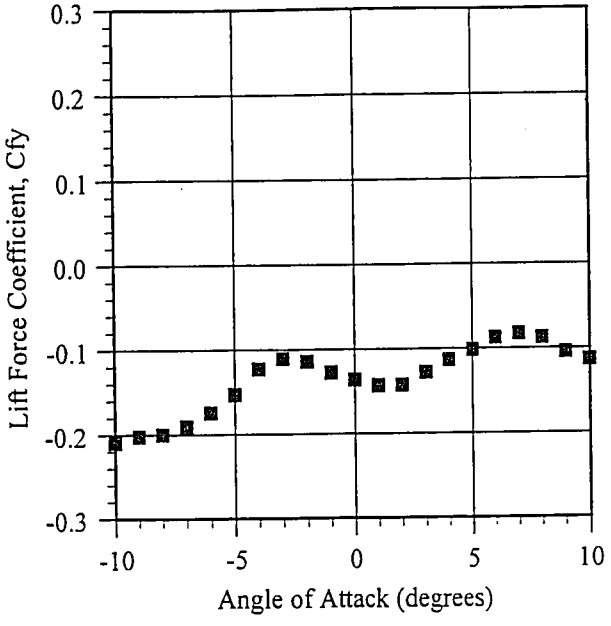

(a)

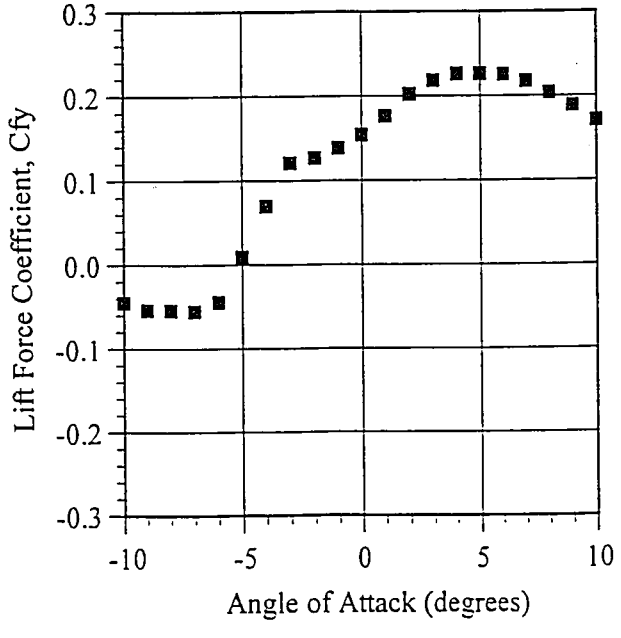

(b)

Figure 3.7 - Lift Force Coefficient, C_{Fy}, Versus Angle of Attack, α, for Specimen TS-3S (One-Half Scale Signal Attachment without Backplate) for (a) Flow From the Front and (b) Flow From the Rear.

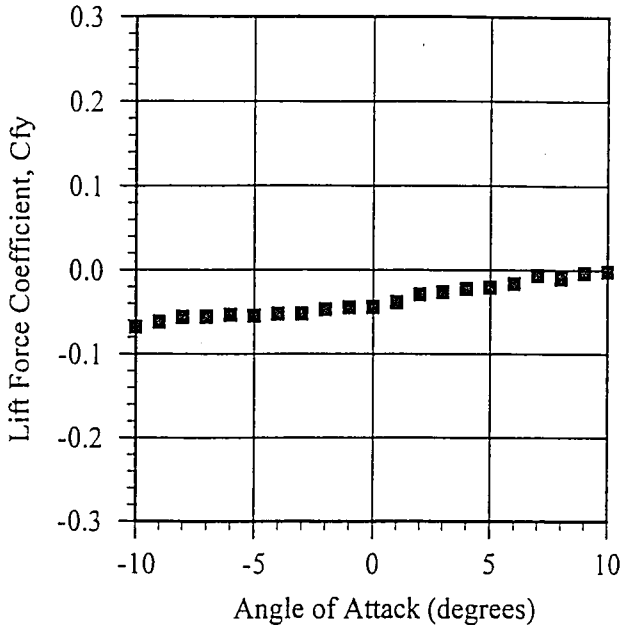

(a)

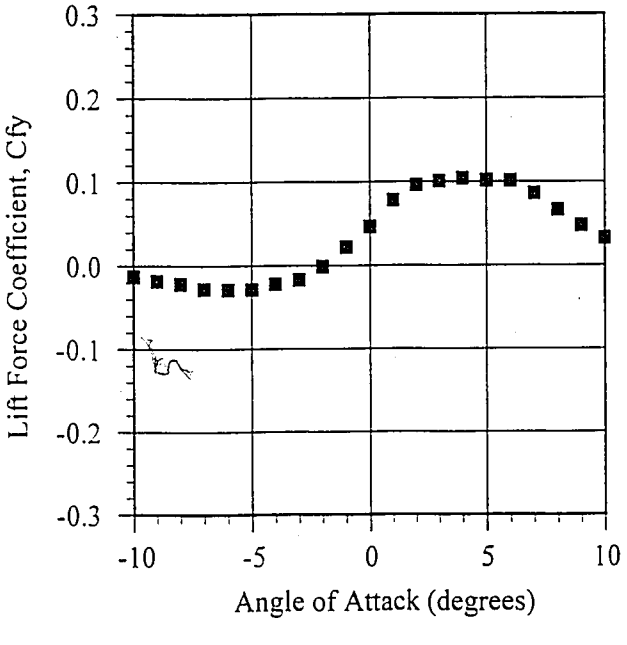

(b)

Figure 3.8 - Lift Force Coefficient, C_{Fy}, Versus Angle of Attack, α, for Specimen TS-4S (One-Half Scale Signal Attachment with Backplate) for (a) Flow From the Front and (b) Flow From the Rear.

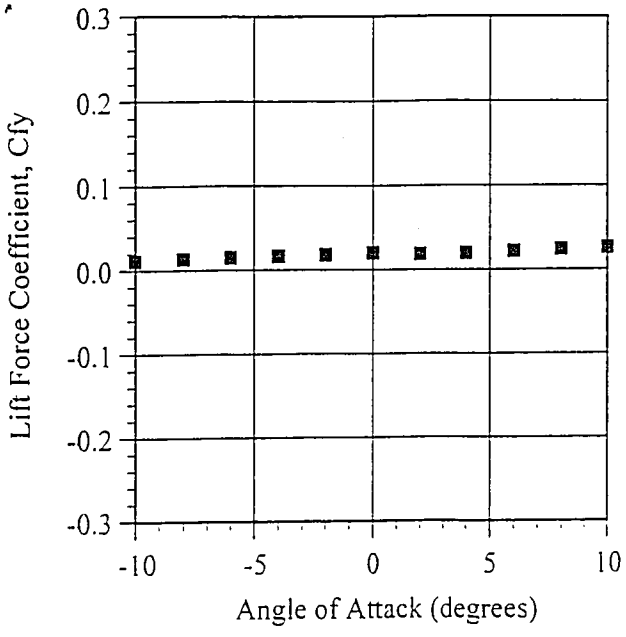

(a)

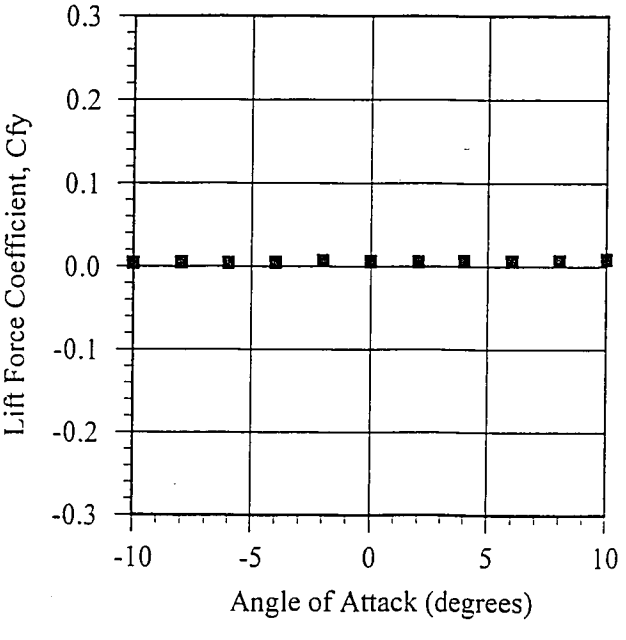

(b)

Figure 3.9 - Lift Force Coefficient, C_{Fy}, Versus Angle of Attack, α, for Specimen RS-1S (One-Eighth Scale "Full-Size" Sign Attachment) for (a) Flow From the Front and (b) Flow From the Rear.

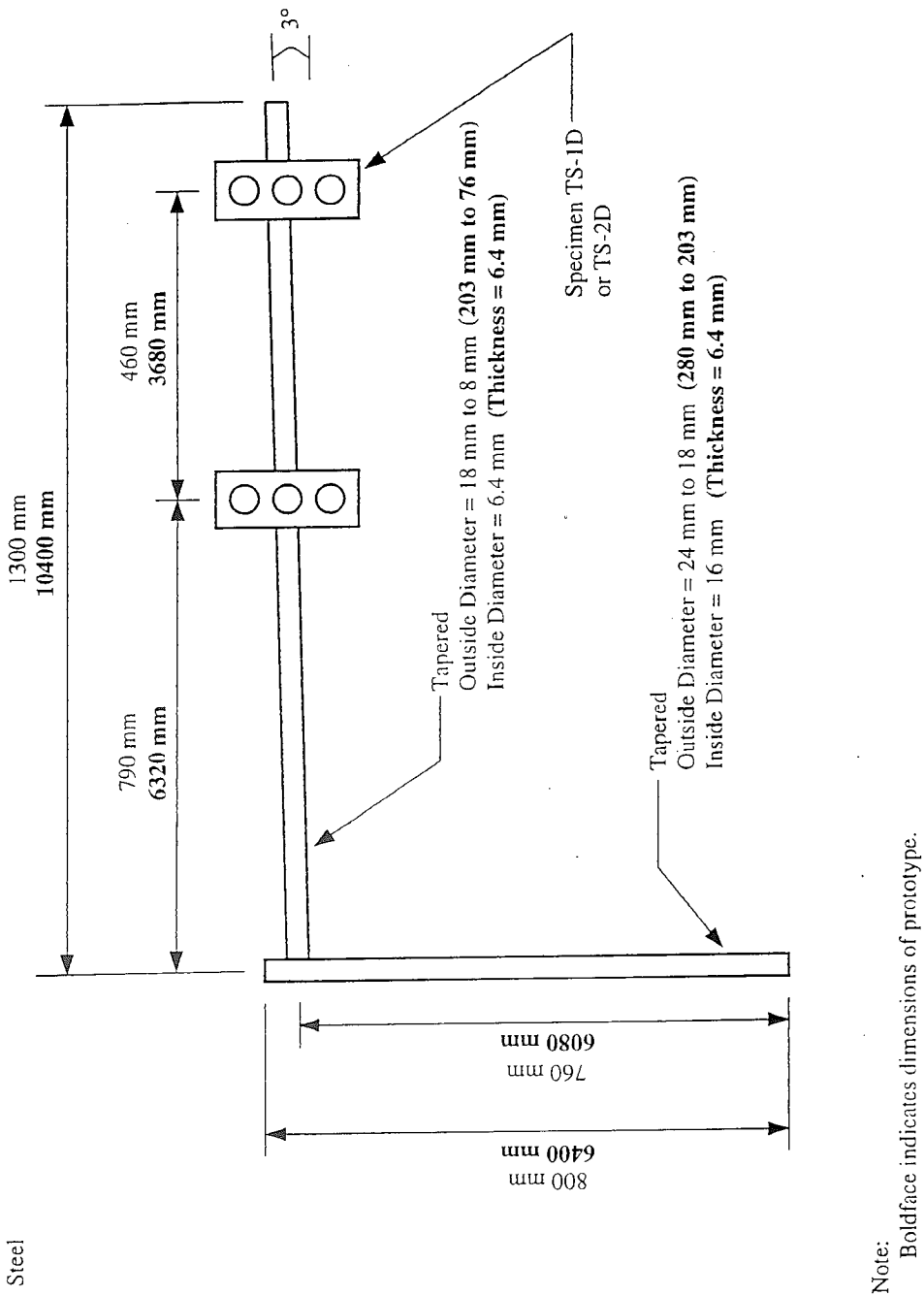

Figure 3.10 - Dimensions of the One-Eighth Scale Cantilevered Signal Support Structure (**Specimen A**) Included in the Aeroelastic Test Program.

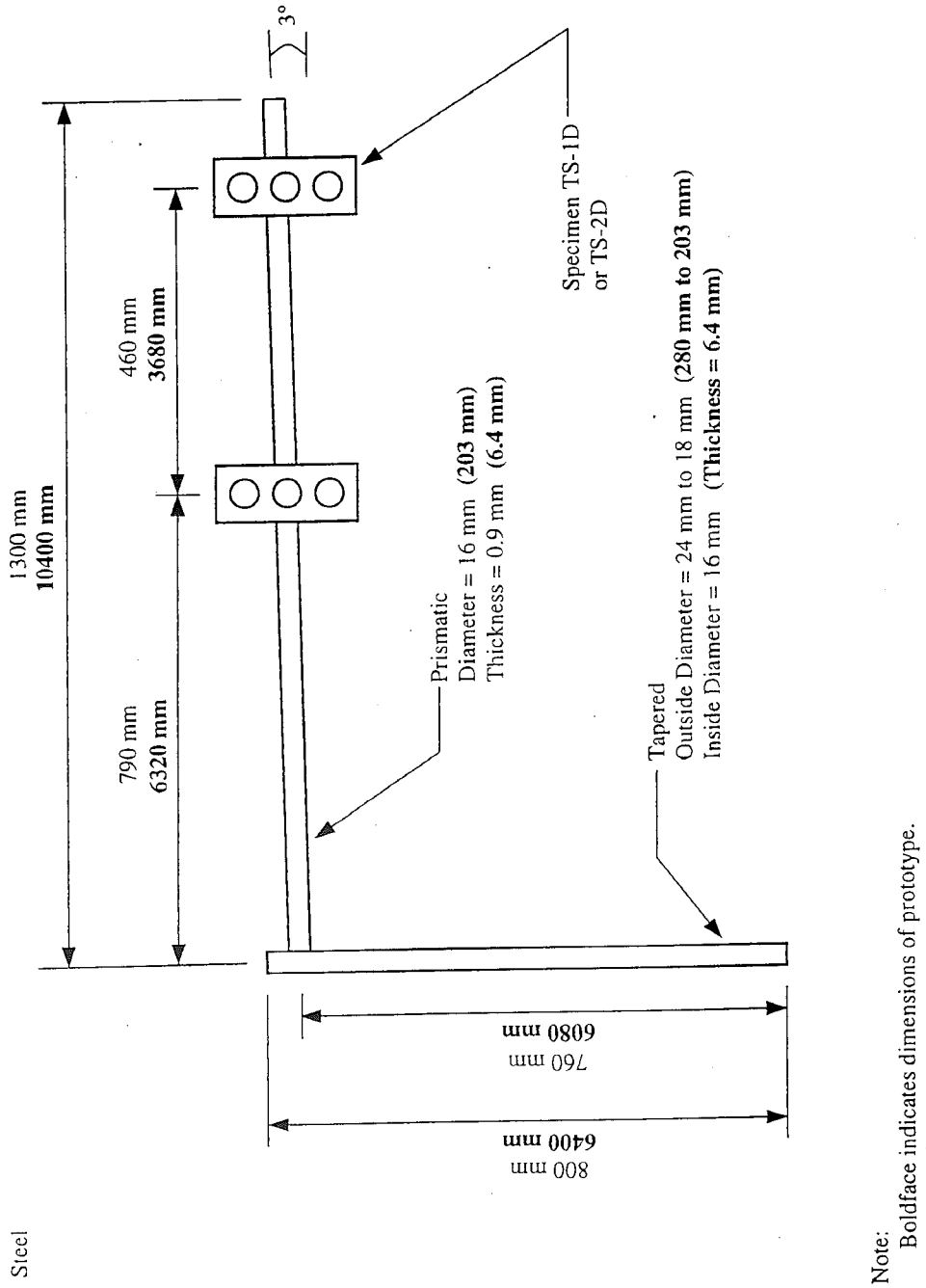

Figure 3.11 - Dimensions of the One-Eighth Scale Cantilevered Signal Support Structure (**Specimen B**) Included in the Aeroelastic Test Program.

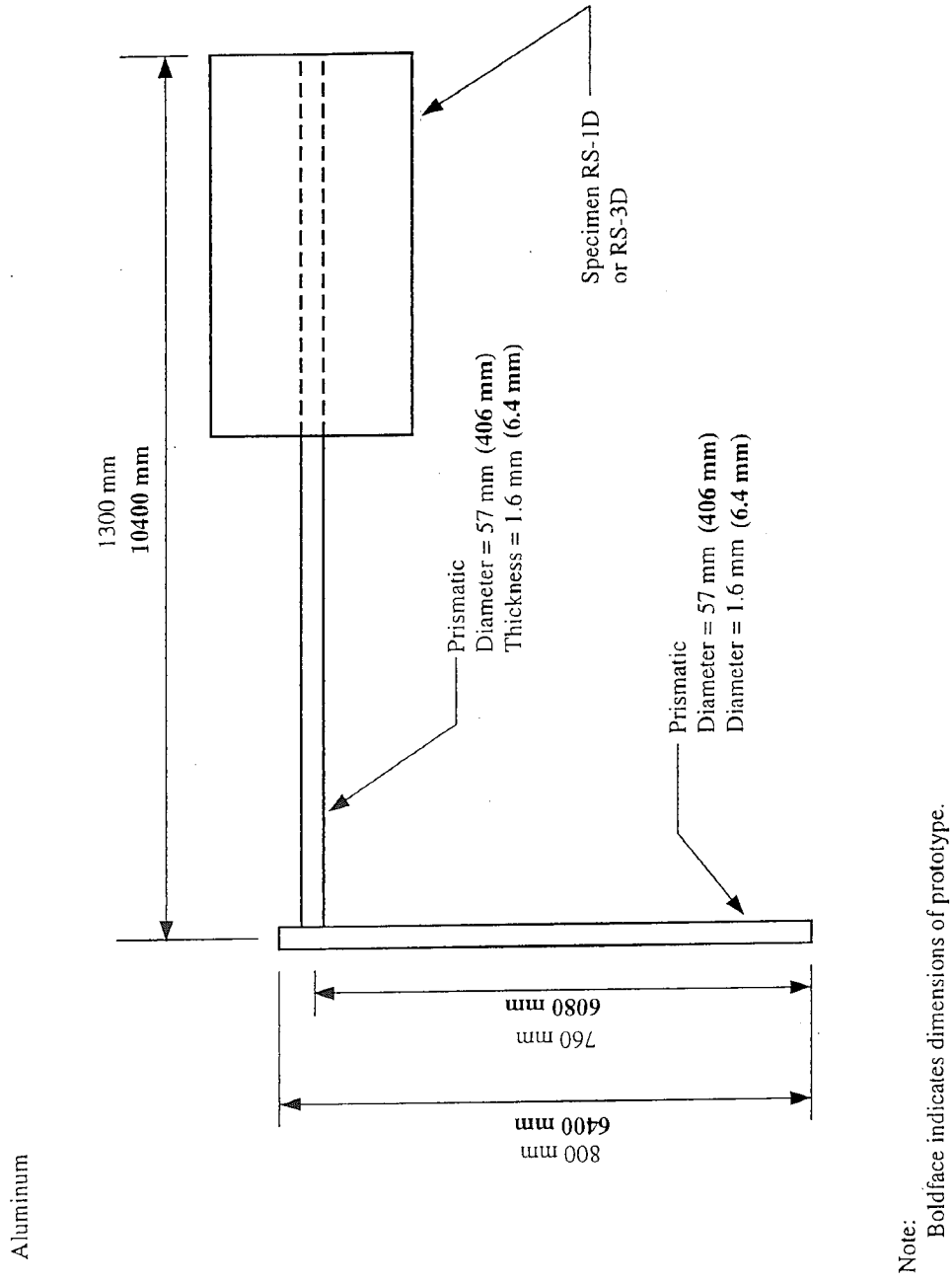

Figure 3.12 - Dimensions of the One-Eighth Scale Cantilevered Sign Support Structure (**Specimen C**) Included in the Aeroelastic Test Program.

Figure 3.13 - Dimensions of the One-Eighth Scale Cantilevered Sign Support Structure (**Specimen D**) Included in the Aeroelastic Test Program.

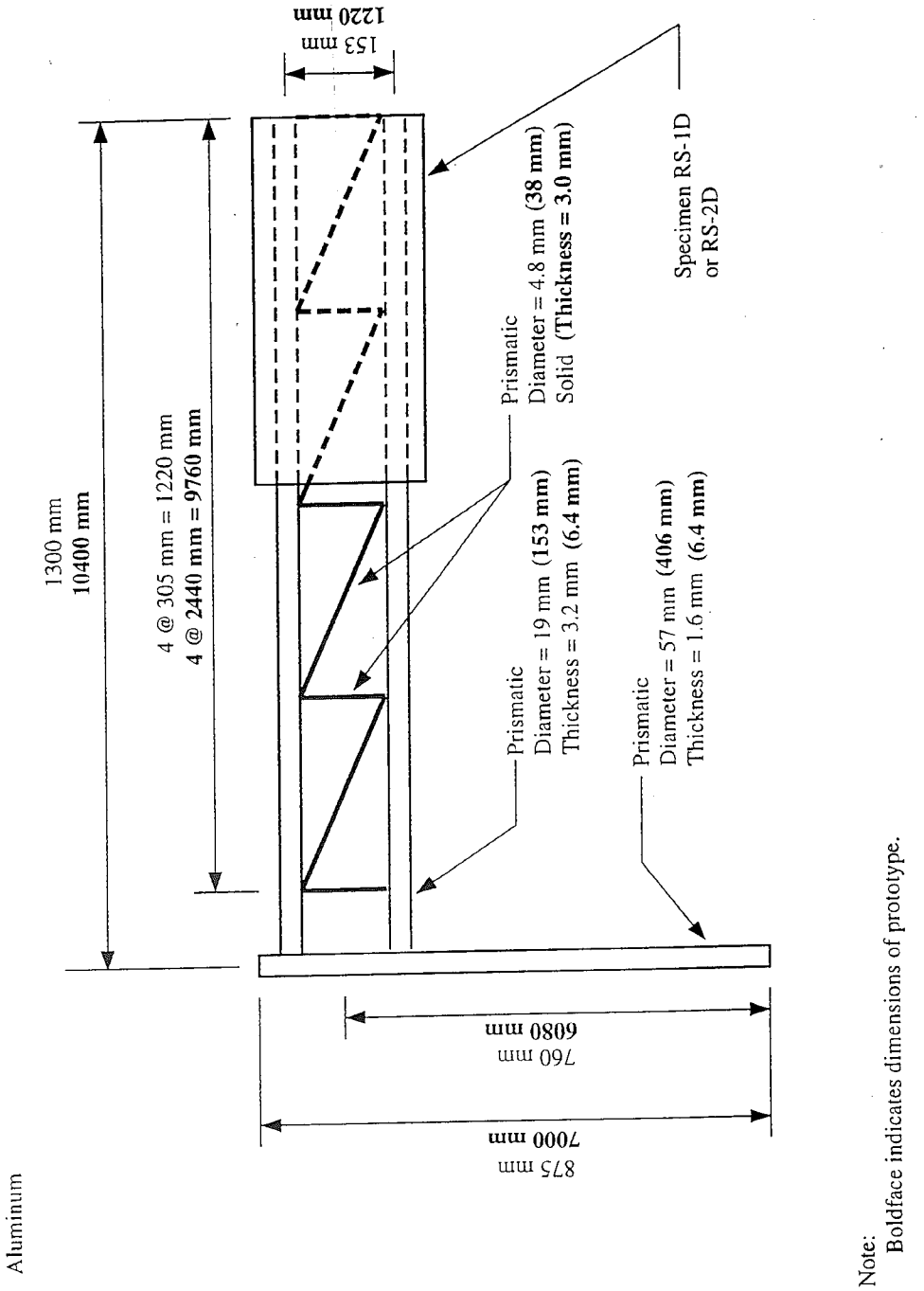

Figure 3.14 - Dimensions of the One-Eighth Scale Cantilevered Sign Support Structure (**Specimen E**) Included in the Aeroelastic Test Program.

Figure 3.15 - Dimensions of the One-Eighth Scale Signal Attachments Mounted to Specimens A and B During the Aeroelastic Tests. **Specimen TS-1D** Denotes Signal Without Backplate. **Specimen TS-2D** Denotes Signal With Backplate.

Weight = 4.2 N

Weight = 3110 N

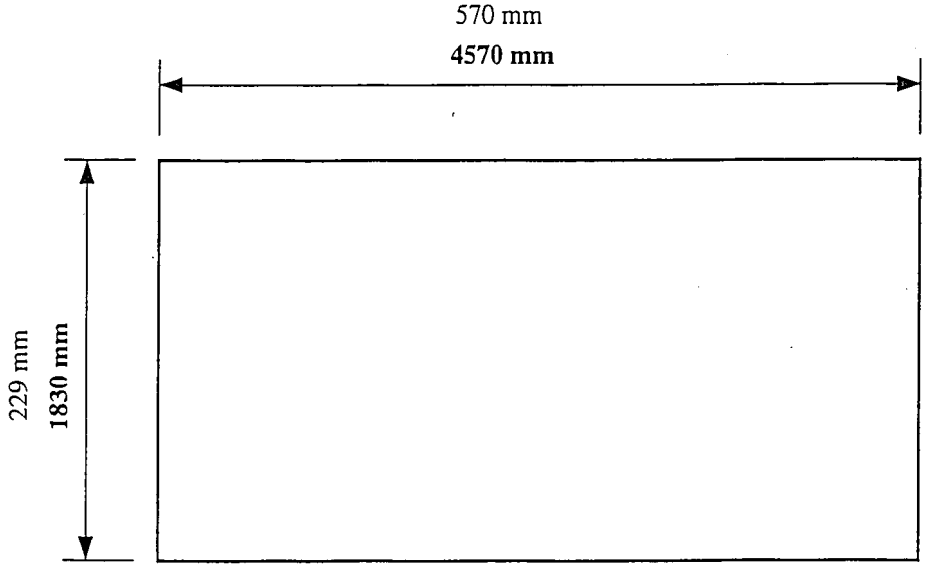

Note:
Boldface indicates dimensions of prototype.

Figure 3.16 - Dimensions of the One-Eighth Scale "Full-Size" Sign Attachment (**Specimen RS-1D**) Mounted to Specimens C and D During the Aeroelastic Tests.

Weight = 2.1 N

Weight = 1560 N

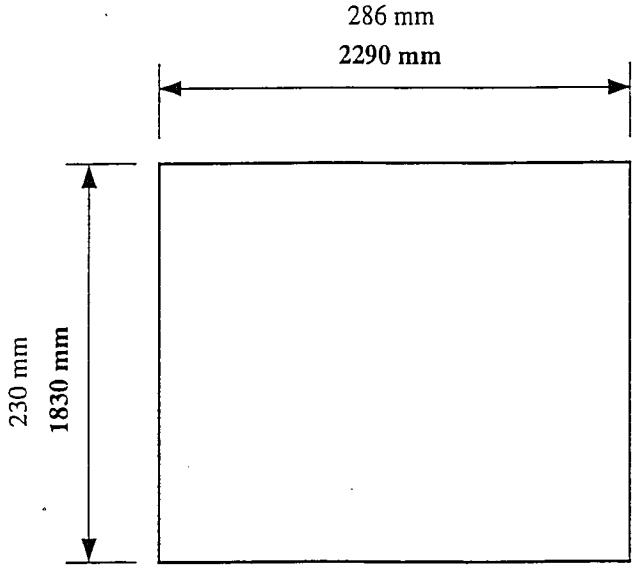

Note:
Boldface indicates dimensions of prototype.

Figure 3.17 - Dimensions of the One-Eighth Scale "Half-Size" Sign Attachment (**Specimen RS-3D**) Mounted to Specimen C During the Aeroelastic Tests.

Weight = 1.0 N

Weight = 3110 N

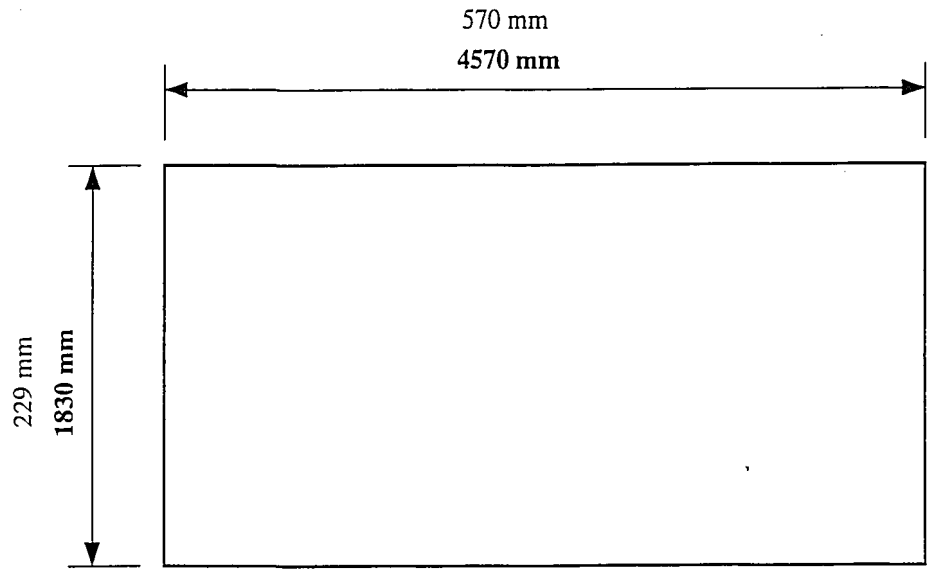

Note:
Boldface indicates dimensions of prototype.

Figure 3.18 - Dimensions of the One-Eighth Scale "Full-Size" Sign Attachment (**Specimen RS-2D**) Mounted to Specimen E During the Aeroelastic Tests.

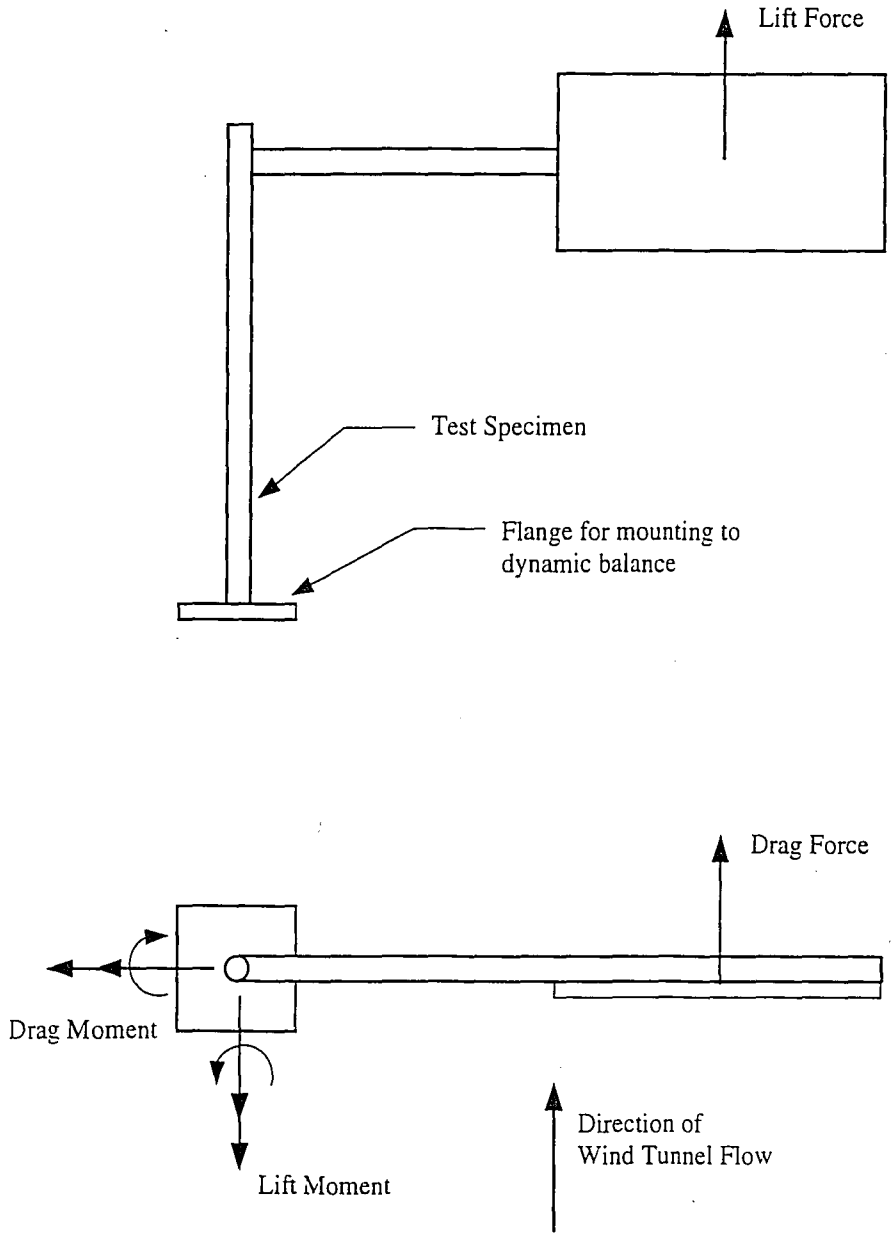

Figure 3.19 - Schematic Showing the Orientation of the Aeroelastic Test Specimens With Respect to the Wind Tunnel Flow and the Orientation of the Lift and Drag Moments Measured by the Dynamic Balance.

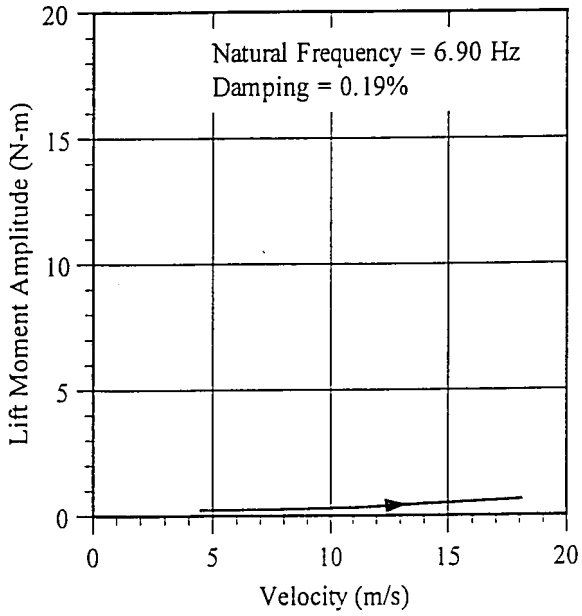

Figure 3.20 - Lift Moment Amplitude Versus Flow Velocity for Test Series I-A (Specimen A Configured with Signal without Backplates) for Flow From the Front. Note the Lack of Significant Across-Wind Response. Results for Flow From the Rear were Similar.

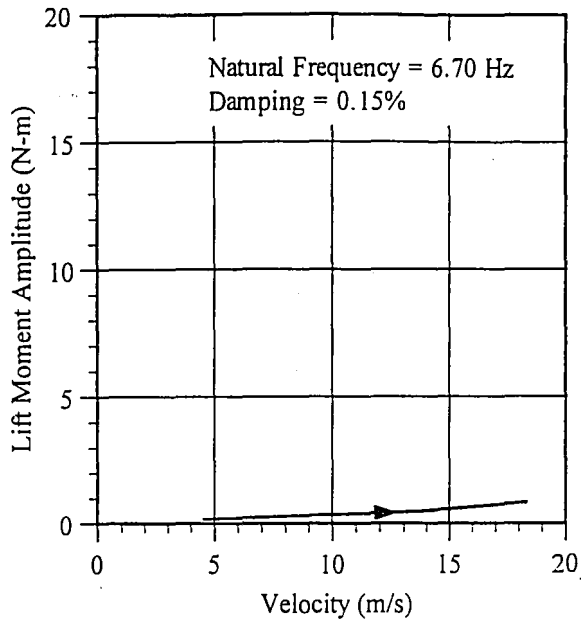

(a)

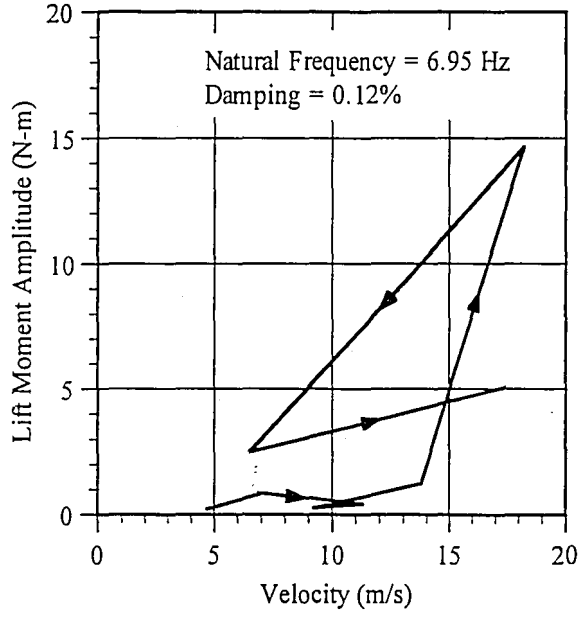

(b)

Figure 3.21 - Lift Moment Amplitude Versus Flow Velocity for Test Series II-A (Specimen A Configured with Signals with Backplates) for (a) Flow From the Front and (b) Flow From the Rear. Note the Across-Wind Galloping Response for Flow From the Rear.

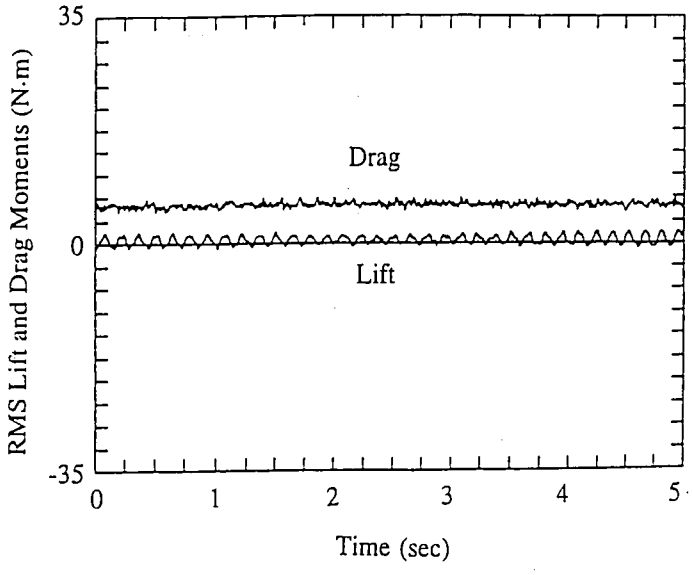

(a)

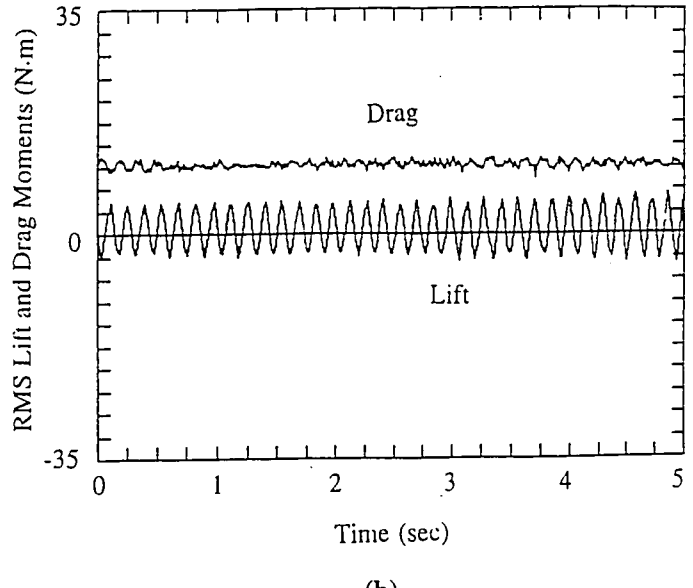

(b)

Figure 3.22 - Time History of the Dynamic Response for Test Series II-A (Flow from Rear) at (a) 13.4 m/s, (b) 17.4 m/s.

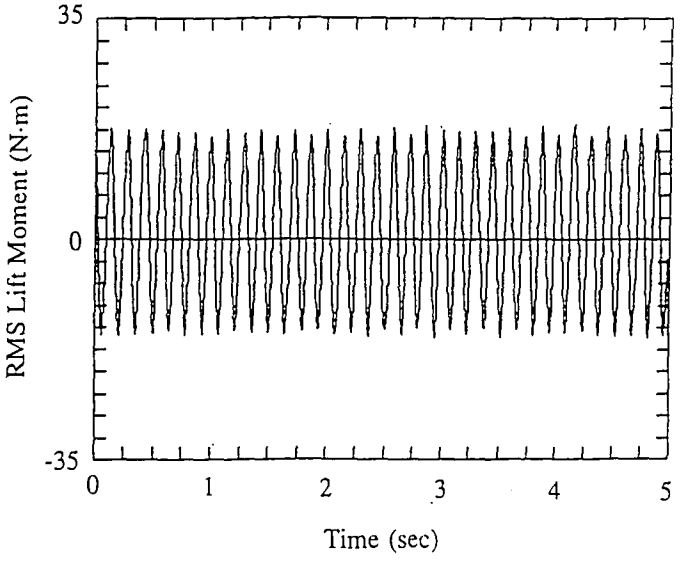

(c)

Figure 3.22 - Time History of the Dynamic Response for Test Series II-A (Flow from Rear) at (c) 18.2 m/s.

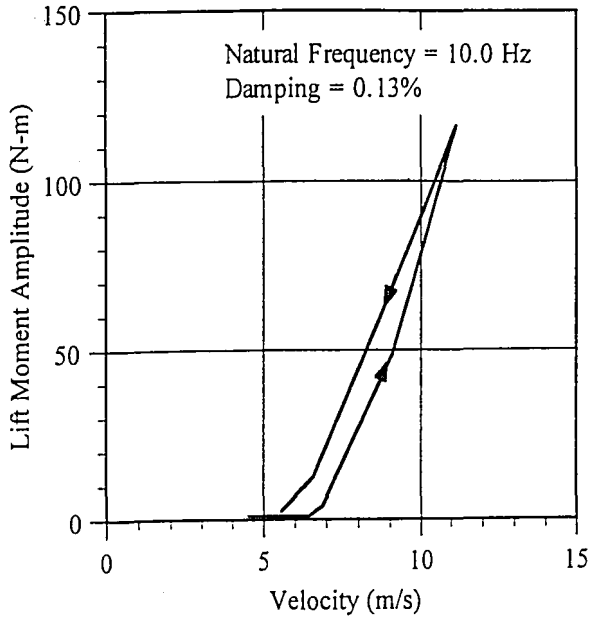

(a)

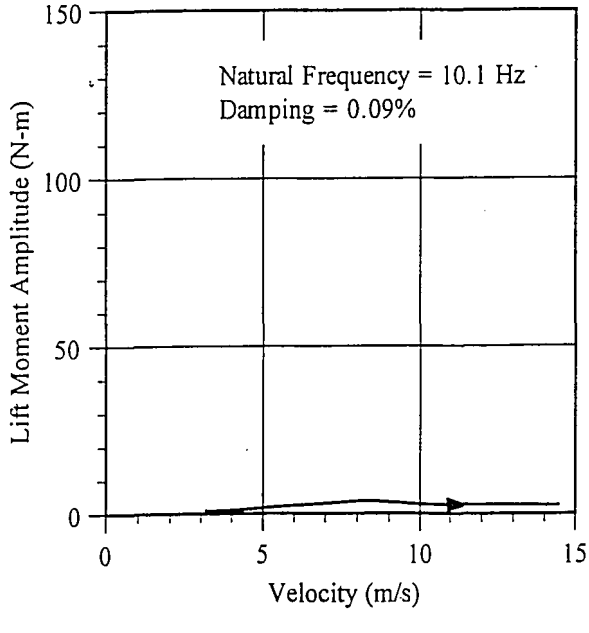

(b)

Figure 3.23 - Lift Moment Amplitude Versus Flow Velocity for Test Series I-C (Specimen C Configured with Sign RS-1D) for (a) Flow From the Front and (b) Flow From the Rear. Note the Across-Wind Galloping Response for Flow From the Front.

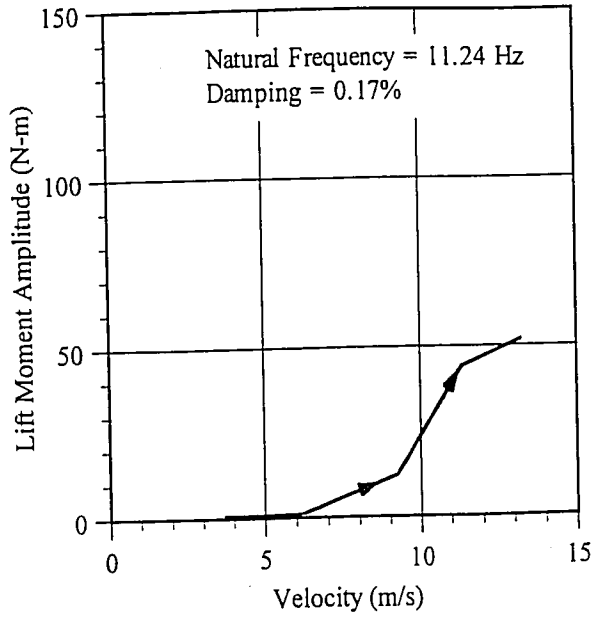

(a)

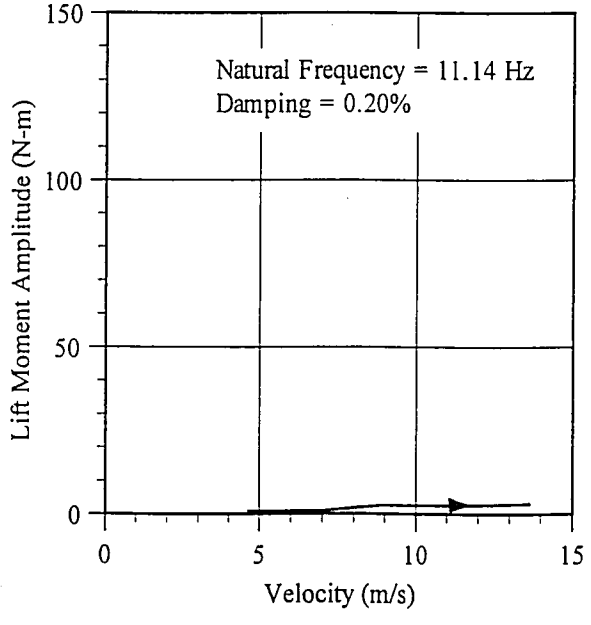

(b)

Figure 3.24 - Lift Moment Amplitude Versus Flow Velocity for Test Series II-C (Specimen C Configured with Sign RS-2D) for (a) Flow From the Front and (b) Flow From the Rear. Note the Across-Wind Galloping Response for Flow From the Front.

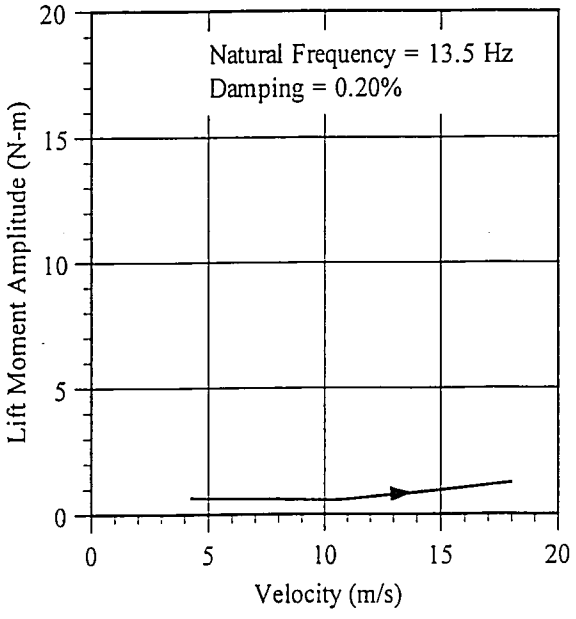

Figure 3.25 - Lift Moment Amplitude Versus Flow Velocity for Test Series I-D (Specimen D Configured with Sign RS-1D) for Flow From the Front. Note the Lack of Significant Across-Wind Response. Similar Results Were Obtained for Flow from the Rear and also for Tests Conducted on Specimen E.

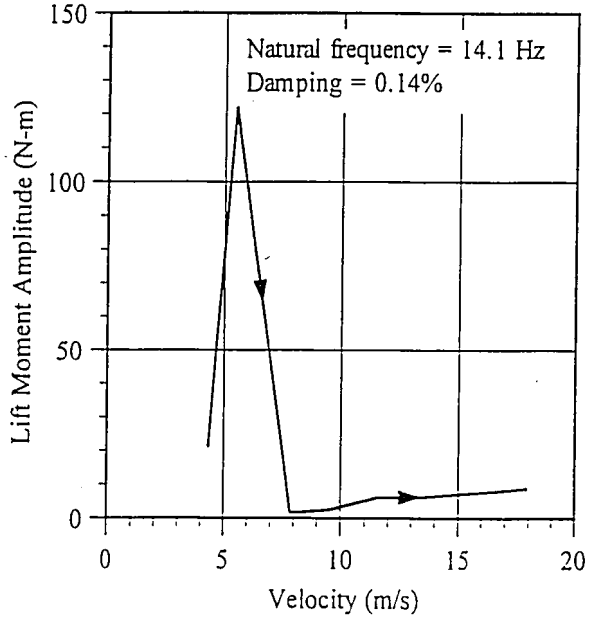

Figure 3.26 - Lift Moment Amplitude Versus Flow Velocity for Test Series I-C (Specimen C Configured with No Attachments). Note the Sharp Peak in the Response Indicative of Vortex Shedding.

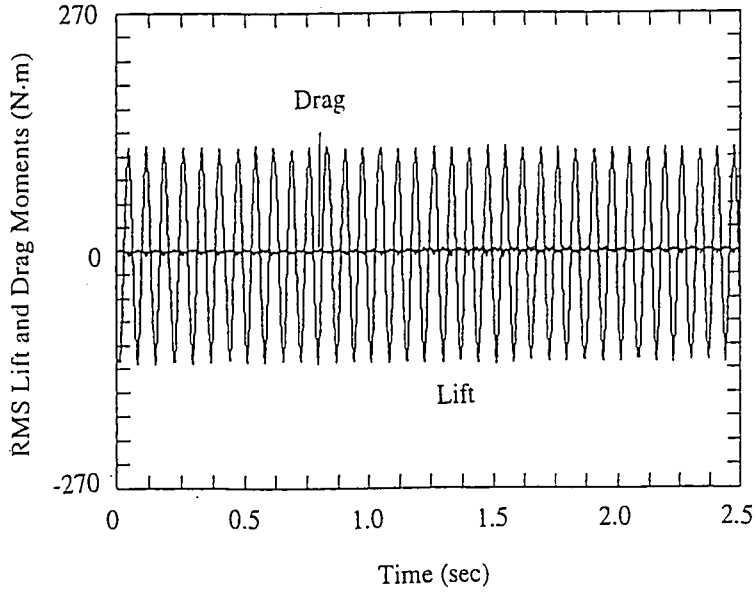

Figure 3.27 - Time History of the Dynamic Response for Test Series I-A (Specimen C Configured With No Attachments) at the Critical Wind Velocity of 5.5 m/s.

Chapter Four

FINITE-ELEMENT ANALYSES

4.1 INTRODUCTION

This Chapter summarizes the results of dynamic and static finite-element analyses which were performed to estimate the magnitude of the across-wind lift pressures to which cantilevered support structures are subjected during occurrences of galloping- and vortex-induced vibrations. The following methods were used to accomplish this objective:

- Finite-element analyses of the wind-tunnel model specimens were performed to estimate the magnitude of the lift pressures required to simulate the across-wind response amplitudes (i.e. lift moment amplitudes at the base of the vertical supports) measured during the aeroelastic wind tunnel tests.

- Finite-element analyses of the wind tunnel prototype specimens were performed to verify that the mass and stiffness of the prototype specimens were reasonably represented by the model specimens. There was good agreement between the prototype and model specimens, indicating that the aeroelastic wind tunnel results are representative of the behavior which would be expected in cantilevered support structures in the field.

- Finite-element analyses of several full-scale cantilevered support structures were performed to evaluate the validity of the experimentally-determined lift pressures. The

structures selected for these analyses were known to have been subjected to across-wind vibrations consistent with galloping. In addition, estimates of at least one dynamic response amplitude from each of these structures was known (either displacements at the tip of the horizontal mast-arm or stress measurements) so that the dynamic response observed in the field could be simulated using finite-element analyses.

The results of the above analyses were used to develop equivalent static load models (in the form of lift pressures) which reasonably estimate the magnitudes of the across-wind loads associated with the galloping and vortex shedding phenomena. These equivalent load models can be used in the design of cantilevered support structures for galloping- and vortex-induced fatigue.

This chapter is organized into six sections. Section 4.2 provides a brief summary of the theoretical dynamic response of a single-degree-of-freedom system to a resonant load. Section 4.3 describes the analytical methods which were used in the finite-element analyses reported herein. Section 4.4 summarizes the results of finite-element analyses of the model wind tunnel specimens. Section 4.5 summarizes the results of finite-element analyses of the prototype wind tunnel specimens. Section 4.6 summarizes the result of finite-element analyses of the full-scale cantilevered support structures. Section 4.7 synthesizes the results of the finite-element analyses reported in the previous sections into equivalent static load models which can be used in the design of cantilevered support structures for galloping- and vortex-induced fatigue.

4.2 GENERAL THEORY OF DYNAMIC RESPONSE

The response of a linear-elastic structural system to a dynamic load is dependent on four parameters: (1) mass, (2) damping, (3) stiffness, and (4) the characteristics of the applied dynamic

load. In the simplest case, the effects of these parameters on the dynamic response of a structure can be investigated through the use of a single-degree-of freedom (SDOF) model.

Figure 4.1 depicts the general model for a SDOF structural system. The mass, m, of the system is constrained to a lateral translation, y(t). The stiffness and damping properties of the system are given by a spring with stiffness equal to k and a damper with damping equal to c, respectively. The response of this system to a dynamic load, F(t), is given by the equation of motion:

$$m\ddot{y} + c\dot{y} + ky = F(t) \tag{4.1}$$

where y, $\dot{y}$, and $\ddot{y}$ are displacement, velocity, and acceleration, respectively; t is time; and the remaining variables are as previously defined.

The undamped circular natural frequency of the system, ω, is related to the stiffness and the mass by the following:

$$\omega = \sqrt{\frac{k}{m}} \tag{4.2}$$

For low levels of damping, the undamped natural frequency is approximately equal to the damped natural frequency [11].

The level of damping possessed by the system is a measure of the structure's ability to dissipate energy and return to the at-rest condition. In typical structural applications, damping is represented as a ratio of the form:

$$\xi = \frac{c}{c_{crit}} = \frac{c}{2m\omega} \tag{4.3}$$

where ξ is the damping ratio, c is the amount of equivalent viscous damping possessed by the structure, and c_{crit} is the minimum amount of equivalent viscous damping for which no oscillation will occur when the structure is subjected to free-vibration.

Substituting Equations 4.2 and 4.3 into Equation 4.1, the equation of motion can be rewritten as:

$$m[\ddot{y} + 2\xi\omega\dot{y} + \omega^2 y] = F(t) \tag{4.4}$$

Thus, for any dynamic loading, F(t), the equation of motion can be solved to determine the response of the structure, y(t). The response is comprised of two components; a transient component and a steady-state component. The transient component represents the response of the structure under damped, free-vibration. The steady-state component represents the response of the structure to the load, F(t). Typically, only the steady-state component is of concern when determining the response of a structure to a forced vibration (i.e. the transient component of the response eventually damps out).

For an externally-applied load, F(t), of the form:

$$F(t) = F_0 \sin\bar{\omega}t \tag{4.5}$$

where F_0 and $\bar{\omega}$ are the amplitude and frequency of the applied load, respectively, the steady-state component of the dynamic response is given by:

$$y(t) = \frac{F_0}{k}\left[\frac{1}{(1-\beta^2)^2 + (2\xi\beta)^2}\right][(1-\beta^2)\sin\bar{\omega}t - 2\xi\beta\cos\bar{\omega}t] \tag{4.6}$$

where β is the ratio of the loading frequency to the natural frequency of the structure (i.e. $\bar{\omega}/\omega$) and the remaining variables are as previously defined. The term F_0/k represents the response of the system under static application of the load F_0. The amplitude of the steady-state response defined by Equation 4.6 is given by:

$$y_{ampl} = \frac{F_0}{k}[(1-\beta^2)^2 + (2\xi\beta)^2]^{-\frac{1}{2}} \quad (4.7)$$

Under resonant conditions, the frequency of the loading is equal to the natural frequency of the structure (i.e. $\beta = 1$). Therefore, at resonance, the amplitude of the steady-state response is given by:

$$y_{ampl} = \frac{F_0}{k}[\frac{1}{2\xi}] \quad (4.8)$$

Equation 4.8 indicates that, at resonance, the maximum dynamic response of a SDOF system is equal to the static response (F_0/k) multiplied by a constant ($1/2\xi$). The constant $1/2\xi$ is termed the dynamic magnification factor. It is the ratio of the resonant steady-state dynamic response amplitude to the static response which would be produced by the force F_0. As is evident from Equation 4.8, the resonant response of a SDOF system is inversely proportional to the amount of damping possessed by the system.

4.3 ANALYTICAL METHODS

The finite-element analyses reported in this chapter were performed using the commercially-available finite-element program ABAQUS [2]. Details of the analytical methods which were used in these analyses are provided in Sections 4.3.1 through 4.3.4.

4.3.1 Analytical Models

The cantilevered support structures considered in the analytical program (i.e. wind-tunnel model specimens, wind-tunnel prototype specimens, and full-scale support structures) were modeled using continuous, three-noded, quadratic beam elements. Structures composed of prismatic structural members were modeled using beam elements of the same corresponding cross-

sectional dimensions (i.e. the actual member dimensions were used in the finite-element model). Structures composed of uniformly tapered structural members were modeled using a series of "equivalent" prismatic elements arranged in a step fashion as is shown in Figure 4.2. The cross-sectional dimension of each "equivalent" prismatic element was equal to the average cross-sectional dimension of the corresponding tapered member.

A relatively fine mesh size was used in the analyses of the full-scale cantilevered support structures and prototype wind tunnel specimens (a nominal element length equal to 305 mm) to ensure adequate representation of the variation in mass and stiffness along the length of the tapered structural members. In order to maintain a reasonable level of consistency between individual analyses, the full-scale cantilevered support structures and prototype wind tunnel specimens which were composed of prismatic structural members were also modeled using the same mesh size.

The wind tunnel model specimens were modeled using a reduced mesh size (i.e. nominal element length equal to 38 mm). The mesh size was reduced in the same proportion as the model scale. As a result, the relative level of mesh refinement between the full-scale cantilevered support structures and wind tunnel model specimens was identical.

Signal attachments were modeled as lumped masses at the nodal points corresponding to the locations of the attachments on the actual support structure. Sign attachments were modeled as a series of lumped masses at the nodal points corresponding to the length of the horizontal support over which the sign was mounted on the actual support structure. The mass at each nodal point was computed as the mass of the actual sign attachment divided by the number of nodal points over which the sign was mounted on the actual support structure.

The base of the vertical support of each of the models was assumed fixed. Effects of foundation flexibility and/or soil-structure interaction were neglected in each of the analyses.

Kaczinski et al. [27] showed that the fixed base assumption results in worst-case estimates of the stress ranges at critical connection details. Therefore, the equivalent static load models developed from these finite-element analyses will conservatively predict the magnitudes of the stress ranges to which cantilevered support structures are subjected during galloping and vortex shedding.

4.3.2 Load Models

Analytical load models for the galloping and vortex shedding phenomena were developed based upon the wind tunnel test results. As was discussed in Chapter Three, galloping of the cantilevered sign and signal model specimens was caused by the aerodynamic forces acting on the attachments to these specimens. As a result, the load model for galloping of the signal support structures was represented in the finite-element analyses as a concentrated load applied in the vertical-plane at the nodal points corresponding to the locations of the signal attachments in the actual structure (see Figure 4.3). The load model for galloping of the sign support structures was represented as a uniformly distributed load applied in the vertical-plane over the length of the sign panel (see Figure 4.4).

The wind tunnel test results indicated that vortex shedding of the cantilevered sign support model specimen (configured without attachments) was caused by the shedding of vortices from the horizontal mast-arm. As a result, the load model for vortex shedding was represented as a uniformly distributed load applied to the structure in the vertical-plane over the length of the horizontal mast-arm (see Figure 4.5).

4.3.3 Analyses

As was discussed in Section 4.1, finite-element analyses were performed to determine the magnitude of the lift pressures required to simulate a known dynamic response amplitude. For

the wind tunnel model and prototype specimens, the known dynamic response amplitude was the magnitude of the lift moment at the base of the vertical support. For the full-scale support structures, the known dynamic response amplitude was either an estimate of the displacement amplitude of the horizontal support or an estimate of the stress range at some location within the structure. Three finite-element analyses were performed on each of the structures considered within the scope of the analytical program. A brief discussion of each of the analyses follows:

Eigenvalue analyses were performed to determine the natural frequencies and mode shapes corresponding to the first six modes of vibration of the structure. The number of modes extracted in the eigenvalue analysis was arbitrarily selected. As will be discussed below, the dynamic response of cantilevered support structures to galloping and vortex shedding is dominated by the first vertical-plane mode of vibration.

Linear modal analyses were performed to determine the steady-state dynamic response of each of the structures to the galloping and/or vortex shedding phenomena. The load to which each of the structures was subjected was assumed a sinusoidal waveform of the form:

$$F(t) = F_0 \sin \omega t \tag{4.9}$$

where F_0 is the amplitude of the dynamic load required to simulate the known dynamic response amplitude, ω is the circular natural frequency of the structure corresponding to the first mode of vibration in the vertical-plane, and t is time. The load given by Equation 4.9 was applied to the structure in accordance with one of the load models discussed in Section 4.3.2. Representation of the loading as a sinusoidal function is consistent with the time history of the dynamic response observed during the wind tunnel tests for which galloping and vortex shedding were observed (see Figures 3.22 and 3.27, respectively). Each of the dynamic analyses was performed by only considering the contribution of the first vertical-plane mode of vibration (generally the second mode of vibration of each of the structures). The superposition of response amplitudes from

higher vertical-plane modes were found to not significantly contribute to the overall dynamic response of the structures.

Static analyses were then performed to determine the magnitude of the static load amplitude required to obtain a response equal to the known dynamic response amplitude for each of the structures. The static load was applied to the structure in accordance with the load models described Section 4.3.2. These analyses were performed to evaluate the accuracy of using equivalent static load models to simulate the forces to which cantilevered support structures are subjected during occurrences of galloping and vortex shedding. The use of equivalent static load models will avoid the necessity for using dynamic analyses for design.

4.4 ANALYSES OF WIND TUNNEL MODEL SPECIMENS

Table 4.1 provides a tabular summary of the data collected from the wind tunnel specimens which exhibited significant vertical-plane vibrations due to either galloping or vortex shedding. The data presented in Table 4.1 are identical to the data presented in Chapter Three. As may be recalled from the discussion in Chapter Three, vortex-induced vibrations were only observed in the sign support specimen (i.e. Specimen C) configured without attachments. The remaining specimens shown in Table 4.1 exhibited galloping-induced vibrations. Member dimensions for each of the model specimens were previously summarized in Chapter Three. The natural frequency (corresponding to the first vertical-plane mode of vibration) and percent critical damping (also corresponding to the first vertical-plane mode of vibration) were determined from free-vibration tests. The wind velocity indicated for each specimen is the velocity at which peak vertical-plane oscillations were observed. Similarly, the column moment amplitude is the lift moment measured at the base of the vertical support of the specimen at the time of peak vertical-plane oscillation.

4.4.1 Results of Dynamic Analyses

Table 4.2 summarizes the dynamic finite-element analysis results for the wind tunnel model specimens. The predicted natural frequencies in the table are for the vertical-plane mode of vibration of the specimen and agree to within 20 percent of the measured values. As is indicated, the damping ratio for each specimen was set equal to the damping ratio obtained from vertical-plane, free-vibration tests of that specimen during the wind-tunnel tests.

The equivalent static pressures indicated in Table 4.2 were calculated using the following relation:

$$Equivalent\ Static\ Pressure = \frac{F_{dynamic}}{(A)(2\xi)} \qquad (4.10)$$

where $F_{dynamic}$ is the dynamic force required to obtain the lift moment amplitude recorded during the wind-tunnel test, A is the projected area of the member subjected to the loading (i.e. signal, sign, or horizontal support), ξ is the damping ratio, and $1/2\xi$ is the dynamic magnification factor for a SDOF system subjected to resonant vibrations (as was discussed in Section 4.2). Note that the equivalent static pressure is a lift pressure amplitude. The remaining columns of Table 4.2 depict the dynamic response amplitudes (i.e. moments and displacements) corresponding to the magnitude of the load required to obtain the lift moment amplitude recorded during the wind tunnel test.

Examination of the equivalent static pressures listed in Table 4.2 indicate that the lift pressures associated with galloping vary from 423 Pa for the signal structure to 739 Pa for the sign structure configured with the "full-size" sign attachment (i.e. Attachment RS-1D). Considering the differences in these structures and the randomness of the galloping phenomenon, this range in equivalent static pressures is remarkably consistent.

A comparison of the results for the sign support structure (i.e. Specimen C) configured with the two sign attachments (i.e. Attachment RS-1D and Attachment RS-3D) indicates that the response is approximately proportional. That is, the response amplitudes associated with Specimen C configured with Attachment RS-1D (the "full-size" sign attachment) are approximately two times greater than the response amplitudes associated with Specimen C configured with Attachment RS-3D (i.e. the "half-size" sign attachment). This result verifies that the magnitude of the across-wind loads to which cantilevered support structures are subjected during occurrences of galloping are proportional to the area of the attachment detail. In other words, the lift pressure associated with galloping is approximately constant for different signs and signals.

The equivalent static pressure for vortex shedding from the mast-arm of the sign structure (i.e. Specimen C) without attachments is 2091 Pa. Comparisons of this equivalent static pressure with the equivalent static pressures computed using the provisions of the present AASHTO Specifications [4] and Ontario Code [35] follows.

As was discussed in Chapter Two, the present AASHTO Specifications [4] contain provisions for the design of simple poles for vortex shedding. The critical wind velocity associated with vortex shedding lock-in, V_{cr}, is given by the Strouhal relation:

$$V_{cr} = \frac{f_n D}{S} \tag{4.11}$$

where f_n is the natural frequency of the structure, D is the across-wind dimension of the element from which vortices are shed, and S is the Strouhal number. The measured natural frequency of Specimen C was 14.1 Hz, the diameter of the horizontal support was 57 mm, and the Strouhal number for vortex shedding from a circular cylinder is 0.18. Substituting this data into the Strouhal relation, the predicted critical wind velocity is:

$$V_{cr} = \frac{(14.1\,Hz)(0.057\,m)}{0.18} = 4.5\,m/s\ (16\,km/hr) \tag{4.12}$$

The equivalent static pressure range is given by:

$$P_t = \frac{P}{2\xi} = \frac{0.0473\,V_{cr}^2 C_d C_h}{2\xi} \tag{4.13}$$

where C_d is the drag coefficient, C_h is the height coefficient, and β is the damping ratio. As is indicated in Table 4.1, the measured damping ratio for Specimen C was 0.14%. Based upon the wind velocity and diameter of the horizontal mast-arm, the AASHTO Specifications specify the use of a drag coefficient equal to 1.10. The height coefficient is assumed to be equal to 1.00 (i.e. the height coefficient does not pertain to the wind tunnel flow condition because the wind tunnel flow velocity does not vary with height). Substituting these data into Equation 4.13, the predicted equivalent static pressure range is:

$$P_t = \frac{(0.0473)(16\,km/hr)^2(1.10)(1.00)}{(2)(0.0014)} = 4760\,Pa \tag{4.14}$$

Therefore, the amplitude of the equivalent static pressure fluctuation predicted by the provisions of the AASHTO Specifications would be equal to 2380 Pa, which agrees very well with the analytically-determined equivalent static pressure amplitude of 2091 Pa.

The Ontario Code [35] also contains provisions for predicting the equivalent static transverse force amplitude per unit length, F_s, associated with vortex shedding from a simple pole:

$$F_s = \frac{0.3}{\xi} C_s D V_{cr}^2 \tag{4.15}$$

The equivalent static transverse pressure amplitude is given by:

$$\frac{P_t}{2} = \frac{0.3}{\xi} C_s V_{cr}^2 \tag{4.16}$$

Substituting the measured damping ratio of 0.14%, a transverse force coefficient equal to 0.71, and a critical wind velocity equal to 4.5 m/s, the predicted equivalent transverse pressure amplitude is:

$$\frac{P_t}{2} = \frac{0.3}{0.0014}(0.71)(4.5 m/s)^2 = 3080 Pa \tag{4.17}$$

Thus, for a measured value of damping, the equivalent static pressure predicted by the Ontario Code [35] is more conservative than the equivalent static pressure predicted by the AASHTO Specifications [4].

Generally, the equivalent static pressures predicted by each of the design specifications correlate well with the equivalent static pressure derived from the dynamic finite-element analysis. As a result, it can be concluded that the design provisions for vortex shedding from a simple pole can be used to estimate the magnitude of the equivalent static pressures to which cantilevered support structures are subjected during occurrences of vortex-induced vibration resulting from the shedding of vortices from the mast-arm. Unfortunately, there are no equivalent load models specified in either the Ontario Code [35] or the AASHTO Specifications [4] for galloping.

4.4.2 Results of Static Analyses

Static analyses of the wind tunnel model specimens were also performed to determine the validity of using an equivalent static load model to estimate the magnitude of the support structure forces to which cantilevered support structures are subjected during occurrences of galloping and

vortex shedding. Table 4.3 summarizes the results of these analyses. The static pressures indicated in Table 4.3 was computed using the following relation:

$$Static\ Pressure = \frac{F_{static}}{A} \tag{4.18}$$

where F_{static} is the amplitude of the load required to simulate the lift moment amplitudes measured during the wind tunnel test and A is the projected area of the member subjected to loading. Note that the static pressure is a lift pressure amplitude. The remaining columns of Table 4.3 depict the static response amplitudes (i.e. moments and displacements) for the magnitude of the load required to simulate the lift moment amplitudes recorded during the wind tunnel test.

A comparison of Tables 4.2 and 4.3 indicates a systematic variation between the dynamic and static response amplitudes between each of the specimens. In particular, the dynamic analysis predicts that the arm moment will be approximately 65 to 75 percent of the column moment while the static analysis predicts that the arm and column moments should be equal. Note that the arm moments indicated in Tables 4.2 and 4.3 were computed at the face of the column while the column moments were computed at the longitudinal axis of the column. As a result, the arm moments computed from the static analyses are slightly less than the column moments. The variation between the static and dynamic results can be attributed to the inertial effects inherent in the dynamic analysis of a multi-degree-of-freedom system which are not accounted for in the single-degree-of-freedom dynamic magnification factor. In view of the considerable variation in the lift pressures to which the model specimens were subjected under galloping, the fact that the static analyses do not precisely simulate the dynamic response amplitudes is not considered significant. It is therefore concluded that equivalent static load models provide a reasonable means by which to simulate the dynamic response amplitudes exhibited by cantilevered support structures subjected to galloping and vortex shedding.

4.5 ANALYSES OF WIND TUNNEL PROTOTYPE SPECIMENS

Dynamic and static finite-element analyses were also conducted on the prototype wind tunnel specimens in a manner identical to that of the model specimens. Details of the dimensions of the prototype specimens were provided in Chapter Three. Scaling of the column moment amplitudes in the model specimens to the column moment amplitudes in the prototype specimens was based upon the one-eighth scaling factor used in the fabrication of the wind tunnel test specimens. The use of this scale factor to obtain the amplitudes of the column moments in the prototype specimens is illustrated in the following example. The column moment amplitude to which the model specimens were subjected is given by the following:

$$(Amplitude\ Column\ Moment)_{model} = [PA_{model}]L_{model} \tag{4.18}$$

where P is the amplitude of the across-wind lift pressure to which the specimen was subjected (note that, based upon aerodynamic and aeroelastic scaling laws, the magnitude of the lift pressure to which the model specimen was subjected is identical to the magnitude of the lift pressure to which the prototype specimen would be subjected), A_{model} is the projected area of the member subjected to the lift pressure, and L_{model} is the length of the moment arm.

The dimensions of the prototype specimens (i.e. dimensions of the support members and attachments) are eight times the dimensions of the model specimens. Therefore, the area of the member subjected to the lift pressure in the prototype specimen is 64 times the area of the member subjected to the lift pressure in the model specimen. In addition, the length of the moment arm in the prototype specimen is 8 times the length of the moment arm in the model specimen. Therefore, the amplitude of the column moment in the prototype specimens is related to the amplitude of the column moment in the model specimens by the following:

$$[Amplitude\ Column\ Moment]_{prototype} = 512[Amplitude\ Column\ Moment]_{model} \quad (4.19)$$

Equation 4.19 was used to calculate the column moment amplitudes to which the prototype specimens would have been subjected. Tables 4.4 and 4.5 summarize the dynamic and static response amplitudes, respectively, for the load magnitudes required to simulate the prototype column moment amplitudes.

Inspection of Tables 4.4 and 4.5 indicates that the magnitudes of the predicted stress ranges at the mast-arm and column exceed 42 MPa for each of the prototype structures. As will be discussed in Chapter Five, these stress ranges would be in excess of the constant amplitude fatigue limits for typical cantilevered support structures connection details. As a result, fatigue damage would be expected had these structures experienced galloping- and/or vortex-induced vibrations in the field.

A comparison of the data presented in Tables 4.4 and 4.5 with the data presented in Tables 4.2 and 4.3 indicates that the mass and stiffness properties of the model specimens were scaled with a reasonable level of accuracy. The laws of similitude indicate that the natural frequencies of the model specimens should be eight times the natural frequencies of the prototype specimens. A comparison of the natural frequencies depicted in Tables 4.2 and 4.4 indicates that this hold true with an error of less than 30 percent, which is considered excellent agreement. Similarly, for a given applied lift pressure, the displacements of the prototype specimens would be expected to be eight times the displacements of the model specimens. Inspection of the data indicates that this holds true with an error of less than 15 percent. As a result, it can be concluded that the dynamic behavior of the model specimens observed during the aeroelastic wind tunnel tests were representative of the behavior which would be exhibited by full-scale cantilevered support structures in the field.

4.6 ANALYSES OF FULL-SCALE SUPPORT STRUCTURES

Finite-element analyses of several full-scale cantilevered support structures were performed to validate the magnitudes of the equivalent static pressures derived from finite-element analyses of the wind tunnel test specimens. The structures included in these analyses were known to have experienced vertical-plane vibrations consistent with galloping. Estimates of at least one dynamic response amplitude was known (either displacements at the tip of the horizontal mast-arm or stress measurements) so that the dynamic response observed in the field could be simulated using finite-element analyses. Details of the full-scale support structures are provided in Figures 4.6 through 4.8.

4.6.1 Signal Structure #1

Figure 4.6 summarizes the details of a cantilevered signal support structure (identified as Signal Structure #1) which was observed to experience vertical-plane vibrations consistent with the galloping phenomenon. The dimensions of Signal Structure #1 are identical to the prototype dimensions of Specimen A (see Figure 3.10) which was tested in the wind tunnel.

Across-wind vibrations of Signal Structure #1 were documented on videotape. Observations of the videotape indicate that the natural frequency of the structure (corresponding to the vertical-plane mode of vibration) was approximately equal to 1.2 Hz. The amplitudes of vibration of the mast-arm were estimated at between 254 mm and 610 mm. Additionally, information obtained from the National Climatic Data Center indicated that the average hourly wind velocity on the day the vibrations were observed was between 11 m/s and 13 m/s with gust velocities up to approximately 18 m/s. As was shown in Chapter Three, these velocities are in good agreement with the velocities at which galloping occurred in Specimen A during the aeroelastic wind tunnel tests.

Finite-element analyses were performed to determine the magnitudes of the equivalent static pressures required to produce mast-arm displacements of 254 mm (indicated as Run A in Table 4.6) and 610 mm (indicated as Run B in Table 4.6). A level of damping equal to 0.75% of critical was assumed in each of the dynamic analyses. This level of damping is representative of the level of damping possessed by signal support structures in the field.

As is indicated in Table 4.6, the frequency corresponding to the vertical-plane mode of vibration predicted by finite-elements (1.13 Hz) correlates well with that observed on the videotape (1.2 Hz). Additionally, the 578 Pa equivalent static pressure required to produce a mast-arm displacement amplitude of 254 mm correlates reasonably well with the equivalent static pressures obtained from finite-element analyses of the wind tunnel specimens. The equivalent static pressure required to produce a displacement amplitude of 610 mm is significantly greater than that obtained from the wind tunnel tests. This large displacement was only observed during a short segment of the videotape and most likely corresponds to a short burst in the response due to gusts. Therefore, it is not necessary to consider an occasional extreme equivalent static pressure such as this in the design of cantilevered support structures for fatigue. It is the cumulative effect of the response over a few hours that dominates the fatigue damage.

4.6.2 Signal Structure #2

Figure 4.7 summarizes the details of a cantilevered signal support structure (identified as Signal Structure #2) which was subjected to a series of full-scale field tests in a research program conducted by McDonald et al. [32]. The scope of this research program was summarized in Chapter Two. The results of these field tests indicated that Signal Support Structure #2 was subjected to a maximum measured stress range in the vertical support (at a location approximately 330 mm from the base) equal to approximately 34 MPa under wind velocities in the range of 4.5

m/s. The results of vertical-plane free-vibration tests indicated that the natural frequency of the structure was 0.74 Hz and the damping was 0.62% of critical.

A dynamic finite-element analysis was performed to determine the equivalent static pressure amplitude required to produce a stress range equal to 34 MPa at a location 330 mm from the base of the vertical support. The results of this analysis are summarized in Table 4.7. As is indicated, good correlation was obtained between the predicted and measured natural frequencies. An equivalent static pressure amplitude equal to 355 Pa was required to produce a stress range in the column equal to 34 MPa.

The equivalent static pressure amplitude required to produce the observed dynamic response in this structure is less than the magnitudes of the equivalent static pressures obtained from the wind tunnel test results. This result would be expected considering that the structure tested by McDonald et al. [32] was only subjected to a 4.5 m/s wind velocity. Furthermore, this result highlights the fact that the load to which cantilevered support structures are subjected is a function of the wind velocity. It can reasonably be assumed that this structure would have been subjected to equivalent static lift pressure amplitudes significantly greater than 355 Pa had higher wind velocities been observed during the testing of this structure.

4.6.3 Sign Structure #1

Figure 4.8 summarizes the details of a cantilevered sign support structure (identified as Sign Structure #1) which collapsed as a result of the propagation of fatigue cracks in the anchor bolts. Fractographic analyses of the failed anchor bolts indicated that the structure was subjected to vertical-plane oscillations which resulted in anchor bolt stress ranges of 69 to 103 MPa [22].

As is indicated in Table 4.8, an equivalent static pressure amplitude of between 347 Pa and 520 Pa is required to produce anchor bolt stress ranges of 69 MPa and 103 MPa, respectively.

Once again, the magnitude of this equivalent static pressure correlates reasonably well with the pressures obtained from finite-element analyses of the wind tunnel model specimens.

4.7 SUMMARY

4.7.1 Galloping

The results of finite-element simulations of the wind tunnel experiments indicate that cantilevered sign and signal support structures are subject to equivalent static lift pressure amplitudes in the range of approximately 420 Pa to 740 Pa during occurrences of galloping-induced vibrations. This range in equivalent static lift pressures is correlated by the results of finite-element analyses of full-scale support structures which were known to experience vertical-plane oscillations consistent with the galloping phenomenon.

Considering the inherent variability in the response of a structure to galloping, the range in equivalent static pressure amplitudes observed in this study are remarkably consistent. Based upon these results, it is recommended that an equivalent static lift pressure amplitude equal to 500 Pa (i.e. an equivalent static lift pressure range equal to 1 kPa) be used in the design of cantilevered sign and signal support structures for galloping-induced fatigue. This equivalent static lift pressure range should be applied vertically (as was indicated in the load models presented in Section 4.3.2) to the projected area of all sign and signal attachments mounted to the horizontal mast-arm.

4.7.2 Vortex Shedding

The results of finite-element simulations of the wind tunnel experiments indicate that cantilevered support structures mounted without attachments should be designed for vortex-induced fatigue provided that the magnitude of the critical wind velocity (as calculated by the

Strouhal relation) is greater than approximately 5 m/s. The magnitude of the equivalent static lift pressure range should be calculated based upon the provisions contained in the present AASHTO Standard Specifications for Structural Supports for Highway Signs, Luminaires, and Traffic Signals. This equivalent static lift pressure range should be applied vertically to the horizontal support of the structure as per the load model described in Section 4.3.2.

Table 4.1 - Observed Wind-Tunnel Test Results.

Support Structure[1]	Attachment Detail[1]	Flow Direction	Natural Frequency[2] (Hz)	Damping[2] (%)	Figure[3]	Flow Velocity[4] (m/s)	Amplitude Column Moment[5] (N-m)
A	TS-2D	Rear	6.95	0.12	3.21(b)	18.2	14.7
C	RS-1D	Front	10.00	0.13	3.23(a)	11.2	116.6
C	RS-3D	Front	11.24	0.17	3.24(a)	13.1	54.5
C	None	-	14.10	0.14	3.26	5.5	122.3

[1]Specimen and attachment details summarized in Chapter Three.
[2]As measured from vertical-plane, free-vibration tests.
[3]Corresponding figure in Chapter Three.
[4]Velocity at which peak vertical-plane response was observed.
[5]Peak column moment amplitude measured at base of vertical support.

Table 4.2 - Dynamic Finite-Element Analysis Results of Wind Tunnel Model Specimens.

Support Structure	Attachment Detail	Natural Frequency (Hz)	Damping (%)	Equivalent Static Pressure (Pa)	Amplitude Column Moment (N-m)	Amplitude Arm Moment (N-m)
A	TS-2D	6.1	0.12	423	14.7	10.3
C	RS-1D	12.4	0.13	739	116.6	83.5
C	RS-3D	13.6	0.17	593	54.5	38.9
C	None	16.6	0.14	2091	122.3	79.4

Support Structure	Attachment Detail	Amplitude Column Displacement (mm)	Amplitude Arm Displacement (mm)
A	TS-2D	2.5	21.9
C	RS-1D	4.1	18.9
C	RS-3D	1.9	8.8
C	None	4.2	18.6

Table 4.3 - Static Finite-Element Analysis Results of Wind Tunnel Model Specimens.

Support Structure	Attachment Detail	Static Pressure (Pa)	Amplitude Column Moment (N-m)	Amplitude Arm Moment (N-m)	Amplitude Column Displ. (mm)	Amplitude Arm Displ. (mm)
A	TS-2D	575	14.7	14.6	2.9	31.1
C	RS-1D	884	116.6	112.9	4.5	23.0
C	RS-3D	724	54.5	53.2	2.1	11.0
C	None	2551	122.3	115.8	4.8	23.0

Table 4.4 - Dynamic Finite-Element Analysis Results of Wind Tunnel Prototype Specimens.

Support Structure	Attachment Detail	Natural Frequency (Hz)	Damping (%)	Equivalent Static Pressure (Pa)	Amplitude Column Moment (N-m)	Amplitude Arm Moment (N-m)
A	TS-2D	1.05	0.12	460	7520	5710
C	RS-1D	1.36	0.13	740	59700	43300
C	RS-3D	1.41	0.17	590	27900	19800
C	None	1.86	0.14	2090	55600	36400

Support Structure	Attachment Detail	Amplitude Column Displ. (mm)	Amplitude Arm Displ. (mm)	Column Stress Range (MPa)	Arm Stress Range (MPa)
A	TS-2D	17	151	42	66
C	RS-1D	32	146	150	108
C	RS-3D	15	67	70	50
C	None	29	127	139	91

Table 4.5 - Static Finite-Element Analysis Results of Wind Tunnel Prototype Specimens.

Support Structure	Attachment Detail	Static Pressure (Pa)	Amplitude Column Moment (N-m)	Amplitude Arm Moment (N-m)	Amplitude Column Displ. (mm)	Amplitude Arm Displ. (mm)
A	TS-2D	575	7530	7520	19	192
C	RS-1D	884	59700	59200	35	177
C	RS-3D	724	27900	27300	16	85
C	None	2550	55600	53200	32	157

Support Structure	Attachment Detail	Column Stress Range (MPa)	Arm Stress Range (MPa)
A	TS-2D	42	77
C	RS-1D	150	129
C	RS-3D	70	68
C	None	139	133

Table 4.6 - Dynamic Finite-Element Analysis Results of Full-Scale Cantilevered Signal Support Structure (**Signal Structure #1**).

Support Structure	Run Number	Natural Frequency (Hz)	Assumed Damping (%)	Equivalent Static Pressure (Pa)	Amplitude Column Moment (N-m)	Amplitude Arm Moment (N-m)
Signal #1	A	1.13	0.75	578	9650	7120
Signal #1	B	1.13	0.75	1390	23200	17100

Support Structure	Run Number	Amplitude Column Displ. (mm)	Amplitude Arm Displ. (mm)	Column Stress Range (Pa)	Arm Stress Range (MPa)
Signal #1	A	30	254	74	113
Signal #1	B	72	610	180	270

Table 4.7 - Dynamic Finite-Element Analysis Results of Full-Scale Cantilevered Signal Support Structure (**Signal Structure #2**).

Support Structure	Natural Frequency (Hz)	Measured Damping (%)	Equivalent Static Pressure (Pa)	Amplitude Column Moment (N-m)	Amplitude Arm Moment (N-m)
Signal #2	0.83	0.62	355	8460	7510

Support Structure	Amplitude Column Displ. (mm)	Amplitude Arm Displ. (mm)	Column Stress Range (Pa)	Arm Stress Range (MPa)
Signal #2	10	151	34	47

Table 4.8 - Dynamic Finite-Element Analysis Results of Full-Scale Cantilevered Sign Support Structure (**Sign Structure #1**).

Support Structure	Run Number	Natural Frequency (Hz)	Assumed Damping (%)	Equivalent Static Pressure (Pa)	Amplitude Column Moment (N-m)	Amplitude Arm Moment Bot. Chord (N-m)
Sign #1	A	1.27	1.0	347	92800	4790
Sign #1	B	1.27	1.0	520	139200	7190

Support Structure	Run Number	Amplitude Column Moment Top Chord (N-m)	Amplitude Column Displ. (mm)	Amplitude Arm Displ. (mm)	Column Stress Range (MPa)	Anchor Bolt Stress Range (MPa)
Sign #1	A	912	24	53	20	69
Sign #1	B	1370	36	80	30	103

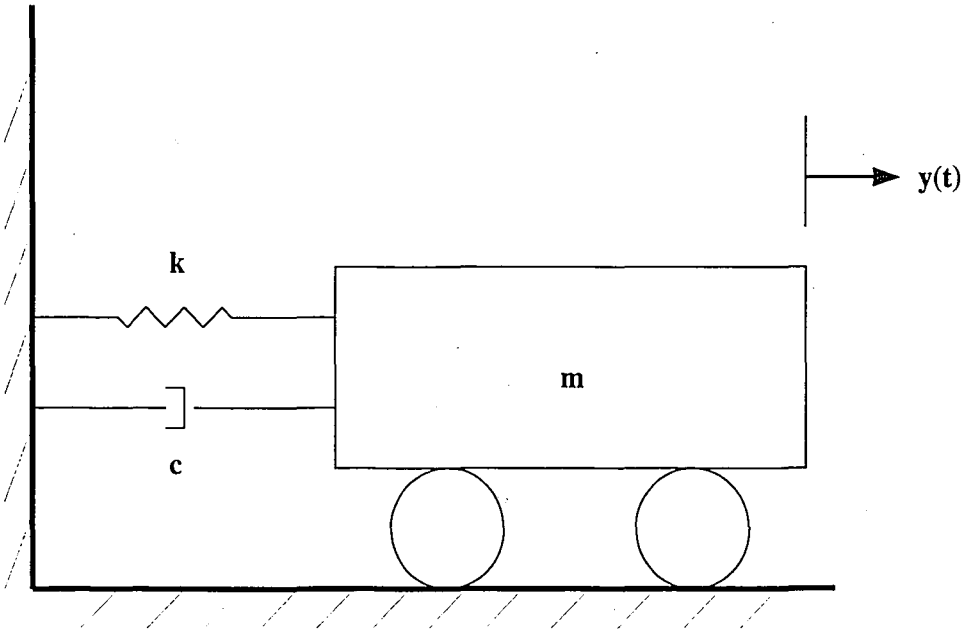

Figure 4.1 - Single-Degree-of-Freedom (SDOF) System.

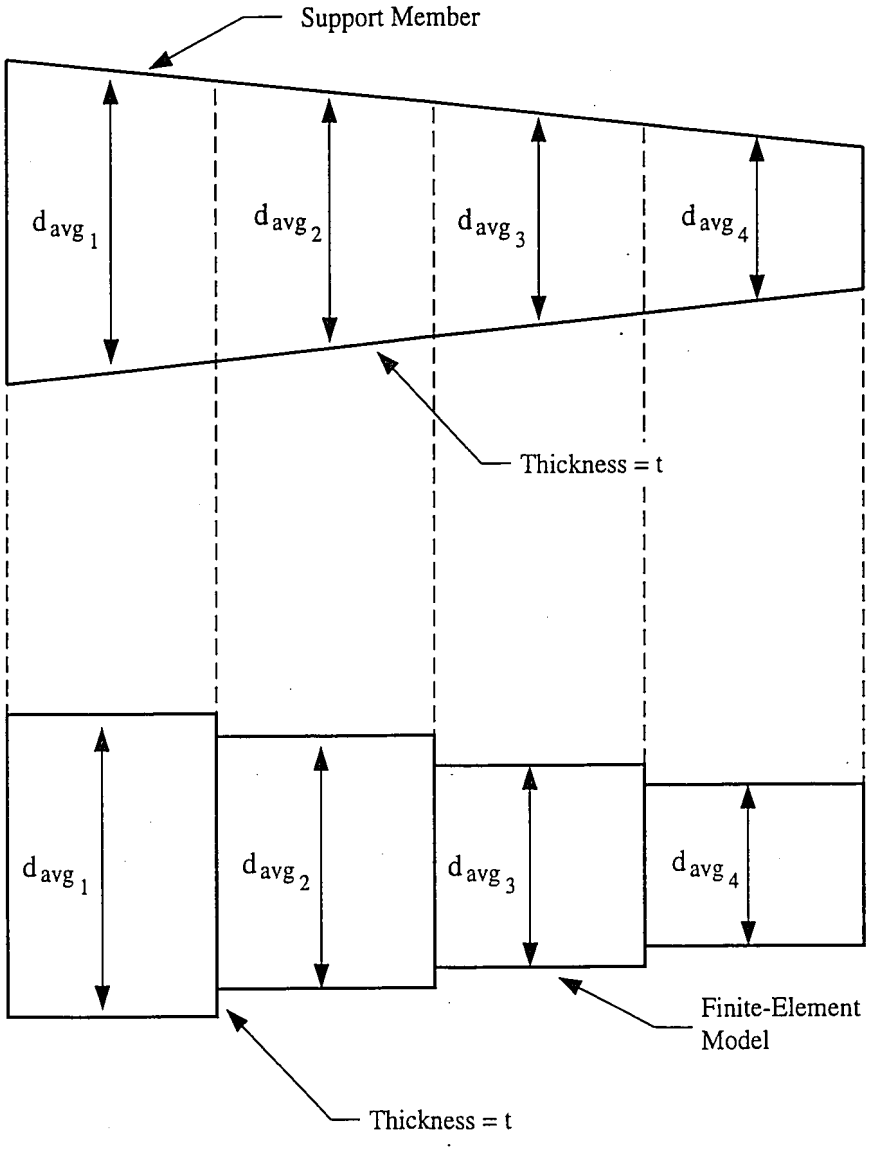

Figure 4.2 - Finite-Element Model of Tapered Members.

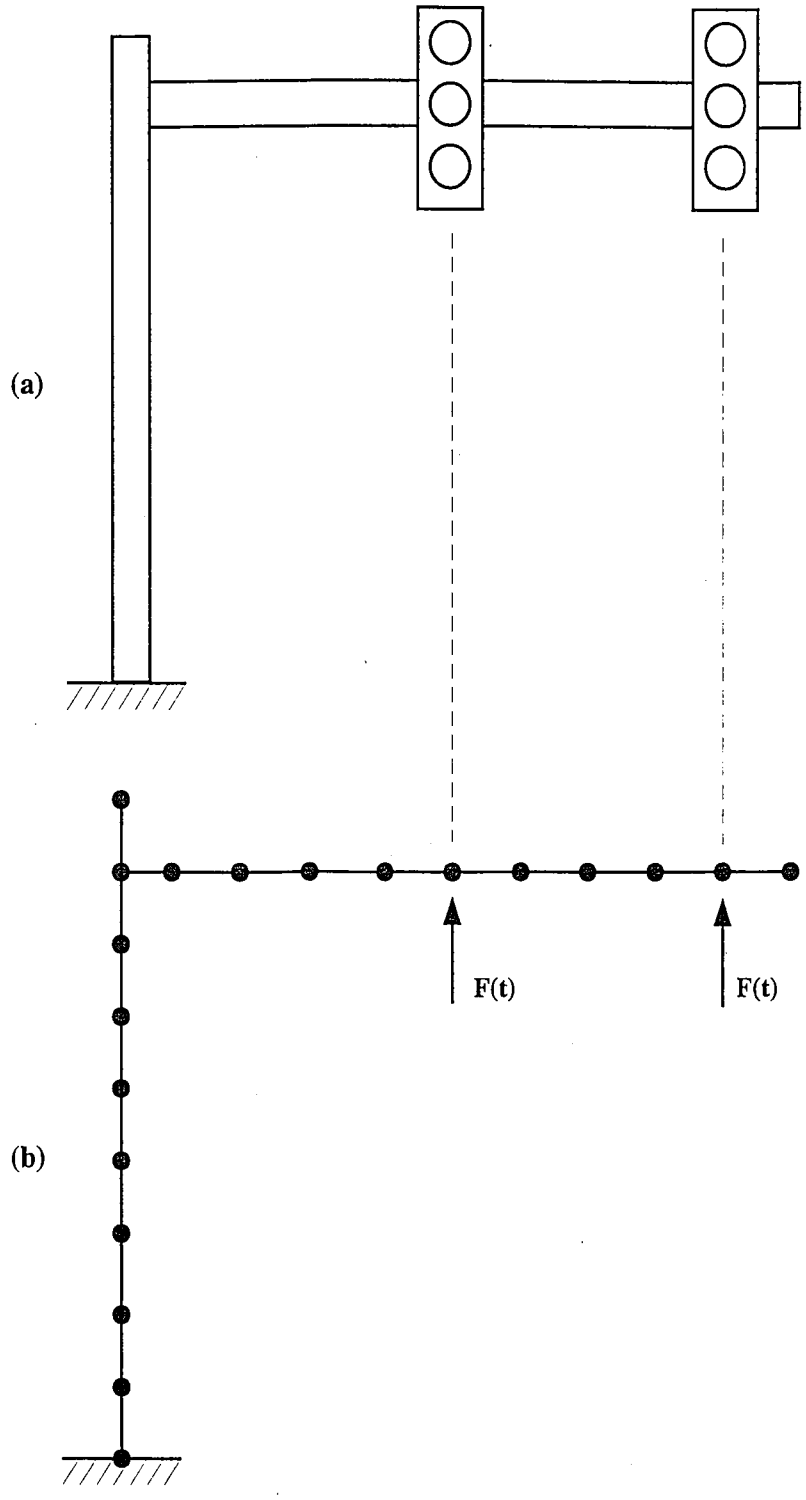

Figure 4.3 - Load Model for Galloping From Signals; (a) Support Structure (b) FEM Model.

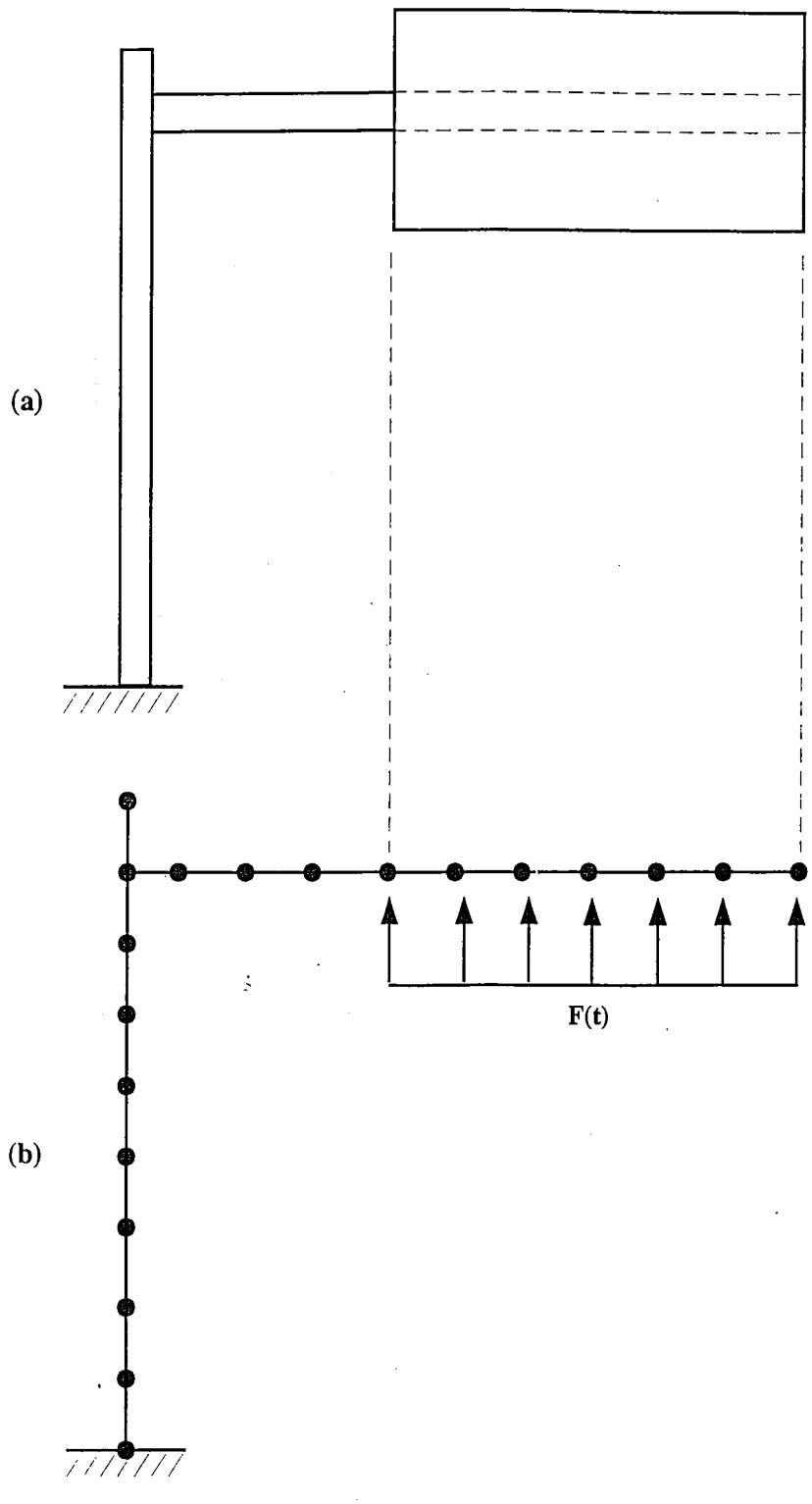

Figure 4.4 - Load Model for Galloping From Signs; (a) Support Structure (b) FEM Model.

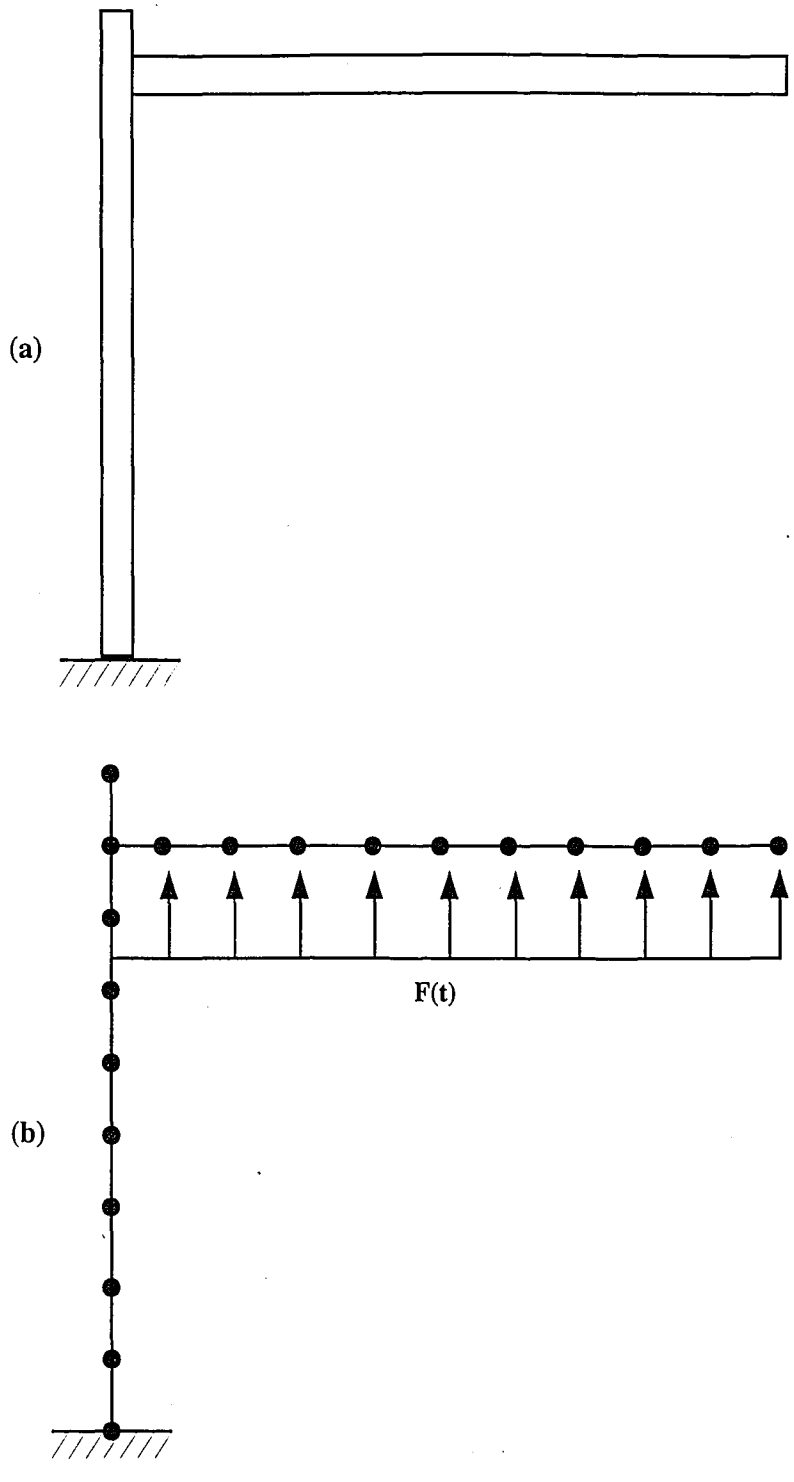

Figure 4.5 - Load Model for Vortex Shedding From Mast-Arm; (a) Support Structure (b) FEM Model.

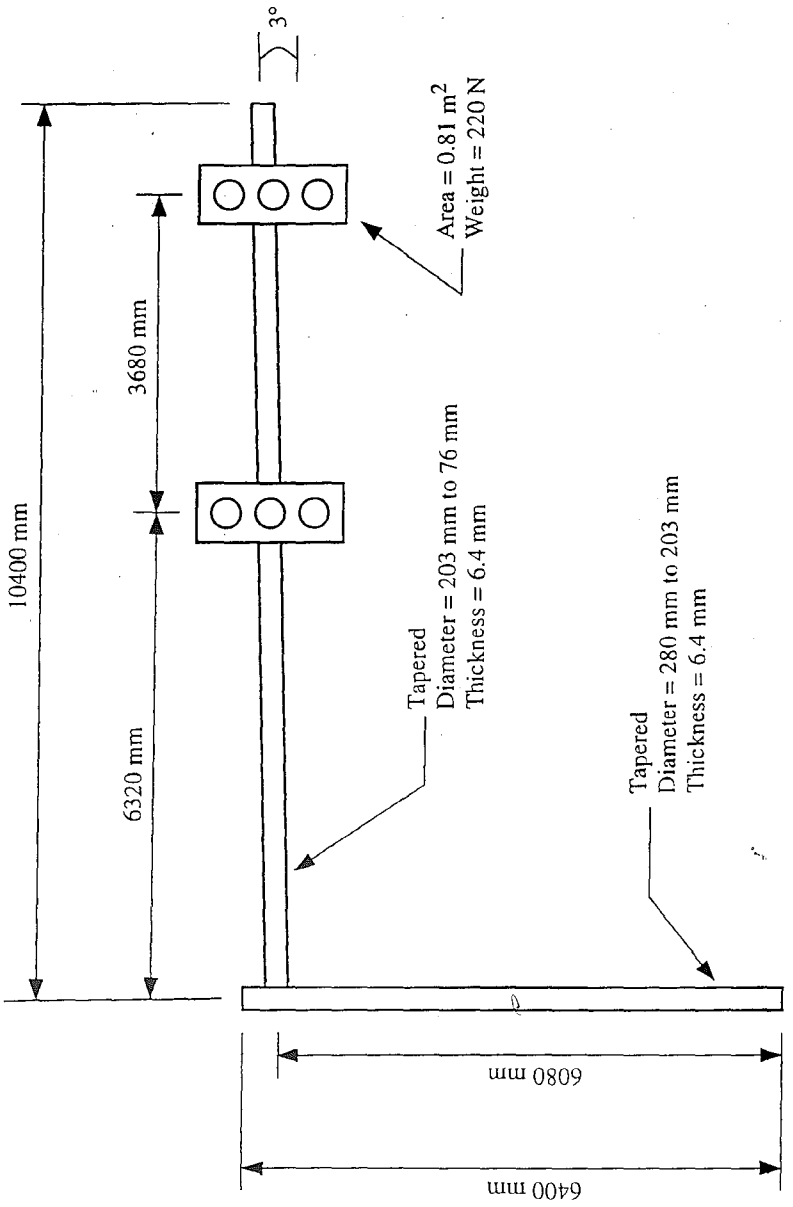

Figure 4.6 - Details of Full-Scale Cantilevered Signal Support Structure (**Signal Support #1**).

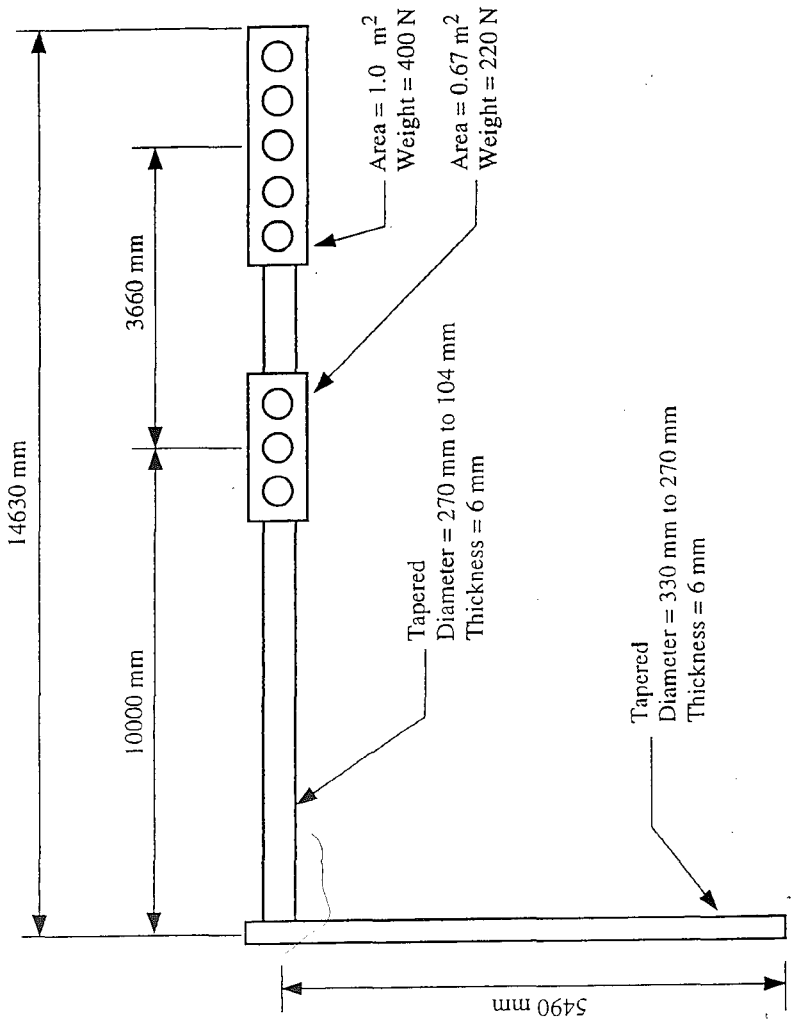

Figure 4.7 - Details of Full-Scale Cantilevered Signal Support Structure (**Signal Support #2**).

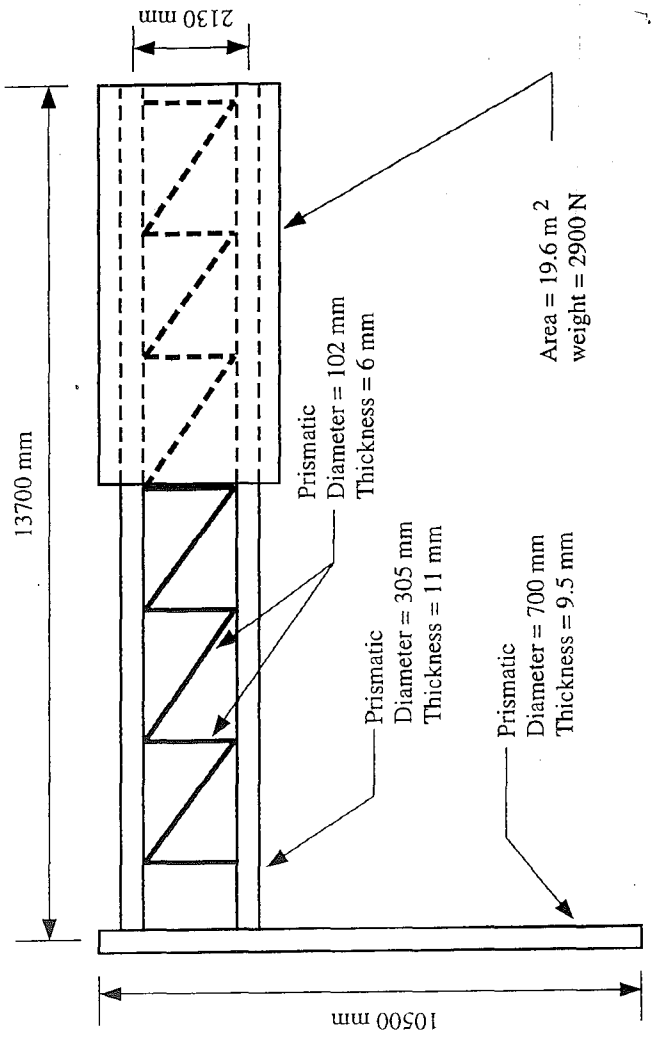

Figure 4.8 - Details of Full-Scale Cantilevered Sign Support Structure (**Sign Support #1**).

Chapter Five

FATIGUE CATEGORIZATION OF CONNECTION DETAILS

5.1 INTRODUCTION

The current AASHTO Standard Specifications for Structural Supports for Highway Signs, Luminaires and Traffic Signals [4] contain provisions which specify that cantilevered support structures should be designed for infinite fatigue life in accordance with the procedures outlined in the AASHTO bridge specifications [3]. The geometrical configuration of typical cantilevered support structure connection details, however, varies significantly from the bridge details found in the AASHTO bridge specifications. As a result, designers are faced with significant uncertainty when attempting to apply the provisions of the AASHTO bridge specifications to the design of cantilevered support structures for fatigue.

This chapter describes the categorization of typical cantilevered support structure connection details to the existing AASHTO and/or AWS fatigue design curves. Section 5.2 summarizes the factors which influence the fatigue strength of welded details. Section 5.3 describes the methodology which was used to categorize typical cantilevered support structure connection details to the existing AASHTO and/or AWS fatigue design curves. The actual categorization of cantilevered support structure connection details is provided in an appendix to this report.

5.2 FATIGUE OF WELDED DETAILS

Fatigue is a complex phenomenon governed by factors which are highly variable and difficult to quantify. The results of previous research [19, 20, 28], however, indicate that the

fatigue resistance of welded details can be characterized by two primary parameters: (1) nominal stress range and (2) notch severity. The notch severity describes the severity of the stress concentration associated with a welded detail. It includes the effects of the global stress concentration associated with the configuration of the detail and the effects of local stress concentration due to the geometry of the weld and the existence of any weld discontinuities.

The provisions of the AASHTO bridge specifications [3] for the design of structures for fatigue are based upon a nominal stress approach in which details are grouped into categories (i.e. S-N curves) according to their relative fatigue resistance. The AASHTO Specifications contain seven design S-N curves labeled A through E′ in order of decreasing fatigue strength (there is also an eighth S-N curve, labeled Category F, for the design of fillet welds loaded in shear. This category rarely controls the design of structures for fatigue). Each design S-N curve possesses a constant amplitude fatigue limit below which infinite fatigue life is obtained under constant amplitude loading. The loading is characterized by the nominal stress range remote from the detail.

The AASHTO fatigue design categories were developed from the results of full-scale, constant amplitude fatigue testing of bridge details. Because fatigue resistance is highly variable, the design categories are based upon a lower-bound 95 percent confidence limit. Thus, the AASHTO S-N design categories implicitly account for variables which are highly variable and difficult to quantify such as local stress concentration associated with weld geometry and weld discontinuities. Details which are grouped within the same design category generally exhibit similar cracking modes and are subject to similar stress concentrations. For example, transverse stiffeners and transverse butt welds with reinforcement are both Category C details. Thus, even though the geometrical configurations of these details are very different, transverse stiffeners and

transverse butt welds with reinforcement exhibit similar fatigue resistance because the severity of the stress concentration associated with each of the details is similar.

5.3 CATEGORIZATION OF CONNECTION DETAILS

The categorization of cantilevered support structure connection details to the existing AASHTO and/or AWS fatigue design curves is based upon a general understanding of fatigue behavior, knowledge of previous research which has led to the development of the existing fatigue design curves, experience with structural failures which have resulted from fatigue, and engineering judgement. The fact that details which possess similar stress concentrations and cause cracks to form at the same location (e.g. the toe of a weld) was used to link the behavior of cantilevered support structure connection details to the existing knowledge base of bridge details which have been subjected to extensive testing. A similar approach has been used previously to categorize the fatigue resistance of ship details to the AASHTO fatigue design curves [23]. Whenever possible, existing data related to the fatigue testing of a particular cantilevered support structure connection detail was reviewed prior to the categorization of that detail to an AASHTO and/or AWS fatigue design curve [21].

The appendix to this report contains the categorization of typical cantilevered support structure connection details to the existing AASHTO [3] and/or AWS [6] fatigue design categories. Identification of the typical cantilevered support structure connection details was based upon a review of: (1) state department of transportation standard drawings of cantilevered sign, signal, and luminaire support structures, (2) literature obtained from cantilevered support structure manufacturers, and (3) literature developed by the AASHTO-AGC-ARTBA Task Force No. 13 [1]. The format of the categorization is similar to the format of the categorization of bridge details found in Reference 3.

Chapter Six

ANCHOR BOLT FATIGUE TESTS

6.1 INTRODUCTION

As was discussed in Chapter Five, previous research [19, 20, 28] indicates that the fatigue strength of welded details is primarily dependent on two parameters: (1) nominal stress range and (2) notch severity. Notch severity is a function of the stress concentration associated with the detail, local weld geometry, and weld discontinuities. Experience with the behavior of welded components under the application of repeated loading indicates that details which possess similar stress concentrations (e.g. the toe of a weld) and are subjected to similar loading (e.g. nominal stresses normal to the axis of the weld) will behave in a similar manner even though the physical appearance of these details may be significantly different. This methodology was used in Chapter Five to categorize welded cantilevered support structure connection details according to the existing AASHTO and/or AWS fatigue design curves.

Anchor bolts, however, are unique with respect to their behavior under the application of repeated loading. For example, fatigue cracking in anchor bolts initiates at the thread root. The stress concentration at the root of a thread is significantly different from the stress concentrations associated with the welded details for which the AASHTO fatigue design curves were developed. Furthermore, being non-welded structural components, the fatigue strength of anchor bolts is influenced by parameters which do not significantly influence the fatigue strength of weldments (e.g. the lack of tensile residual stresses resulting from the welding process make stress parameters such as maximum stress significant with respect to the fatigue strength of anchor bolts). As a

result, existing knowledge of the fatigue strength of welded details cannot be used to predict anchor bolt fatigue strength.

Several research programs, which will be summarized in Section 6.2.1, have been previously conducted to evaluate the fatigue strength of anchor bolts. The results of these research programs indicate that the lower-bound fatigue strength of axially-loaded, snug-tight anchor bolts is consistent with the AASHTO Category E′ fatigue design curve in the regime of finite life (e.g. less than two million cycles). Similarly, the fatigue strength of axially-loaded, fully-tightened anchor bolts in the regime of finite life has been found to be consistent with the AASHTO Category E fatigue design curve. No data, however, have been acquired below a stress range of approximately 69 MPa. As a result, it is unknown whether the AASHTO Category E and E′ fatigue design curves accurately represent the fatigue strengths of fully-tightened and snug-tight anchor bolts, respectively, in the regime of infinite life (e.g. greater than two million cycles).

A series of fatigue tests were conducted within the scope of the current research program to extend the existing anchor bolt fatigue database into the infinite life regime. Specifically, the objective of these tests was to determine a lower-bound estimate of the constant amplitude fatigue limit (CAFL) of double-nutted, snug-tight anchor bolts subjected to axial tension. In order to accomplish this objective, the test program was arranged so as to evaluate the effects of: (1) maximum stress, (2) yield strength, (3) thread forming method, (4) bolt pretension, and (5) misalignment. The fatigue design recommendations presented in Section 6.5 are based upon a worst-case condition so that the effects of these secondary variables need not be explicitly considered in the design process. Material property tests were also performed to ensure that the strength, ductility, and fracture toughness of the specimens obtained for this study were in accordance with existing anchor bolt material property specifications.

The effects of bolt diameter, thread series, and galvanizing were not explicitly considered in the experimental program following a review of previous research (described in Section 6.2.1) which indicated that these variables do not significantly influence the fatigue strength of anchor bolts. Furthermore, the influence of thread fit on the fatigue strength of anchor bolts was not specifically considered within the scope of the test program. Rather, thread fit was considered a random variable, the effects of which were incorporated in the sample of test specimens.

Chapter Six is organized into five sections. Section 6.2 provides a summary of the previous research pertaining to anchor bolt fatigue strength and discusses the provisions for the design of bolts for fatigue which are contained in existing design specifications. Section 6.3 summarizes the specimen details, experimental set-up, and test procedures used in this test program. The results of the fatigue tests are presented and discussed in Section 6.4. Finally, recommendations for the design of anchor bolts for fatigue are presented in Section 6.5.

6.2 BACKGROUND

6.2.1 Previous Research

Frank [24] performed fatigue tests to evaluate the effects of type of steel, thread series, nominal diameter, galvanizing, thread forming method (i.e. cut vs rolled), and stress range on the fatigue strength of "snug-" and "fully-tightened" anchor bolts subjected to axial tension. In Frank's tests, snug was defined by a level of torque equal to 271 N-m. Fully-tightened was defined as one-third-of-a-turn beyond snug. The tests included anchor bolts fabricated from ASTM A36, ASTM A193 Grade B7, and AISI 4340 (heat treated) steels in nominal diameters ranging from 35 mm to 51 mm. Thread series consisting of 8UN, 6UNC, and 4½UNC were included in the test program. Single- and double-nutted anchor bolts (i.e. anchor bolts configured with one nut on either side of the baseplate) were also considered. Frank conducted each of the

fatigue tests at a maximum stress corresponding to 75 percent of the minimum specified yield strength of the material.

The results of Frank's research indicated that the effects of nominal diameter, thread series, galvanizing, type of steel, and thread forming method were negligible with respect to the fatigue strength of anchor bolts.. The results of tests on the fully-tightened specimens indicated that tightening of the nuts to one-third-of-a-turn beyond snug resulted in increased fatigue strengths as compared to the double-nutted, snug-tight specimens and the single-nut specimens. Failure of the single-nut specimens was consistently observed to occur at the first engaged thread of the exterior nut. Failure of the double-nutted, snug-tight specimens was observed at either: (1) the first engaged thread of the exterior nut or (2) at multiple threads within the exterior nut. Tightening of the double-nutted anchor bolts to one-third-turn-beyond snug was found to shift the mode of failure to the threaded region outside of the connection (i.e. below the leveling nut).

The shift in failure mode from the first engaged thread of the exterior nut to the threaded region below the leveling nut in fully-tightened, double-nutted anchor bolts can be attributed to a variation in the distribution of the applied load which occurs in the fully-tightened connection. In double-nutted, snug-tight anchor bolts subjected to axial tension, the entire applied load range is carried by the exterior nut. Furthermore, a majority of the load is transferred to the bolt at the first engaged thread. As a result, the first engaged thread is subjected to the largest stress range and is the critical location with respect to the initiation of fatigue cracks. Tightening of the double-nutted connection to one-third-of-a-turn beyond snug pretensions the short length of bolt between the interior and exterior nuts, creating a clamping force which results in a more even distribution of the applied load between the exterior and interior nuts. This effect was evident in strain gage measurements made by Frank during testing of the fully-tightened, double-nutted anchor bolts. These measurements indicated that approximately one-third of the applied load was

taken by the interior nut. Furthermore the distribution of load within the nuts of fully-tightened, double-nut connections is more uniform (i.e. the transfer of load is not concentrated at the first engaged thread). As a result, the critical location for the initiation of fatigue cracks in fully-tightened, double-nutted anchor bolts shifts from the first engaged thread of the exterior nut to the free-length of bolt below the leveling nut which is not subjected to pretensioning.

The beneficial effects of pretension in conventional bolted connections loaded in tension is well known and is described extensively in Reference 30. However, the behavior of conventional bolted connections subjected to axial tension is inherently different from that of fully-tightened, double-nutted anchor bolts. In a conventional connection, the entire length of bolt is subjected to the pretension force. In fully-tightened, double-nutted anchor bolt connections, the exposed length of bolt below the leveling nut is not subjected to the beneficial effects of pretensioning. As a result, fully-tightened, double-nutted anchor bolts are, in general, more susceptible to fatigue cracking at this location.

Dusel et al. [16] conducted a similar test program to evaluate the effects of type of steel, nominal diameter, bolt length, and stress range on the fatigue strength of snug- and fully-tightened (i.e. tightened to one-third-of-a-turn beyond snug) double-nutted anchor bolts subjected to axial tension. The tests included anchor bolts fabricated from ASTM A307 and ASTM A449 steels in nominal diameters ranging from 25 mm to 44 mm. Snug-tight was defined by a level of torque equal to 136 N-m. Furthermore, the tests were conducted at maximum stress levels ranging from approximately 10 percent to 100 percent of the yield strength of the material.

Similar to the results of the research performed by Frank [24], Dusel et al. [16] found that the effects of nominal diameter, type of steel, and bolt length were insignificant. The results of tests on the fully-tightened specimens indicated that tightening of the nuts to one-third-of-a-turn beyond snug resulted in increased fatigue strengths as compared to the snug-tight specimens.

Failure of all of the snug-tight specimens was observed at the first engaged thread of the exterior nut. Failure of the fully-tightened specimens was observed at one of three locations: (1) the first engaged thread of the exterior nut; (2) within the threads of the interior nut; or (3) within the threaded region outside of the connection (i.e. below the leveling nut).

The database of fatigue test results generated by Frank [24] and Dusel et al. [16] for single-nutted and double-nutted, snug-tight anchor bolts subjected to axial tension is depicted in Figure 6.1. As will be discussed in Section 6.4.3, the magnitude of the maximum stresses to which anchor bolts are subjected significantly influences the fatigue strength. Increases in the magnitude of the maximum stress tend to decrease the fatigue strength. Therefore, the data shown in Figure 6.1 include only those tests conducted at maximum stresses greater than 60 percent of the minimum specified yield strength of the material. A maximum stress equal to 60 percent of the minimum specified yield strength corresponds to the allowable static design stress for anchor bolts [4]. As a result, the data shown in Figure 6.1 represent a worst-case condition in terms of the fatigue strength of snug-tight anchor bolts. Under actual service load conditions, anchor bolts are not expected to be subjected to maximum stresses greater than 60 percent of the material yield strength. For a given applied load range, bolts which are less efficiently designed would be expected to have longer fatigue lives than are exhibited in Figure 6.1.

The results of a statistical analysis of the data in Figure 6.1 (the methods of which were discussed in Chapter Five) indicates that the lower-bound, corresponding to the mean minus two-times the standard deviation, falls between the AASHTO Category E and E′ fatigue design curves. Therefore, the fatigue strength of axially-loaded, snug-tight anchor bolts is conservatively rounded down to the nearest AASHTO fatigue design curve, i.e. Category E′. Note that this conclusion is only applicable in the regime of finite life (i.e. less than two million cycles).

The database of fatigue test results generated by Frank [24] and Dusel et al. [16] for double-nutted anchor bolts tightened to one-third-of-a-turn beyond snug and subjected to axial tension is depicted in Figure 6.2. Again, the data shown in Figure 6.2 include only those tests conducted at maximum stresses corresponding to greater than 60 percent of the minimum specified yield strength of the material. The results of a statistical analysis of the database indicates that the lower-bound falls between the AASHTO Category D and E fatigue design curves. Therefore, the fatigue strength of axially-loaded, fully-tightened anchor bolts is conservatively approximated by the AASHTO Category E fatigue design curve in the regime of finite life (i.e. less than two million cycles).

6.2.2 Review of Existing Design Specifications

The following summarizes the provisions contained in three design specifications (i.e. AISC LRFD [5], BS7608 [9], and Eurocode 3 [18]) known to have provisions for the design of bolts for fatigue. It should be noted that none of the above design specifications specifically addresses the design of anchor bolts for fatigue. It is useful, however, to compare the provisions contained in these specifications to the available test data related to the fatigue strength of anchor bolts.

In the AISC LRFD Specifications [5], bolted joints loaded in direct tension are evaluated in terms of the maximum unfactored tensile load attributed to each bolt, including any prying force. Provisions for the calculation of prying loads are provided in Part 11 of the LRFD Manual. The AISC LRFD procedure for the design of bolts for fatigue is identical to the AISC ASD procedure and is based upon a specification developed by the Research Council on Structural Connections (RSCS) [37]. Typically, the AISC provisions are applied to hanger-type or bolted flange connections where the bolts are tensioned against the plies.

The AISC LRFD Specifications for the design of bolts for fatigue are based upon the maximum applied load rather than the applied stress range because the fraction of the externally applied stress range to which fully-tightened, axially-loaded bolts are subjected is highly variable and very difficult to estimate analytically [30]. In the AISC Specifications, the fatigue strength of high strength bolts is given in terms of the nominal unthreaded area of the bolt. The allowable total service load in fatigue for more than 500,000 cycles (i.e. infinite life) is 25 percent of the product of the nominal area of the bolt and the ultimate tensile strength.

In a majority of design specifications, the design of bolts for fatigue is typically based upon the tensile stress area of the bolt. The tensile stress area is defined as:

$$A_T = \frac{\pi}{4}(d - \frac{0.9743}{n})^2 \qquad (6.1)$$

where A_T is the tensile stress area (in^2), d is the nominal diameter of the unthreaded portion of the bolt (in), and n is the number of thread per inch. In order to convert the tensile stress area to metric units (mm^2), the tensile stress area computed using the above equation should be multiplied by 645. Generally, the tensile stress area is approximately 75 percent of the nominal area of the bolt. Thus, for the purposes of comparison to other specifications, the allowable service stress for greater than 500,000 cycles permitted in the AISC Specifications is actually about 0.33 times the ultimate tensile strength of the bolt.

In BS7608 [9] a slightly different approach is used for the design of axially-loaded, fully-tightened bolts for fatigue. As in the AISC provisions, the problem of calculating the actual stress range in bolts in fully-tightened connections is deemed intractable. In order to circumvent this problem, BS7608 assumes that the stress range acting on the tensile stress area of the bolt is 20 percent of the total applied load, regardless of the magnitude of the actual fluctuating portion of the load. This assumption represents a conservative estimation of the actual stress range to which

fully-tightened bolts are subjected under fatigue loading in a variety of connections. The S-N fatigue design curve is given as a proportion of the tensile strength of the bolt, so that for high-strength bolts with a tensile strength of 785 MPa, the resulting S-N curve falls between the AASHTO Category E and E′ design curves for less than 2 million cycles. In BS7608, the tensile strength may not be taken as greater than 785 MPa even when higher strength bolts are used. The CAFL for bolts is given as 6 percent of the tensile strength, with a slight reduction for bolts larger than 25 mm in diameter.

For example, for fully-tightened AASHTO Grade 105 anchor bolts with a tensile strength equal to 862 MPa, the tensile strength would be taken as 785 MPa under the BS7608 provisions, and the S-N design curve for less than 2 million cycles would fall between the AASHTO Category E and E′ design curves. For greater than 2 million cycles, the CAFL would be taken as 6 percent of the allowable tensile strength (785 MPa), or 47 MPa (which is very close to the CAFL for the AASHTO Category D fatigue design curve). For fully-tightened Grade 55 anchor bolts with a tensile strength equal to 517 MPa, the S-N design curve for less than 2 million cycles would fall below the AASHTO Category E′ design curve. For greater than 2 million cycles, the CAFL would be taken as 6 percent of the tensile strength (517 MPa), or 31 MPa (which is very close to the CAFL for the AASHTO Category E fatigue design curve).

If the assumed stress range of 20 percent of the peak load is applied to the AISC provisions, the AISC provisions would imply a CAFL of 20 percent of 0.33 times the ultimate tensile strength (for greater than 500,000 cycles). This is equivalent to 6.6 percent of the tensile strength. Given this assumed stress range, the provisions of the AISC and BS7608 Specifications for the design of bolts for infinite life are approximately in agreement.

In the Eurocode 3 [18], the design S-N curve for axially-loaded bolts is specified to be approximately equivalent to the AASHTO Category E′ fatigue design. Furthermore, the design

S-N curve is independent of the tensile strength of the bolt. The Eurocode S-N curve for bolts is approximately equivalent to the BS7608 S-N curve (and therefore the AISC provisions) for high-strength bolts with yield strengths greater than 785 MPa. AISC and BS7608 would be more conservative than the Eurocode 3 for lower strength bolts. The CAFL in the Eurocode 3 is 23 MPa for all types of bolts, which is significantly more conservative than the CAFL of 47 MPa specified in the BS7608 provisions or the CAFL of 52 MPa implied by the AISC provisions.

The fatigue strength in the Eurocode 3 Specifications is based upon the actual stress range acting on the tensile stress area of the bolt. For snug-tight bolts, this calculation is straightforward (i.e. the stress range within the bolt is equal to the applied load range divided by the tensile stress area of the bolt). For fully-tightened bolts, however, calculation of the actual stress range acting on the tensile stress area is uncertain, and the Eurocode 3 Specifications do not suggest how such calculations are to be performed. However, assuming such a calculation can be performed, the provisions of Eurocode 3 permit a slightly improved fatigue strength for fully-tightened bolts due to the fact that the reduced stress range acting within the fully-tightened connection would be compared to the S-N fatigue design curve.

Generally, the provisions contained in the above design specifications are consistent with the results of previous research programs [16, 24] which have been performed to determine the fatigue strength of anchor bolts in the regime of finite life. As was shown in Figures 6.1 and 6.2, the lower-bound fatigue strengths exhibited by snug- and fully-tightened anchor bolts in the regime of finite life are consistent with the AASHTO Category E′ and Category E design curves, respectively. These design S-N curves are generally in agreement with the provisions of the AISC LRFD, BS7608, and Eurocode 3 Specifications for the design of bolts for finite life.

There does, however, appear to be disagreement with respect to the magnitudes of the constant amplitude fatigue limits recommended by the three Specifications. Within each of the

design Specifications, the magnitude of the CAFL appears to be arbitrarily set without regard to referenced test data. As a result, significant uncertainty exists with respect to the design of bolts for fatigue in the regime of infinite life.

6.3 DESCRIPTION OF EXPERIMENTS

6.3.1 Test Specimens

A total of 47 specimens were included in the fatigue test program. Table 6.1 summarizes the details of the four types of specimens which were tested. As is shown, the test specimens consisted of 38 mm diameter AASHTO Grade 55 and AASHTO Grade 105 anchor bolts with a 6UNC thread series. Selection of the diameter and thread series to be tested was based upon a review of state department of transportation standard drawings of cantilevered support structures. Thirty-eight millimeter diameter anchor bolts with a 6UNC thread series were identified as being typical for a majority of cantilevered support structure installations. As is shown in Table 6.1, approximately one-half of the specimens within each material grade were obtained with cut threads. The remaining specimens were obtained with rolled threads.

The basic specimen geometry is depicted in Figure 6.3. As is shown, the specimens were 914 mm long with a 203 mm long threaded region at each end and were supplied with four washers and four Grade 2H heavy hex nuts. All of the specimens, nuts, and washers were obtained from two independent commercial vendors in order to simulate the thread quality of anchor bolts used in actual construction and to minimize any bias in the test results due to a specific manufacturing process. Furthermore, all of the specimens, nuts, and washers were obtained galvanized in order to simulate the condition of anchor bolts used in typical cantilevered support structure installations. The nuts were re-tapped by the supplier following galvanizing, as is typical.

6.3.2 Experimental Set-Up and Procedures

A schematic of the experimental set-up used for the concentrically-loaded tests is depicted in Figure 6.4. As is shown, test fixtures were designed to transfer load directly from a servohydraulic actuator directly to the exterior nuts on each end of the specimen through bearing plates measuring 140 mm x 146 mm x 38 mm thick. Figure 6.5 shows a photograph of a complete test set-up.

As is indicated in Figure 6.6, the effects of misalignment were introduced by fabricating holes in the bearing plates which were offset from the longitudinal axis of the servohydraulic actuator. The amount of offset was set so as to subject the misaligned specimens to a 1:40 vertical misalignment, thereby introducing stresses caused by axial tension and non-uniform bending along the longitudinal axis of the specimens.

Selection of the amount of misalignment to which the anchor bolts would be subjected was based upon a review of current state department of transportation specifications for anchor bolt installation which indicated 1:40 as a maximum amount of anchor bolt misalignment permitted for cantilevered support structure installations [12]. In addition, bevelled washers were used at each end of the misaligned test specimens to minimize any localized bending effects resulting from non-uniform bearing of the nuts against the bearing plate. Bevelled washers are typically used in cantilevered support structures in which the anchor bolts are installed at misalignments less than 1:40 [12]. Generally, state department of transportation require that anchor bolts installed at misalignments greater than 1:40 be rejected for use in cantilevered support structure foundations. As a result, misalignments greater than 1:40 were not considered within the scope of the test program.

Each of the specimens were snug-tightened against the bearing plates using a standard torque wrench without the aid of additional lubrication. For the purposes of this research

program, snug-tight was defined as tightening of the nuts to a torque of 271 N-m. A constant torque value was used to define snug-tight to ensure a reasonable level of consistency between individual tests and to permit a direct comparison with the results obtained by Frank [24]. It should be noted that defining snug-tight by a torque of 271 N-m was arbitrary and does not correspond to any specific level of bolt pretension. However, the definition of snug-tight adopted for the purposes of this research program resulted in levels of bolt pretension below those achieved using the generally accepted definitions of snug-tight (which are discussed in the following paragraphs). As a result, the data obtained from these tests are slightly conservative. For those tests conducted at greater than snug-tight, tightening of the nuts was achieved with the use of a hydraulic wrench. Beeswax was applied to the threaded and bearing surfaces of these specimens to reduce the level of torque required to obtain the desired level of nut tightness.

Several specifications currently contain provisions which specify minimum requirements for obtaining the snug-tight condition. The AISC LRFD Specifications [5] define snug-tight as the "tightness that exists when all of the plies in a joint are in firm contact." This requirement is generally not applicable to anchor bolt installations because the nuts in a double-nut connection are tightened against a single base-plate (i.e. multiple plies do not exist in anchor bolt installations). AASHTO recently issued supplemental specifications for AASHTO M164 (ASTM A325) [39] which define snug-tight as 10 percent of the specified proof load. The proof load is determined from tensile tests and is defined as the "applied load fasteners must resist without evidence of permanent deformation." The level of torque required to achieve the minimum specified bolt tension corresponding to snug-tight is determined from calibrations in a Skidmore-Wilhelm Calibrator. For galvanized bolts, all tests in the AASHTO supplemental specifications are to be performed following galvanizing. The application of these provisions to the installation of anchor bolts, however, is uncertain. For example, double-nutted anchor bolts are subject to

pretensioning in the short length of bolt between the double nuts. Such a short length of bolt cannot be calibrated in a Skidmore-Wilhelm Calibrator. As a result, the level of torque required to achieve a bolt pretension of 10 percent of the specified proof load would be unknown.

It is recommended that, in actual anchor bolt installations, snug-tight be defined by the level of torque corresponding to the full-strength of a man using an ordinary spud wrench. This represents the definition previously used by AISC to define snug-tight. Based upon the results of the research reported herein, defining snug-tight as the full-strength of a man will always result in a level of torque greater than the definition of snug-tight adopted for this research program (i.e. 271 N-m). As a result, anchor bolts tightened in the field will possess a greater level of pretension and will exhibit a slightly higher fatigue strength than specimens tested in this research program.

All specimens were tested in a double-nut configuration, i.e. one nut on each side of the bearing plate, under constant-amplitude, tension-tension loading. A computer-controlled, 245 kN capacity servohydraulic actuator was used to subject the test specimens to sinusoidal loading at frequencies between 10 and 25 Hz. The variable controlled during each of the tests was the stress range on the tensile stress area of the bolt. Except where noted, the maximum stress on the tensile stress area for all tests on the Grade 55 anchor bolts was held constant at approximately 60 percent of the minimum specified yield strength of the material. Due to limitations on the capacity of the testing machine used in this experimental program, the maximum stress on the tensile stress area for the Grade 105 bolts was held constant at either 32 percent or 38 percent of the minimum specified yield strength of the material.

The dynamic load range induced in the test specimens during testing was monitored by a load cell mounted between one of test fixtures and the crosshead of the test machine. Prior to the start of the fatigue test program, however, several concentrically-loaded test specimens were

instrumented with a series of strain gages and statically tested to ensure adequate calibration of the load cell and to evaluate the magnitude of any bending induced in the specimens due to seating. The specimens were instrumented with a series of four strain gages mounted at 90 degree intervals on the unthreaded portion of the bolt midway between the bearing plates. The results of the static tests indicated good correlation between the bolt load indicated by the load cell and the bolt load computed from the average of the four strain gages readings. Furthermore, bending stresses due to seating of the specimens were found to be negligible. As a result, the load cell was considered an adequate means by which to monitor the dynamic load range induced in the specimens during testing.

Each specimen was tested under load control with failure defined by the propagation of a crack through the entire specimen cross-section. The experimental set-up and specimen geometry permitted two data points to be obtained from each specimen (i.e one data point from each of the two threaded regions). As a result, all specimens which failed at one end with sufficient threads remaining were retested until failure at the opposite end was obtained. This procedure effectively limited the extended period of time required to conduct fatigue testing in the regime of infinite life. Inclusion of multiple data from each of the specimens was found not to significantly influence the results of statistical analyses of the data. The lower-bound corresponding to the first observed failure was found to be identical to the lower-bound when failures at both ends of the specimens were included in the statistical analysis.

6.4 RESULTS OF EXPERIMENTS

A tabular summary of the fatigue test results is provided in Tables 6.2 through 6.6. Each table summarizes the specimen series and test number, test condition (snug-tight or number of turns beyond snug), stress range, maximum stress, number of cycles, test result (failure or runout),

and failure location if a failure was obtained. All of the stress parameters are summarized in terms of the tensile stress area. The nomenclature defining the failure location is discussed in Section 6.4.1. Specimens with two numbers of cycles indicated were tested until failure at each of the threaded regions was obtained. Specimens marked with an asterisk were tested to runout at a lower stress range and then retested at the stress range indicated. The failure surfaces of each of these specimens were inspected following failure to ensure that significant fatigue damage did not occur at the lower stress range (this was the case for all of the specimens retested at a higher stress range). Any undetectable fatigue damage which may have occurred at the lower stress range was not considered in the calculation of the stress range (i.e. an effective stress range was not computed). Neglecting any potential fatigue damage at the lower stress range would result in slightly more conservative estimates of the lower-bound fatigue strength. Sections 6.4.2 through 6.4.7 summarize the fatigue test results in terms of S-N curves.

6.4.1 Fatigue Crack Initiation and Propagation

Due to the inherent geometrical configuration of bolted connections, visual inspection for fatigue cracking was not possible during the course of the testing program. However, post-test inspections of the fatigue specimens indicated that failure was caused by the propagation of a single crack which formed in one of two locations, as is indicated in Figure 6.7. The majority of specimen failures occurred at the first fully-engaged thread from the loaded face of the exterior nut of the double-nutted connection, identified as failure location 1 in Figure 6.7. In addition, several specimens failed in the threaded region outside of the double-nutted connection, identified as failure location 2 in Figure 6.7. All but one of the specimens which failed outside of the connection were tightened to greater than snug-tight.

Inspection of the failure surfaces indicated that fatigue cracks initiated at multiple points at the thread root that coalesced into a single primary crack which resulted in failure. This prolonged "initiation" or coalescence period is the primary source of the effect of yield strength on anchor bolt fatigue strength. This is in contrast to weldments which have more significant microdefects and therefore possess insignificant initiation lives.

Generally, the primary crack propagated along a straight-line front towards the center of the cross-section of the specimen. In all cases, the primary crack propagated through approximately 65% to 75% of the specimen cross-section prior to fracture. Figure 6.8 shows photographs of typical fatigue crack surfaces.

6.4.2 Fatigue Strength of Snug-Tight Specimens

Figure 6.9 summarizes the fatigue test results for the concentrically-loaded, snug-tight specimens in the form of an S-N curve. The data includes tests conducted on both Grade 55 and Grade 105 specimens with rolled and cut threads. As is indicated in Figure 6.9, the lower-bound to the test data is approximately equal to the AASHTO Category E fatigue design curve. Furthermore, inspection of the data in the regime of infinite life indicates no failures were obtained below a stress range of 62 MPa. The next lower CAFL would be the fatigue limit corresponding to the AASHTO Category D fatigue design curve (48 MPa). Thus, the constant amplitude fatigue limit of axially-loaded, snug-tight anchor bolts is conservatively approximated by the fatigue limit corresponding to the AASHTO Category D fatigue design curve (48 MPa).

Figure 6.10 compares the results of the present research program with the results obtained by previous researchers [16, 24]. The current data falls within the range of scatter exhibited by the previous data. Statistical analysis of the entire database indicates that the lower-bound to the test data falls between the AASHTO Category E and E′ fatigue design curves. As a result, the

lower-bound S-N design curve representative of the fatigue strength of axially-loaded, snug-tight anchor bolts is a unique curve given by the AASHTO Category E′ fatigue design curve with a constant amplitude fatigue limit corresponding to the AASHTO Category D fatigue design curve (48 MPa).

Comparison of the lower-bound estimates of the anchor bolt fatigue test data with the recommendations of other design specifications (as was discussed in Section 6.2.2) indicates that the recommended fatigue design strengths for anchor bolts and the provisions contained in these other design specifications are generally consistent for Grade 105 anchor bolts but slightly liberal with respect to the design of Grade 55 anchor bolts. This can generally be expected, since the design Specifications discussed in Section 6.2.2 are oriented towards the design of high-strength structural bolts for fatigue.

6.4.3 Effects of Maximum Stress

Figures 6.11 through 6.14 summarize the results of tests conducted to determine the effects of maximum stress on the fatigue strength of anchor bolts. The data in these figures are from tests conducted on Grade 55 anchor bolts with both rolled and cut threads at stress ranges varying from 138 MPa to 69 MPa. At each stress range, longer fatigue lives were obtained for tests conducted at lower magnitudes of maximum stress. This behavior is typical for non-welded structural components, which have small residual stresses, and has been observed in fatigue testing of other types of non-welded steels [7].

The maximum stress effect can be attributed to the fact that fatigue life in non-welded structural steels is strongly dependent upon the initiation of fatigue cracks. Fatigue crack initiation (and thus the fatigue life corresponding to the initiation period) is strongly dependent upon the magnitude of the maximum stress. At lower values of maximum stress, the initiation life

increases, resulting in a total fatigue life which is composed of the number of cycles required to initiate a crack and propagate the crack to failure. The same effect is not observed in welded details for two reasons. First, welded details are subject to a pre-existing tensile stress (resulting from the residual stress caused by welding), the magnitude of which is on the order of the yield strength of the material. Second, it is generally assumed that weldments possess crack-like defects. As a result, the fatigue life of welded details is controlled by the number of cycles required to propagate a pre-existing crack to failure (i.e. the fatigue life of weldments is not composed of a significant initiation life).

The effects of maximum stress can be conveniently accounted for in the design of anchor bolts for fatigue by basing the design S-N curve on tests conducted at worst-case (highest) maximum stress levels. Thus, maximum stress need not be explicitly considered in the design process. Anchor bolts which are subjected to a lower value of maximum stress in service will exhibit fatigue lives greater than that predicted by the design S-N curve.

6.4.4 Effects of Thread Forming Method

Figures 6.15 and 6.16 summarize the effects of thread forming method (cut vs rolled) for the Grade 55 and Grade 105 specimens, respectively. As is shown in Figure 6.15, thread forming did not significantly influence the fatigue strength exhibited by the Grade 55 specimens.

Thread forming, however, did influence the fatigue strength exhibited by the Grade 105 specimens. As is shown in Figure 6.16, Grade 105 specimens with rolled threads consistently exhibited longer fatigue lives at each of the stress ranges considered. The difference in fatigue strengths between the cut and rolled specimens may be attributed to two factors. First, anchor bolts fabricated with cut threads generally possess a smaller thread root radius than anchor bolts fabricated with rolled threads. The stress concentration associated with the cut thread, therefore,

is more severe. As a result, anchor bolts fabricated with rolled threads would be expected to exhibit a slightly greater fatigue strength than anchor bolts fabricated with cut threads. Second, anchor bolts fabricated with rolled threads possess compressive residual stresses at the thread root resulting from the rolling process. The compressive residual stresses tend to shield the critical thread root area from part of the applied tensile stress range, resulting in an increase in fatigue strength in comparison to anchor bolts fabricated with cut threads.

The effects of thread forming method are observed in the Grade 105 specimens and not in the Grade 55 specimens for two reasons. First, the magnitude of the compressive residual stresses resulting from the rolling process are proportional to the material yield strength. For the Grade 105 specimens (with a higher yield strength), the compressive residual stresses are larger in magnitude than the magnitude of the compressive residual stresses in the Grade 55 specimens (which have a lower yield strength). Therefore, for a given stress range, the magnitude of the residual stresses in the Grade 105 specimens provide a greater benefit with respect to fatigue strength (i.e. the greater compressive residual stresses in the Grade 105 specimens negate a greater portion of the applied tensile stress range than in the Grade 55 specimens).

Second, the effects of thread forming method are also more apparent in the Grade 105 specimens because limitations on the capacity of the hydraulic actuator used in this test program prevented the Grade 105 specimens from being tested at a maximum stress greater than approximately 38 percent of the minimum specified yield strength of the material. At lower values of maximum stress, the effect of stress concentration on fatigue strength is more apparent (i.e. the effects of stress concentration decrease with increasing maximum stress). At higher values of maximum stress, fatigue damage occurs regardless of the severity of the stress concentration. As a result, no significant variations in fatigue strength were observed in the Grade 55 specimens (which were tested at 60 percent of the material yield strength) with cut and rolled

tests. In addition, the relatively low maximum stress to which the Grade 105 specimens were subjected was not large enough to fully negate the beneficial effects of the compressive residual stresses at the thread root. On the other hand, the Grade 55 specimens, which were tested at a maximum stress corresponding to approximately 60 percent of the minimum specified yield strength of the material, did not exhibit a significant variation in fatigue strength between the cut and rolled specimens (as is shown in Figure 6.15). It can be reasonably theorized that the beneficial effects of the compressive residual stress induced by the rolling process were effectively negated by the high applied tensile load.

In other words, when the magnitude of the minimum tensile stress exceeds the maximum value of the compressive residual stress at the thread root, the applied stress range will be fully tensile. Under these conditions, the beneficial effects of the compressive residual stresses at the root of a rolled thread would not be apparent. As a result, the Grade 105 specimens with rolled threads exhibited slightly longer fatigue lives when compared to the Grade 105 specimens with cut threads. Based upon the results of these tests, it is not clear if this benefit would still be obtained if the Grade 105 bolts had been tested at a maximum stress corresponding to 60 percent of the yield strength of the material.

The results of tests conducted by Frank [24] suggest that the higher fatigue strengths exhibited by the Grade 105 would not have been observed at higher levels of maximum stress. As may be recalled from the discussion in Section 6.2.1, the maximum stress in each of the tests conducted by Frank was held constant at 75 percent of the minimum specified yield strength of the material. Frank observed from the results of these tests that the effects of thread forming method were insignificant. Therefore, it appears that the effects of thread forming were minimized in Frank's experiments due to the application of a high maximum tensile stress.

6.4.5 Effects of Yield Strength

Figures 6.17 and 6.18 summarize the effects of yield strength for the specimens with cut and rolled threads, respectively. The data in each of these figures were obtained from tests conducted at approximately equivalent absolute magnitudes of maximum stress. Based on the data in Figures 6.17 and 6.18, yield strength does not appear to significantly influence the fatigue strength of anchor bolts fabricated with either rolled or cut threads under these conditions. This conclusion is consistent with the results of Frank [24] and Dusel [16].

As was previously discussed, however, limitations on the capacity of the actuator prevented the Grade 55 and Grade 105 specimens from being tested at magnitudes of maximum stress which were similar in terms of percentage of material yield strength. As was discussed in Section 6.4.3, the fatigue strength of anchor bolts is governed, in part, by the magnitude of the maximum stress, i.e. larger values of maximum stress decreases the apparent fatigue strength of anchor bolts. Based upon the results presented in Section 6.4.3, it can be reasonably concluded that, under levels of maximum stress identical with respect to the percentage of material yield strength, Grade 55 anchor bolts would exhibit longer fatigue lives than Grade 105 anchor bolts. This apparent increase in fatigue strength would occur because, at values of maximum stress similar with respect to the percentage of material yield, Grade 55 anchor bolts would be subjected to an absolute maximum stress lower than the maximum stress in the Grade 105 anchor bolts.

As was discussed in the Section 6.1, the approach adopted with respect to the design of anchor bolts for fatigue is to represent the lower-bound behavior of all types of anchor bolts and loading conditions. In this way, the effects of secondary variables such as maximum stress, yield strength, and thread forming method need not be explicitly considered in the design process. It is possible that the worst-case maximum load effects were not considered in the tests of the Grade 105 specimens. The results of previous research, however, suggest that higher strength bolts do

not exhibit significant degradation in fatigue strength at higher magnitudes of maximum stress. For example, Frank [24] tested high-strength bolts at maximum stress levels equal to 75 percent of the minimum specified yield strength of the material. The results of these tests did not indicate that there was a significant decrease in fatigue strength in comparison to the lower strength anchor bolts tested at the same percentage of yield.

In an optimally designed structure, proportioned such that the maximum anchor bolt stresses associated with the extreme wind-loading event (e.g. 50-year wind) correspond to the allowable static design stress, Grade 55 anchor bolts would be subjected to a smaller maximum stresses than Grade 105 anchor bolts (in terms of absolute values of maximum stress). Based upon the previous discussion, for a given fatigue stress range, the Grade 55 anchor bolts would be expected to exhibit a longer fatigue life than the Grade 105 anchor bolts. Therefore, there is a slightly greater margin of safety or reliability level for the lower strength anchor bolts. It is also likely that the higher strength bolts would be used at higher stress ranges, which makes Grade 105 anchor bolts even more "fatigue critical."

6.4.6 Effects of Misalignment

Figure 6.19 shows data from tests conducted on the misaligned test specimens under snug-tight conditions. The data include test results from Grade 55 and Grade 105 specimens with rolled and cut threads. Figure 6.19 also includes a comparison of the misaligned test results with the test data obtained from the concentrically-loaded test specimens. All of the data indicated in Figure 6.19 were obtained under snug-tight conditions.

The data are presented in terms of the nominal axial stress range acting on the tensile stress area. The bending stress range resulting from the misaligned configuration is not included in the stress calculation. The bending is "built-into" the S-N curve and is reflected by the lower

apparent fatigue strength relative to the concentrically-loaded test specimens. However, it appears that, even with the inclusion of the misaligned test data, the AASHTO Category E′ design curve still represents a reasonable lower-bound to both the misaligned and concentric test data.

Comparison of the misaligned fatigue test results with the results of a full-scale cantilevered support structure foundation fatigue test suggest that the level of end-restraint provided by the test fixture used in this test program was similar to the level of end restraint provided by an actual base-plate. As a result, the bending stress ranges to which the misaligned test specimens were subjected are expected to be similar to the bending stress ranges to which misaligned anchor bolts are subjected in an actual cantilevered support structure foundation.

As is shown in Figure 6.19, no failures were obtained in the misaligned specimens below a stress range of 55 MPa. Therefore, the constant amplitude fatigue limit corresponding to the AASHTO Category D design curve (48 MPa) can also be used to design anchor bolts for infinite life with misalignments up to 1:40 (provided that bevelled washers are used during installation) without explicit consideration of the bending stresses created by the misaligned configuration. It should be noted that, without bevelled washers, misaligned anchor bolts may be subject to additional localized bending stresses due to non-uniform bearing of the nut against the base-plate. Under these conditions, the apparent constant amplitude fatigue limit may be lower than the AASHTO Category D fatigue limit.

6.4.7 Effects of Bolt Preload

Figure 6.20 depicts the fatigue lives exhibited by anchor bolts subjected to varying levels of bolt pretension (one-third-of-a-turn beyond snug, one-sixth-of-a-turn beyond snug, and one-twelfth-of-a-turn beyond snug) at a 138 MPa nominal stress range. No attempt was made to calculate the actual stress range between the double-nuts. Specimens tested at one-third and one-

sixth-of-a-turn beyond snug did not exhibit failures during the testing program. Specimens tested at one-twelfth-of-a-turn beyond snug failed at a number of cycles significantly greater than the snug-tight specimens tested at an identical stress range (see Figure 6.9). Furthermore, two of the three failures observed in the specimens tightened to one-twelfth-of-a-turn beyond snug occurred outside of the connection (i.e. failure location 2 as identified in Figure 6.7).

The limited number of tests conducted at greater than snug-tight prevents any definitive conclusions to be made regarding the effect of this parameter on the fatigue strength of anchor bolts in the infinite life regime. However, an evaluation of the existing database of fatigue tests conducted at one-third-of-a-turn beyond snug permits several statements to be made concerning the effects of pretensioning.

As was previously discussed, the results of a statistical analysis of the existing database of anchor bolt tests conducted at one-third-of-turn past snug (as is shown in Figure 6.21) indicates that the fatigue strength of fully-tightened anchor bolts in the regime of finite life is conservatively approximated by the AASHTO Category E fatigue design curve. Furthermore, examination of the data in the regime of infinite life indicates that Frank [24] obtained failures at stress ranges as low as 69 MPa. As a result, the constant amplitude fatigue limit for fully-tightened anchor bolts is below the fatigue limit corresponding to the AASHTO Category C fatigue design curve. Furthermore, it is reasonable to conclude that the constant amplitude fatigue limit for snug-tight anchor bolts (i.e. the fatigue limit defined by AASHTO Category D) is a worst-case condition. Thus, the actual constant amplitude fatigue limit for fully-tightened anchor bolts likely falls between the fatigue limits corresponding to AASHTO Categories C and D. It is therefore recommended that the fatigue limit corresponding to AASHTO Category D (48 MPa) be utilized for the design of fully-tightened anchor bolts for infinite life.

As discussed above, the results of previous research indicate that the fatigue strength of anchor bolts in the finite life regime can be improved by one fatigue category (to Category E) by tightening the nuts to one-third-of-a-turn past snug. The improvement in fatigue strength afforded by tightening to one-third-of-a-turn beyond snug can be attributed to a reduction in load carried by the external nut. Frank [24] determined that, under fully-tightened conditions, approximately one-third of the externally applied load is taken by the interior nut. In a majority of the fatigue tests on fully-tightened anchor bolts, the transfer of load from the exterior to interior nuts shifted the failure mode from the first engaged thread of the exterior nut to the threaded region below the levelling nut. The limited number of tests conducted at greater than snug-tight in the current research program suggest that the shift in failure modes from the first engaged thread of the exterior nut to the threaded region below the levelling nut can be achieved by tightening to as little as one-twelfth-of-a-turn beyond snug.

Although an improvement in the constant amplitude fatigue limit for fully-tightened anchor bolts (above the Category D fatigue limit associated with snug-tight bolts) has not been suggested, it should be stressed that tightening to one-third-of-a-turn beyond snug is the preferred method for anchor bolt installation. Snug-tight bolts may potentially become loose under service-load conditions, altering the distribution of load to each of the remaining anchor bolts in the foundation assembly. The remaining bolts may be subjected to stress ranges greater than those assumed in design. This is, of course, detrimental to the performance of the anchor bolt assembly with respect to fatigue. Tightening to one-third-of-a-turn beyond snug eliminates the possibility of anchor bolts becoming loose under service conditions. As a result, it is the preferred method for anchor bolt installation.

6.4.8 Material Property Tests

A series of material property tests were performed to ensure that strength, ductility, and fracture toughness of the anchor bolt test specimens were in accordance with existing anchor bolt material property specifications. One anchor bolt was randomly selected from each of the four specimen series summarized in Table 6.1 and subjected to a series of material property tests. Three standard 13 mm diameter tensile specimens (50 mm gage length) and three standard Charpy V-Notch impact specimens were fabricated from each of the four randomly selected anchor bolts.

Two specifications currently specify minimum material property requirements for anchor bolts. The first, AASHTO M314-90, specifies minimum tensile properties for Grade 36, Grade 55, and Grade 105 anchor bolts. The second, ASTM F1554-94, specifies minimum tensile properties for Grade 36, Grade 55, and Grade 105 anchor bolts along with supplemental requirements specifying minimum fracture toughness for Grade 55 and Grade 105 anchor bolts.

The tensile property requirements for the AASHTO and ASTM specifications are identical for each anchor bolt grade. In addition ASTM F1554-94 also specifies two supplemental fracture toughness requirements denoted as S4 and S5. The first supplemental requirement, S4, is applicable to both Grade 55 and Grade 105 anchor bolts and requires a minimum Charpy impact energy at 5 degrees Celsius. The second supplemental requirement, S5, is applicable only to Grade 105 anchor bolts and requires a minimum Charpy impact energy at -29 degree Celsius. Table 6.7 summarizes the tensile and fracture toughness requirements for Grade 55 and Grade 105 anchor bolts. Note that the Grade 55 Charpy V-Notch specimens were tested in accordance with supplemental S4 while the Grade 105 Charpy V-Notch specimens were tested in accordance with the more stringent supplemental S5.

The material property test results are summarized in Table 6.8. As is indicated, the tensile and fracture toughness properties of each of the anchor bolts selected from the four specimen series surpassed the minimum requirements specified in AASHTO M314-90 and ASTM F1554-94.

6.5 RECOMMENDATIONS FOR FATIGUE DESIGN OF ANCHOR BOLTS

The results of the experimental program reported herein indicate that:

- The AASHTO Category E′ design curve should be used to design axially-loaded, snug-tight anchor bolts in the regime of finite life,

- The AASHTO Category E design curve should be used to design axially-loaded anchor bolts tightened to one-third-of-a-turn beyond snug in the regime of finite life,

- The constant amplitude fatigue limit corresponding to AASHTO Category D (48 MPa) should be used to design axially-loaded, snug- and fully-tightened anchor bolts in the regime of infinite life,

- Whenever practical, anchor bolts should be installed in the fully-tightened condition (i.e. tightened to one-third-of-a-turn beyond snug). Although no benefit is recommended when designing fully-tightened anchor bolts for infinite life, it should be noted that the fully-tightened condition precludes the possibility of anchor bolts becoming loose under service-load conditions. As a result, the fully-tightened condition is inherently better with respect to the fatigue performance of anchor bolts. It should also be noted that, in general, large diameter bolts will require the use of a

hydraulic wrench with external lubrication of the threaded and bearing surfaces in order to achieve one-third-of-a-turn beyond snug.

- The bending stress range resulting from misalignments up to 1:40 need not be explicitly considered in stress calculations when designing anchor bolts for infinite life provided that bevelled washers are utilized in the installation of such bolts. It should be noted, however, that anchor bolts may be subject to prying forces resulting from localized distortion of the base-plate. The increase in stress range associated with prying is, of course, detrimental with respect to the behavior of anchor bolts under fatigue loading. As a result, the effects of prying should be minimized in actual anchor bolt installations through the use of base-plates with adequate thickness.

In addition to the above design recommendations, the results of this research indicate that:

- The magnitude of the maximum stress to which anchor bolts are subjected significantly influences the fatigue strength. A worst-case assumption, i.e. maximum stress levels of about 60 percent of the minimum specified yield strength of the material, is implicit in the above recommendations. Test results indicate that decreases in the magnitude of the maximum stress below 60 percent of the yield strength can significantly increase the apparent fatigue strength and CAFL.

- In cases where the magnitude of the maximum stress is relatively low (i.e. less than approximately 30 percent of the minimum specified yield strength of the material), anchor bolts fabricated with rolled threads exhibit greater fatigue resistance than anchor

bolts fabricated with cut threads. The effect is particularly apparent in higher strength bolts. At larger magnitudes of maximum stress, the effects of thread forming method become negligible as the larger values of applied minimum tensile stress overcome the compressive residual stresses at the root of rolled threads induced by the rolling process. Additional tests should be performed to fully quantify the potential advantages of using anchor bolts fabricated with rolled threads.

- For a given magnitude of maximum stress (in terms of absolute stress), Grade 55 and Grade 105 anchor bolts exhibit approximately identical fatigue strengths. However, the test results suggest that, at maximum stresses which are a similar percentage of material yield strength, Grade 55 anchor bolts exhibit slightly higher fatigue strength than Grade 105 anchor bolts. Furthermore, in actual structural applications, when higher strength bolts are proportioned for strength only, the result will be smaller diameter (or fewer) bolts than would be needed for lower strength bolts. This reduction in size will have the effect of increasing the magnitude of the stress ranges for a given load range. Therefore, it is critical that higher strength anchor bolts be proportioned for fatigue. The constraints of the fatigue requirements, which are equal for both anchor bolt strength levels, may preclude any benefit (with respect to smaller bolt diameters) obtained from using the higher strength bolts.

The above design recommendations are based upon the worst-case stress conditions (i.e. only data consisting of fatigue tests conducted at maximum stresses greater than 60 percent of the minimum specified yield strength of the material were included in the regression analyses to determine the lower-bounds to the snug- and fully-tightened databases). In typical structural

applications, the maximum stresses to which anchor bolts will be subjected will be significantly less than 60 percent of the yield strength of the material (i.e. at typical service loads, the maximum stresses in anchor bolts due to dead load plus fatigue loads will be less than 60 percent of the material yield strength). Furthermore, the design recommendations assume worst-case conditions with respect to parameters such as yield strength and thread forming method. As a result, these secondary parameters need not be considered in the design of anchor bolts for fatigue. Generally, the recommended fatigue design provisions provide a conservative approximation of anchor bolt fatigue strength.

It should be noted, however, that the design recommendations are generally consistent with the provisions of other design recommendations for the design of bolts for fatigue (as was discussed in Section 6.2.2). Although there appears to be some discrepancies between the provisions contained within these various specifications, the recommendations derived from the results of the current research program are generally in agreement with these various design specifications.

Specimen Series	Material Grade[1]	Yield Strength[2] (MPa)	Nominal Diameter (mm)	Thread Series	Thread Type
H55	55	379	38	6UNC	cut
F55	55	379	38	6UNC	rolled
H105	105	724	38	6UNC	cut
F105	105	724	38	6UNC	rolled

[1]AASHTO Specification M314-90 (ASTM F1554-94)
[2]Minimum specified

Table 6.1 - Specimen Details.

Specimen	Test Condition	Stress Range (MPa)	Maximum Stress (MPa)	Cycles	Result	Failure Location**
H55-1	snug	138	142	402,490 589,304	failure	1
H55-16*	snug	97	100	21,071,250	runout	-
H55-16	snug	83	85	32,905,506	runout	-
H55-15	snug	69	73	51,448,200	runout	-
H55-22*	snug	110	228	275,500 400,989	failure	1
H55-20	snug	97	228	546,803 832,855	failure	1
H55-23	snug	83	228	1,569,189 1,737,325	failure	1
H55-22	snug	69	228	15,215,394	runout	1
H55-24	snug	69	228	4,187,632	failure	1
H55-19	snug	62	228	22,263,038	runout	1
H55-7	one-third	138	228	5,142,843	runout	-
H55-13	one-third	138	228	7,983,794	runout	-
H55-14	one-twelfth	138	228	10,104,447	runout	-

*Indicates a specimen previously tested at a different stress range to runout.
**See Figure 6.7

Table 6.2 - Test Results for Concentrically-Loaded Grade 55 Specimens with Cut Threads.

Specimen	Test Condition	Stress Range (MPa)	Maximum Stress (MPa)	Cycles	Result	Failure Location**
F55-9	snug	138	197	591,588 668,378	failure	1
F55-2	snug	138	162	2,279,100 5,621,718	failure	1
F55-10	snug	138	142	3,969,951 10,558,134	failure runout	1 -
F55-13	snug	110	114	20,344,932	runout	-
F55-21	snug	69	72	35,423,100	runout	-
F55-21*	snug	138	276	304,418 391,324	failure	1
F55-23	snug	110	276	530,702 604,914	failure	1
F55-18	snug	83	276	1,319,896 1,958,215	failure	1
F55-16	snug	69	228	3,877,091 4,469,315	failure	1
F55-17	snug	62	228	7,268,961 26,896,630	failure runout	1 -
F55-11	snug	55	228	56,576,300	runout	-
F55-15	one-third	138	228	5,593,491	runout	-
F55-3	one-sixth	138	228	1,939,420	failure	2
F55-20	one-twelfth	138	228	1,512,264 4,469,977	failure	1 2

*Indicates a specimen previously tested at a different stress range to runout.
**See Figure 6.7

Table 6.3 - Test Results for Concentrically-Loaded Grade 55 Specimens with Rolled Threads.

Specimen	Test Condition	Stress Range (MPa)	Maximum Stress (MPa)	Cycles	Result	Failure Location**
H105-5	snug	138	228	191,476 243,733	failure	1
H105-2	snug	110	228	312,835 351,813	failure	1
H105-6	snug	83	228	699,734 1,287,072	failure	1
H105-4	snug	69	228	1,468,555 2,743,177	failure	1
H105-7	snug	55	228	20,000,000	runout	-

*Indicates a specimen previously tested at a different stress range to runout.
**See Figure 6.7

Table 6.4 - Test Results for Concentrically-Loaded Grade 105 Specimens with Cut Threads.

Specimen	Test Condition	Stress Range (MPa)	Maximum Stress (MPa)	Cycles	Result	Failure Location**
F105-8	snug	138	276	431,843 505,807	failure	1
F105-3	snug	110	276	677,173 744,477	failure	1
F105-7*	snug	110	228	913,567	failure	1
F105-7*	snug	97	228	6,524,723	runout	-
F105-2	snug	97	228	2,508,168 8,900,087	failure runout	1 -
F105-7*	snug	83	228	7,735,351	runout	-
F105-7	snug	69	228	10,366,776	runout	-
F105-6	one-third	138	276	5,030,282	runout	-

*Indicates a specimen previously tested at a different stress range to runout.
**See Figure 6.7

Table 6.5 - Test Results for Concentrically-Loaded Grade 105 Specimens with Rolled Threads.

Specimen	Test Condition	Stress Range (MPa)	Maximum Stress (MPa)	Cycles	Result	Failure Location**
H55-12	snug	69	228	866,230	failure	1
H55-18	snug	69	228	817,509	failure	2
H55-18	snug	55	228	9,857,097	runout	-
H55-21	snug	41	228	17,225,294	runout	-
F55-24	one-third	138	228	527,116	failure	2
F55-28	snug	69	228	1,179,952	failure	1
F55-4	snug	55	228	4,727,263	failure	1
F55-8	snug	41	228	21,614,308	runout	-
H105-1	snug	69	239	589,190	failure	1
H105-3	snug	55	239	7,656,769	runout	-
F105-1*	snug	83	276	4,150,352	failure	1
F105-5	snug	69	276	6,453,989	runout	-
F105-4	snug	69	276	1,586,963	failure	1
F105-1*	snug	69	276	10,254,594	runout	-
F105-1	snug	55	276	15,581,946	runout	-

*Indicates a specimen previously tested at a different stress range to runout.
**See Figure 6.7

Table 6.6 - Test Results for Misaligned Grade 55 and Grade 105 Specimens.

Tensile Property*	Grade 55	Grade 105
Tensile Strength (MPa)	517 - 655	862 - 1034
Yield Strength**, min (MPa)	380	724
Elongation in 50 mm, min (%)	21	15
Reduction in Area, min (%)	30	45

*AASHTO M314-90 (ASTM F1554-94)
**0.2% Offset

(a)

Material	Minimum Energy, (J)		Test Temperature (deg. C)
	Ave. 3 Tests	One Test	
Grades 55 & 105	20	16	5*
Grade 105	20	16	-29**

*ASTM F1554-94 S4
**ASTM F1554-94 S5

(b)

Table 6.7 - ASTM F1554-94 (a) Tensile and (b) Charpy Impact Requirements for Anchor Bolts.

Tensile Property	Grade 55**		Grade 105**	
	H55	F55	H105	F105
Tensile Strength (MPa)	580	596	964	1048
Yield Strength*, min (MPa)	421	420	823	930
Elongation in 50 mm, min (%)	32.8	30.9	19.3	18.4
Reduction in Area, min (%)	67.9	62.2	52.0	56.1

*0.2% Offset
**Average of Three Tests

(a)

Material	Impact Energy, (J)		Test Temperature (deg. C)
	Ave. 3 Tests	Lowest Test	
H55	44	37	5
H105	52	47	-29
F55	71	65	5
F105	52	38	-29

(b)

Table 6.8 - (a) Tensile and (b) Charpy Impact Test Results.

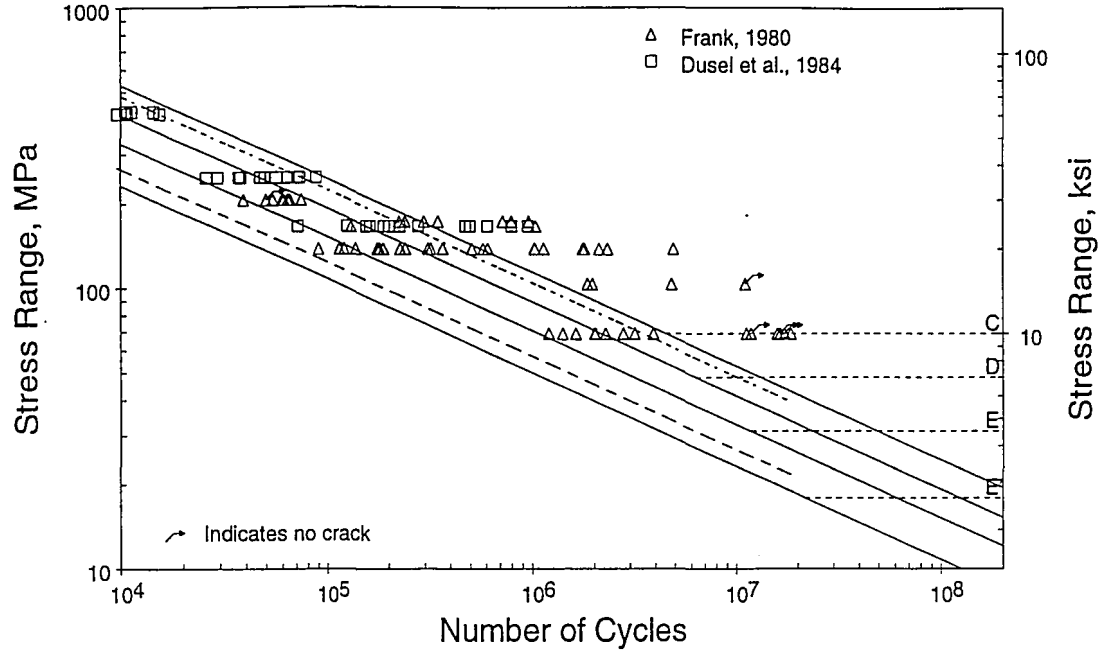

Figure 6.1 - Previous Database of Snug-Tight Anchor Bolt Fatigue Tests (Includes Only Those Data Obtained From Tests Conducted at Maximum Stresses Corresponding to Greater Than $0.6F_y$). Dotted lines are Mean and Mean Minus Two Standard Deviations of the Data. Solid Lines are the AASHTO S-N Design Curves. Horizontal Dashed Lines Indicate CAFL of Each AASHTO Design Curve.

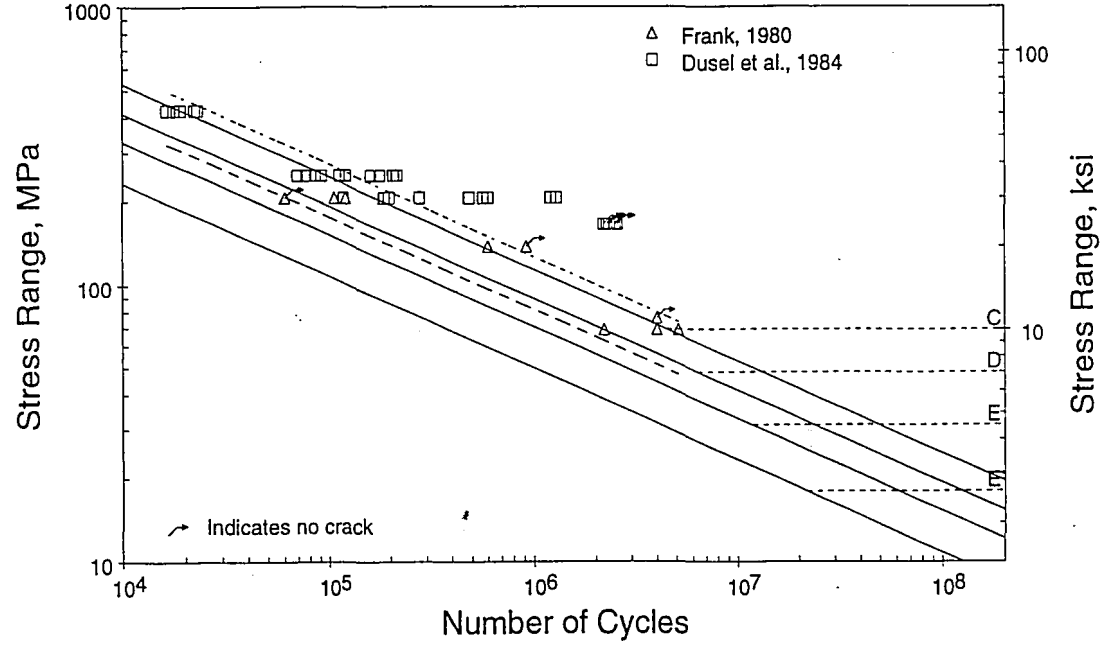

Figure 6.2 - Previous Database of Fully-Tightened Anchor Bolt Fatigue Tests (Includes Only Those Data Obtained From Tests Conducted at Maximum Stresses Corresponding to Greater Than $0.6F_y$).

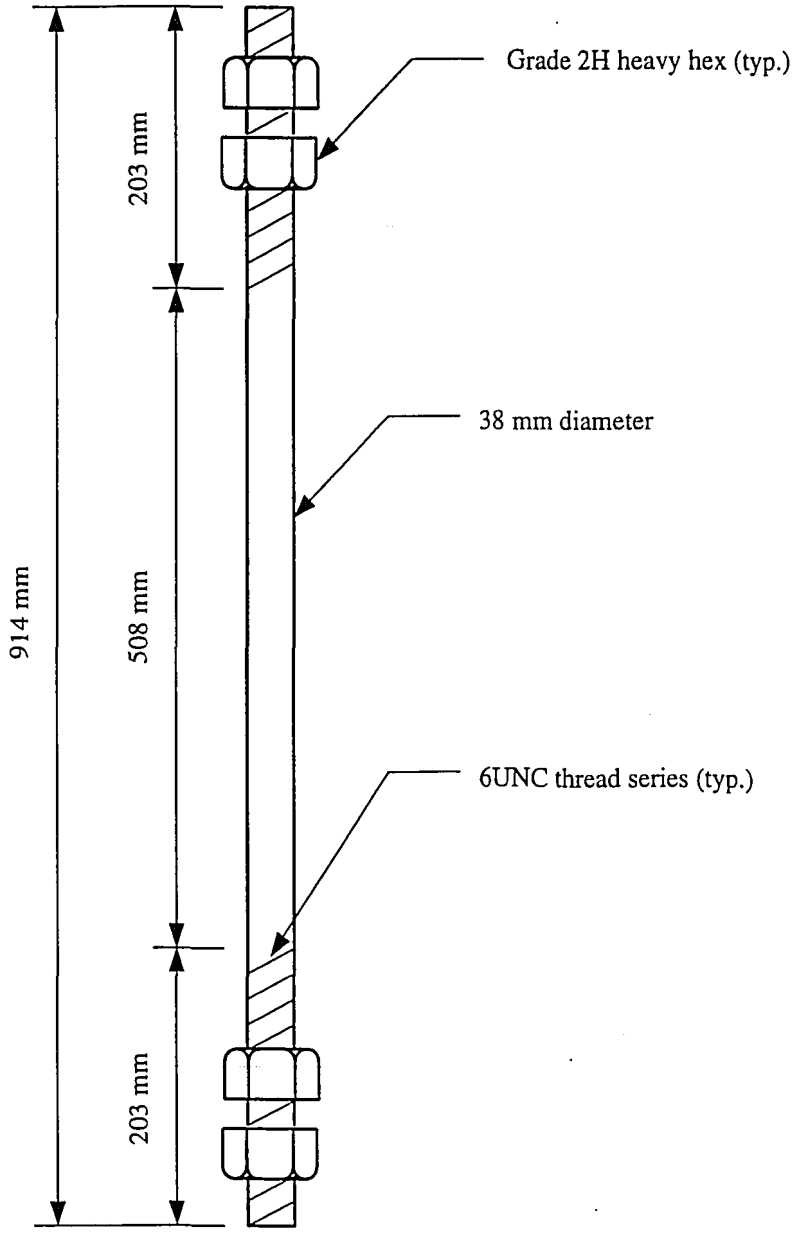

Figure 6.3 - Specimen Geometry.

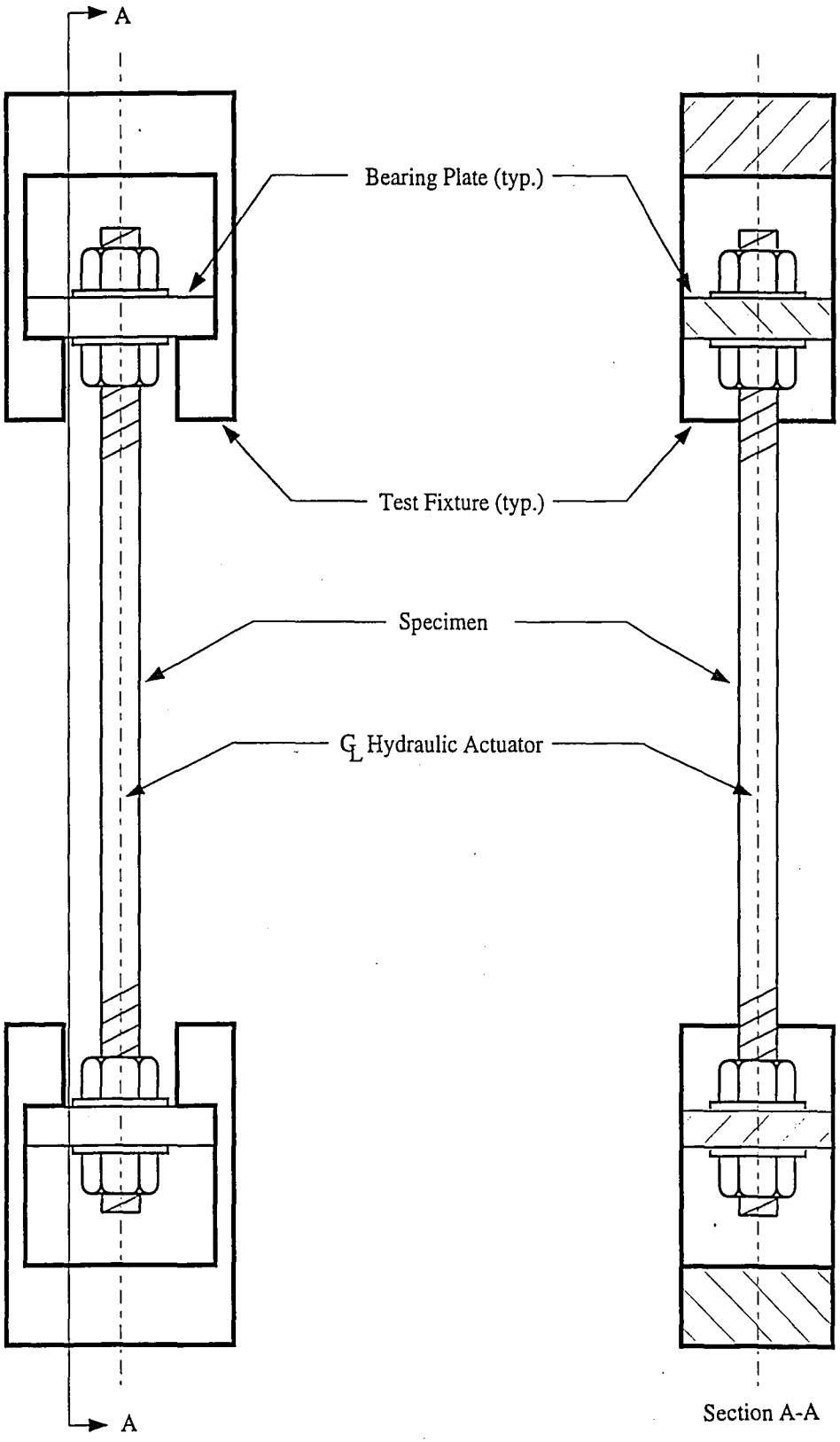

Figure 6.4 - Experimental Set-Up for Concentrically-Loaded Tests.

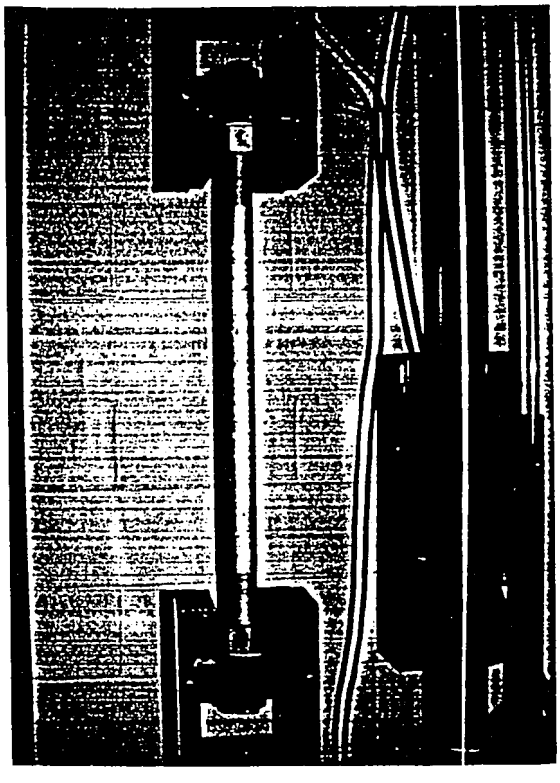

Figure 6.5 - Photograph Showing Test Set-Up for Concentrically-Loaded Tests.

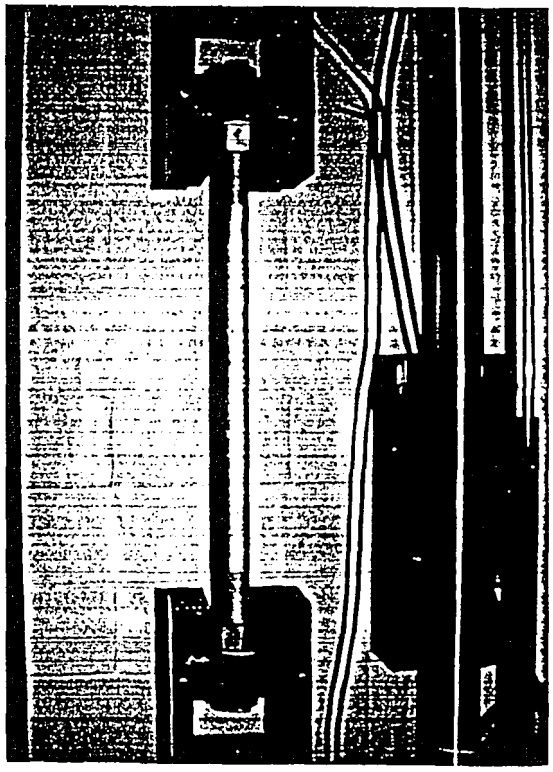

Figure 6.5 - Photograph Showing Test Set-Up for Concentrically-Loaded Tests.

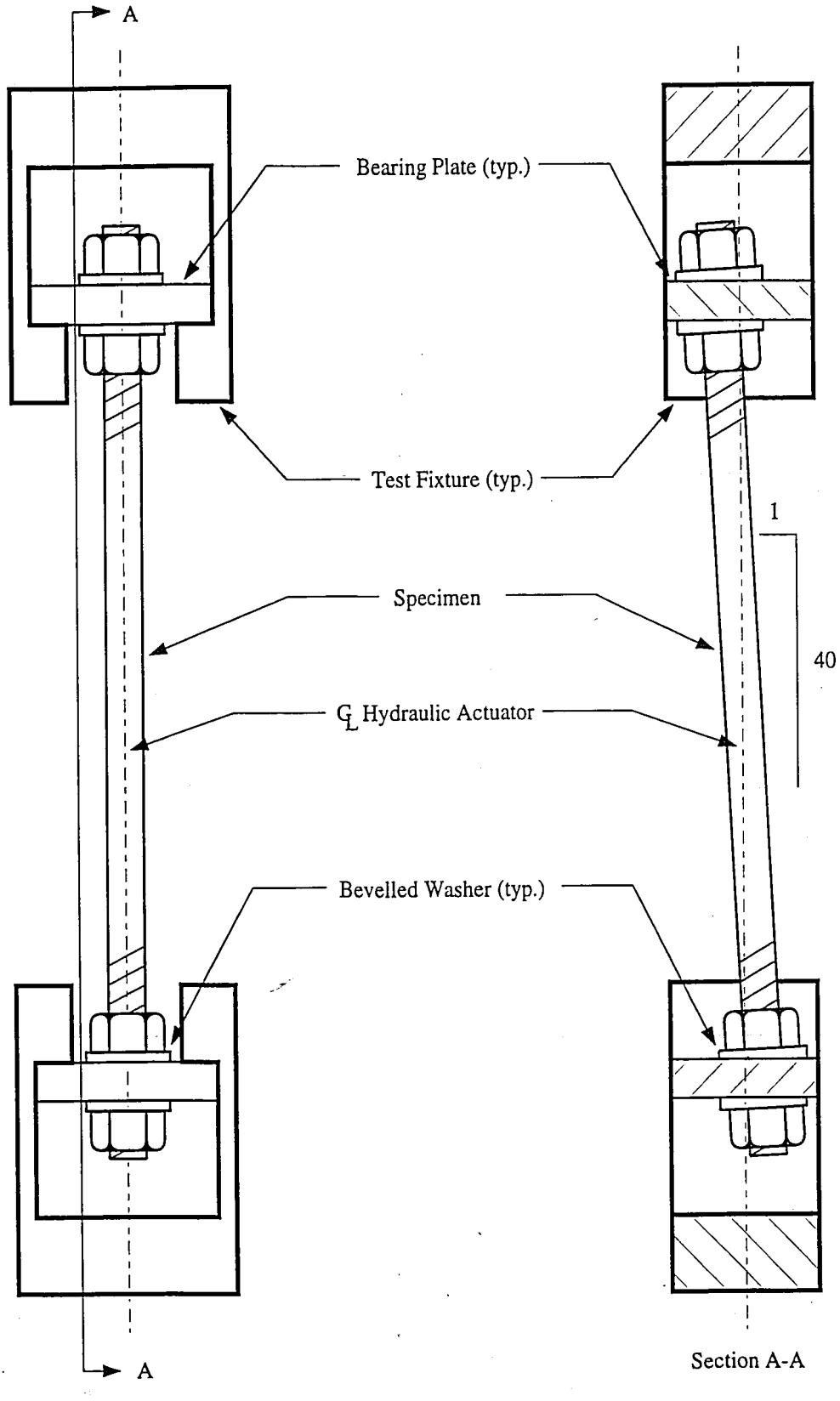

Figure 6.6 - Experimental Set-Up for Misaligned Tests.

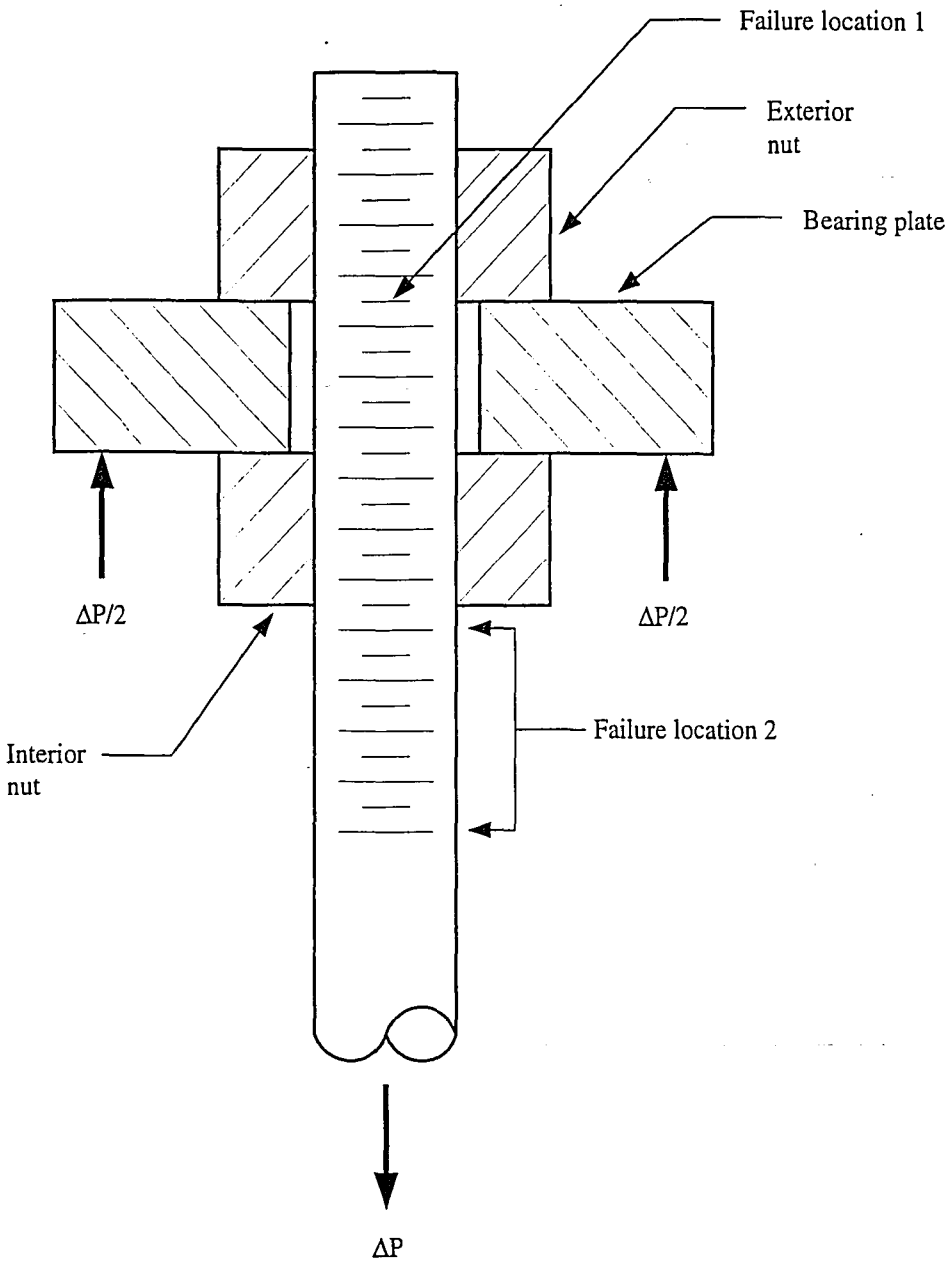

Figure 6.7 - Schematic Defining Failure Locations.

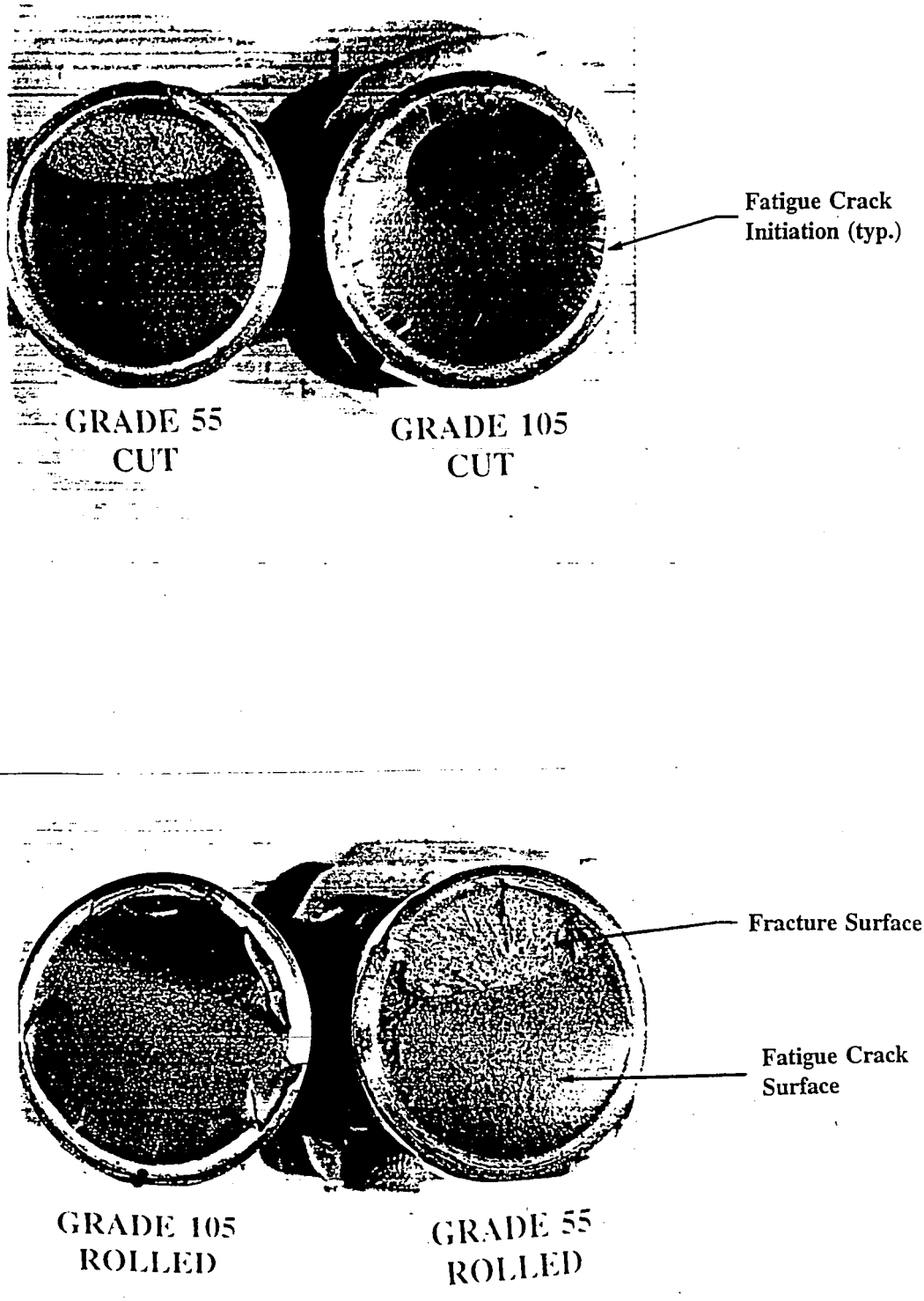

Figure 6.8 - Photographs Showing Typical Cracked Specimens.

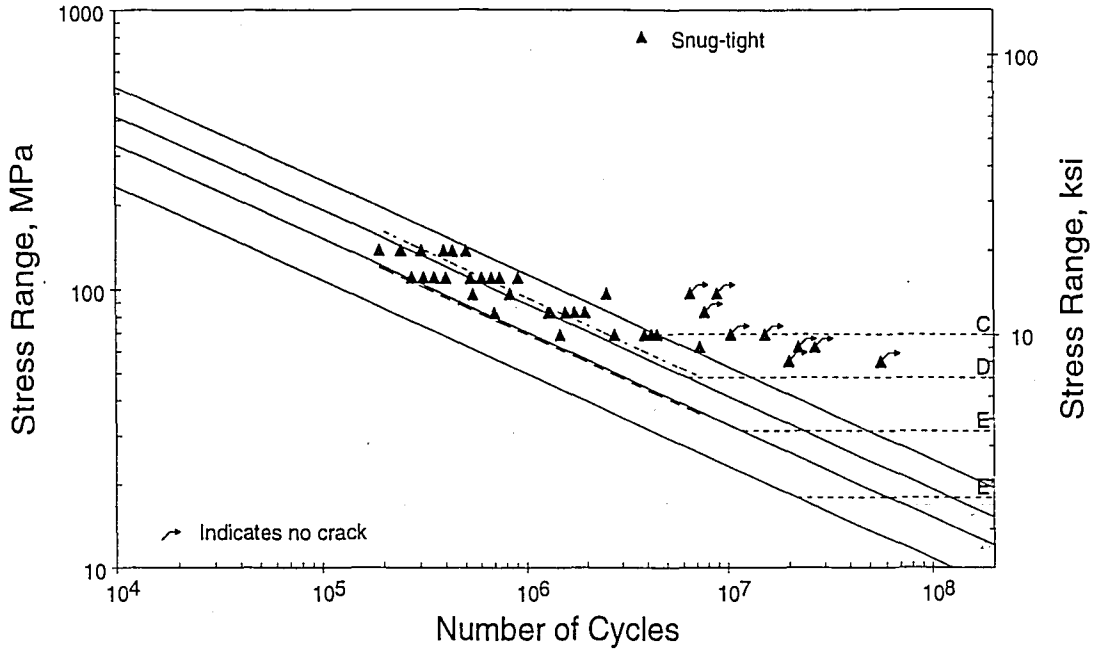

Figure 6.9 - S-N Curve Showing Concentrically-Loaded, Snug-Tight Test Data.

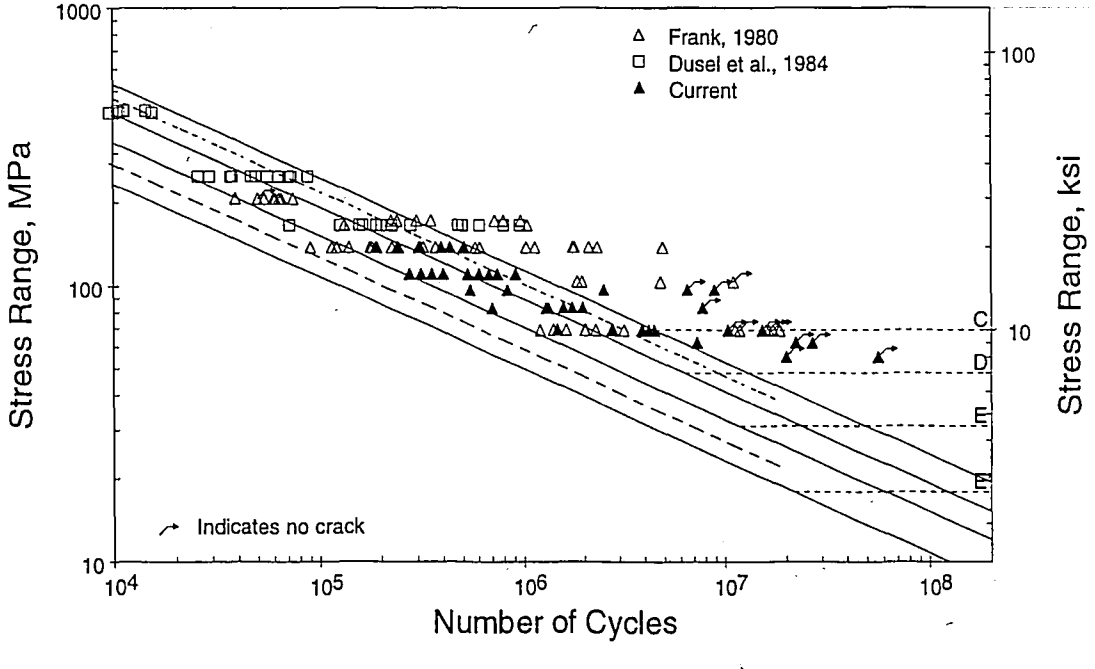

Figure 6.10 - S-N Curve Comparing Concentrically-Loaded, Snug-Tight Test Data with Previous Database.

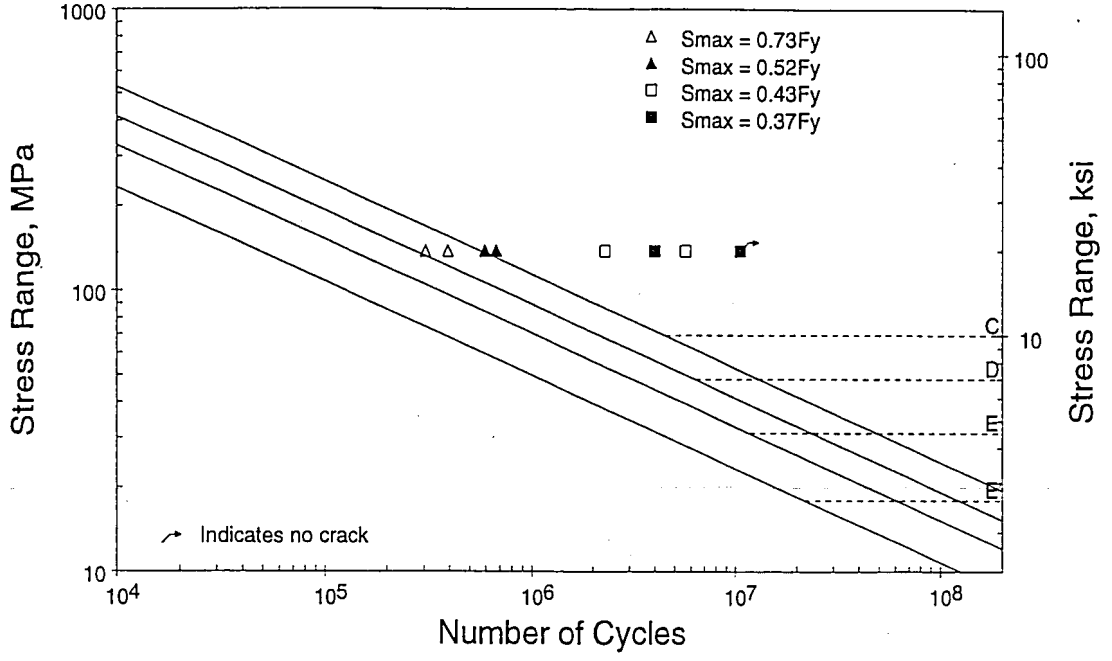

Figure 6.11 - S-N Curve Showing Effects of Maximum Stress for Grade 55 Specimens with Rolled Threads at 138 MPa Stress Range.

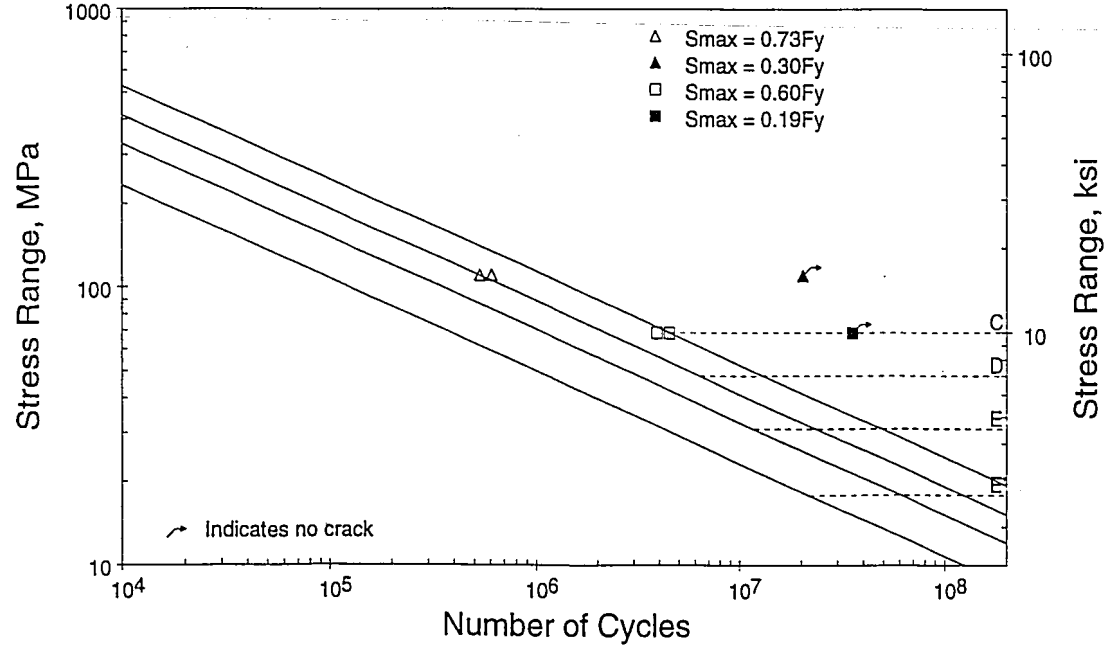

Figure 6.12 - S-N Curve Showing Effects of Maximum Stress for Grade 55 Specimens with Rolled Threads at 110 MPa and 69 MPa Stress Ranges.

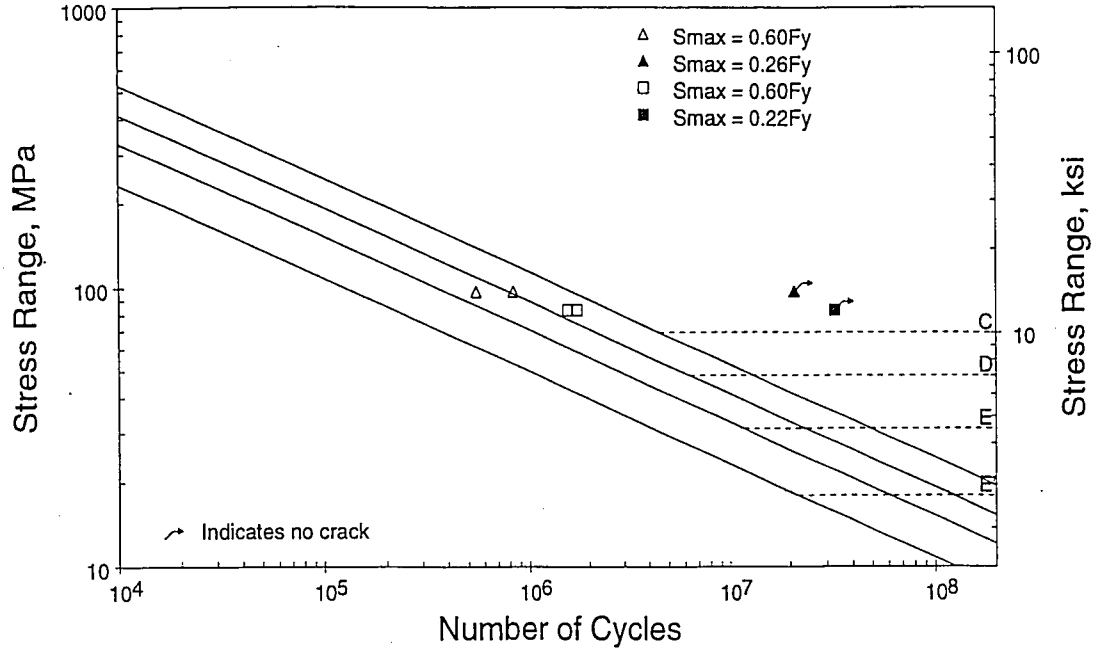

Figure 6.13 - S-N Curve Showing Effects of Maximum Stress for Grade 55 Specimens with Cut Threads at 97 MPa and 83 MPa Stress Ranges.

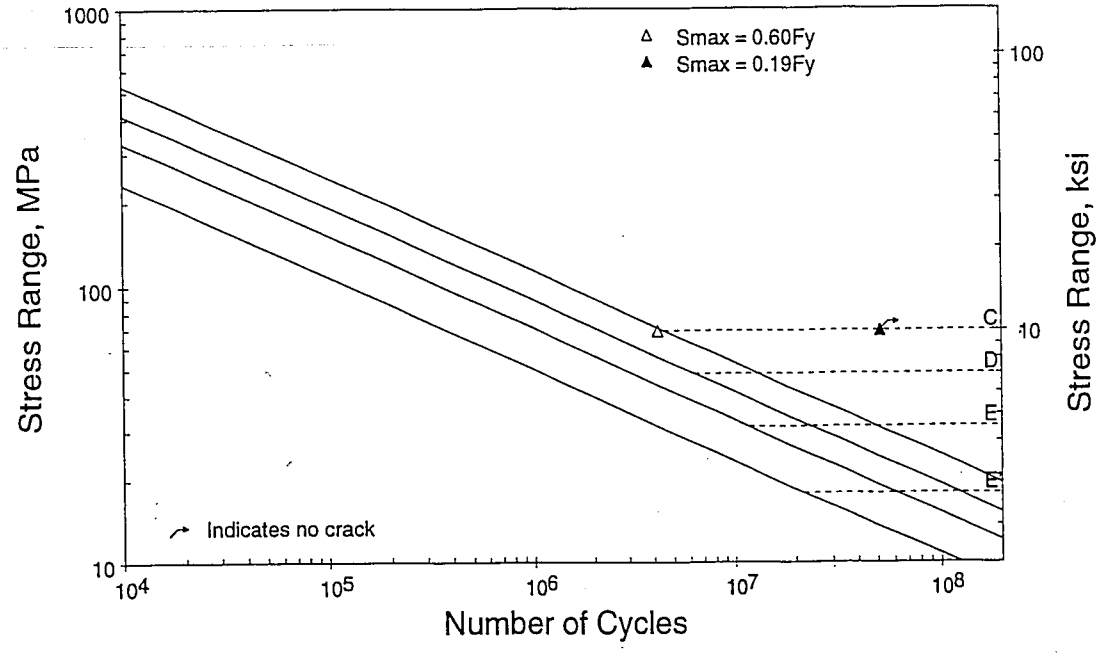

Figure 6.14 - S-N Curve Showing Effects of Maximum Stress for Grade 55 Specimens with Cut Threads at 69 MPa Stress Range.

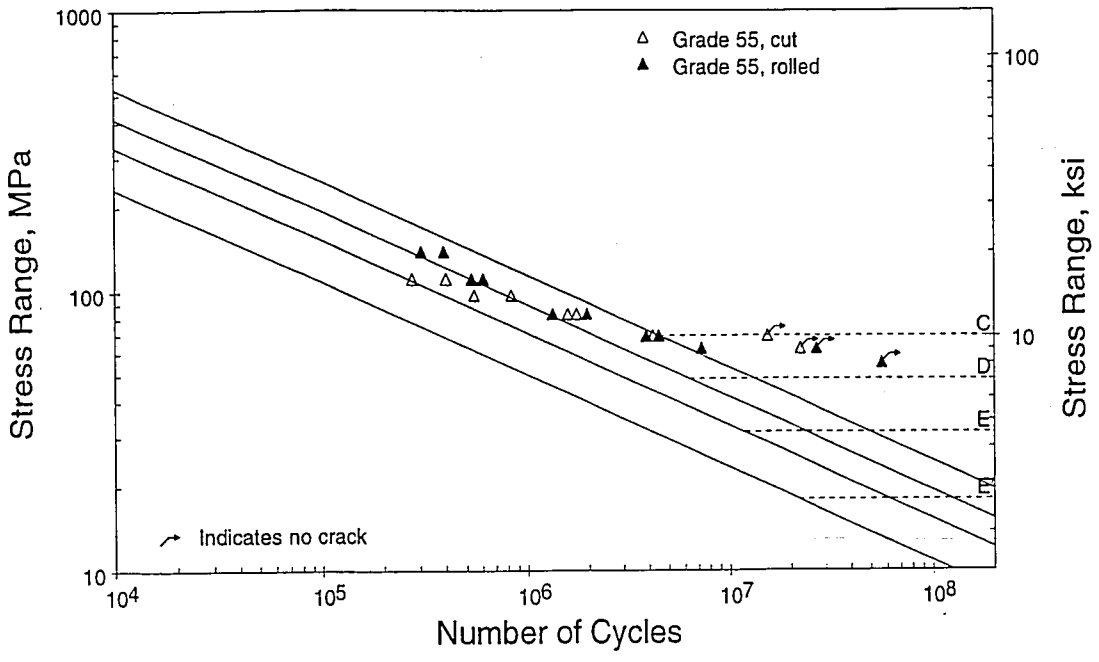

Figure 6.15 - S-N Curve Showing Effects of Thread Forming Method for Grade 55 Specimens.

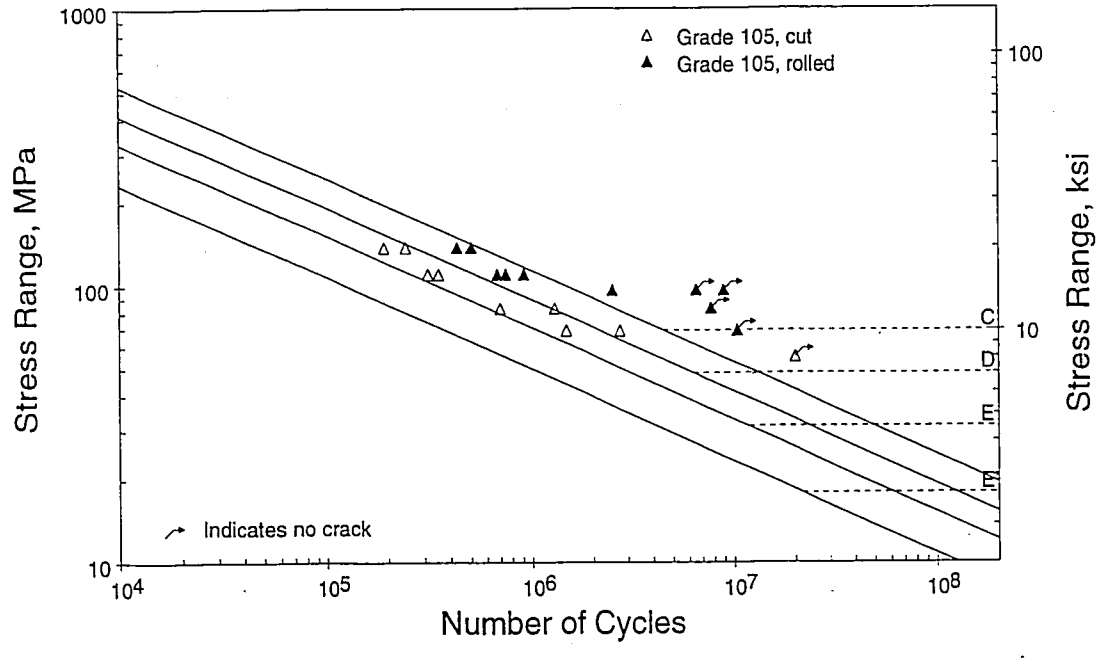

Figure 6.16 - S-N Curve Showing Effects of Thread Forming Method for Grade 105 Specimens.

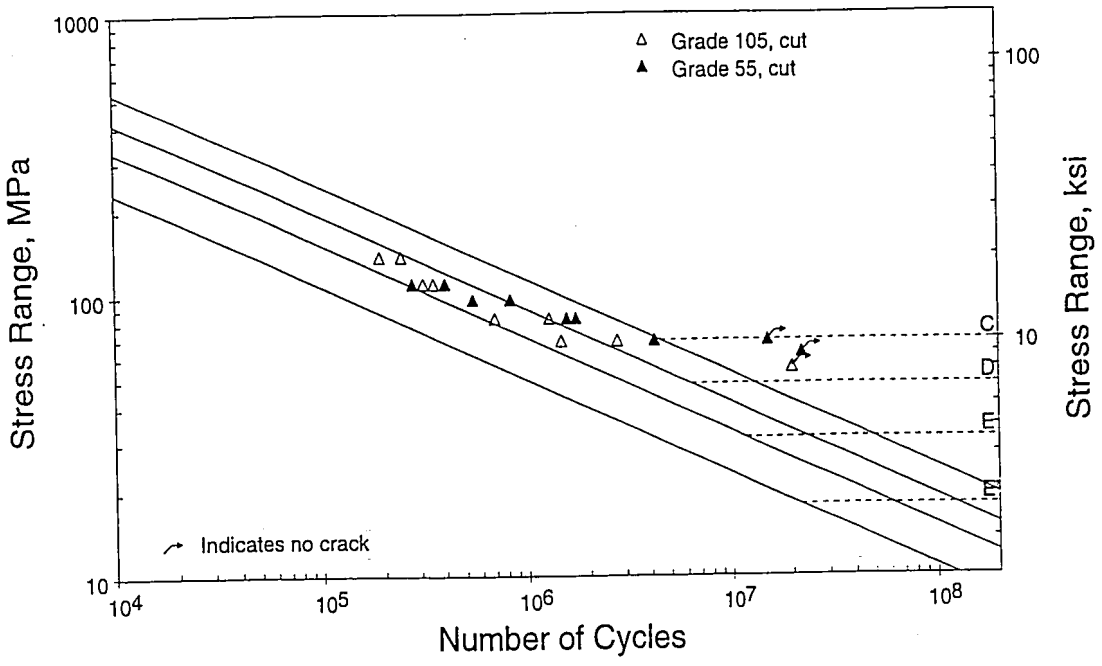

Figure 6.17 - S-N Curve Showing Effects of Material Grade For Specimens with Cut Threads (Tests Conducted at Approximately Same Absolute Maximum Stress).

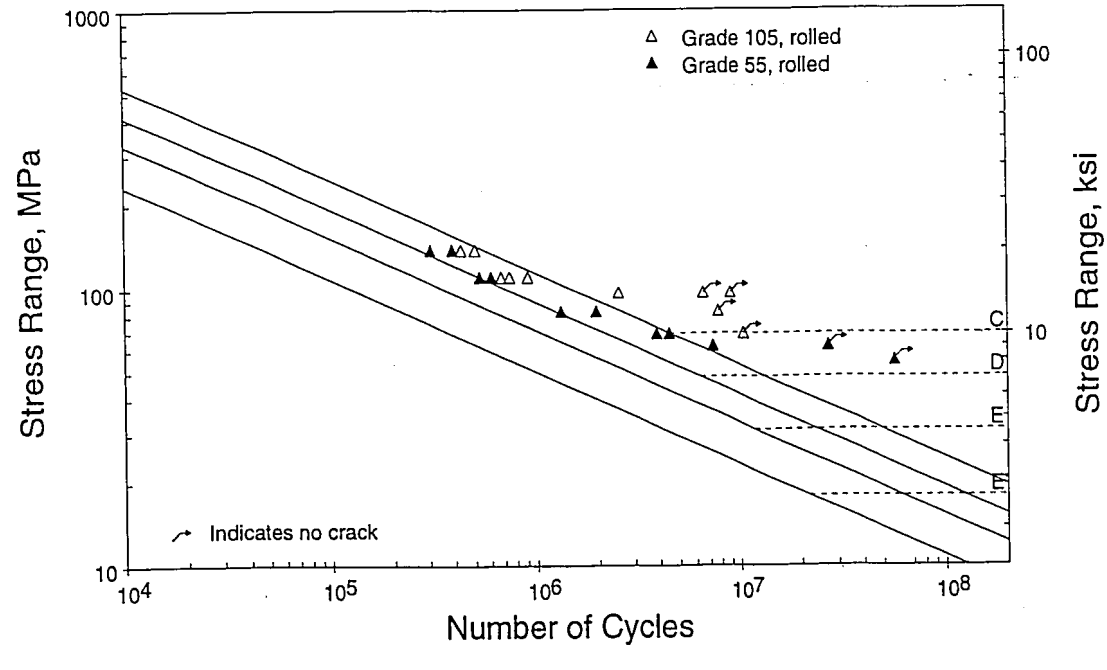

Figure 6.18 - S-N Curve Showing Effects of Material Grade For Specimens with Rolled Threads (Tests Conducted at Approximately Same Absolute Maximum Stress).

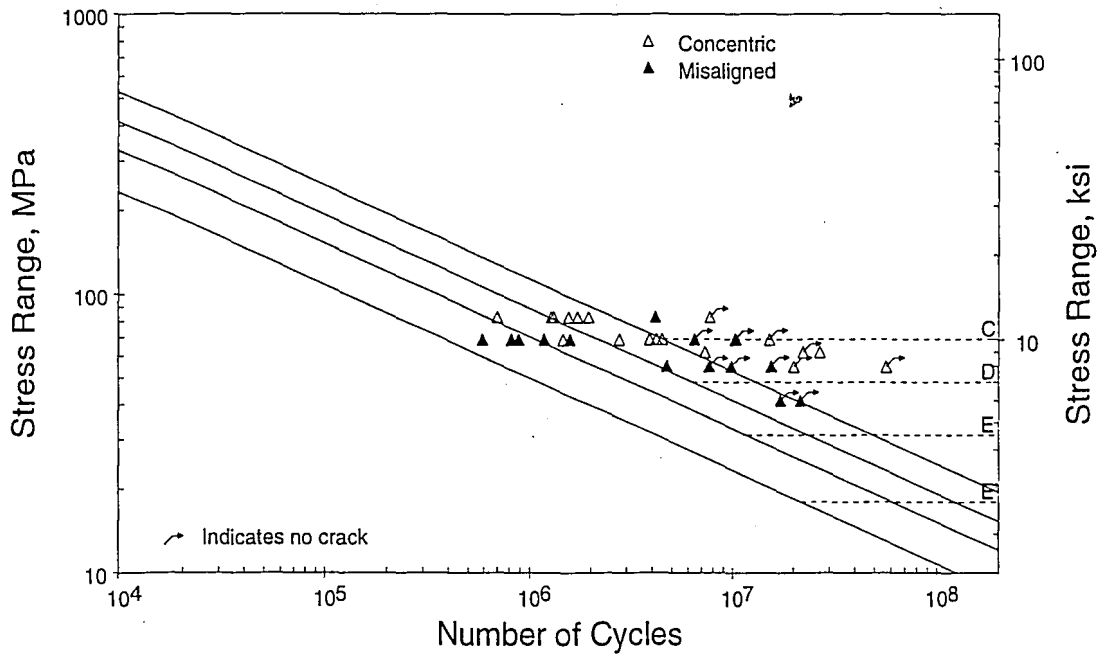

Figure 6.19 - S-N Curve Comparing ~~Snug~~-Tight Misaligned and Concentrically-Loaded Specimens

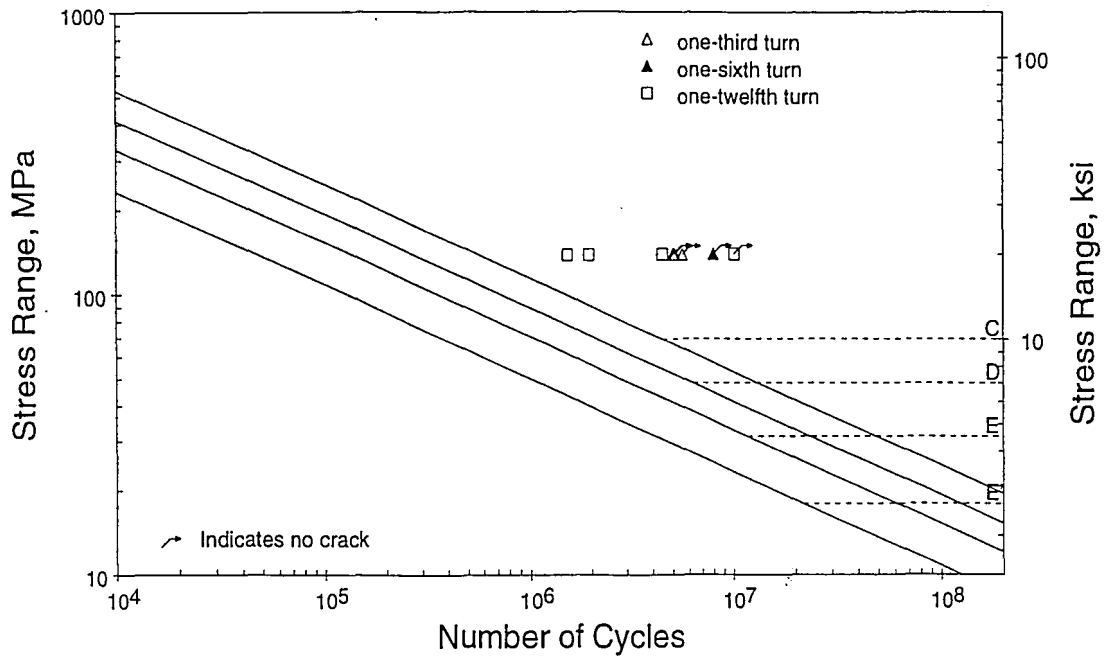

Figure 6.20 - S-N Curve Showing Effects of Bolt Pretension

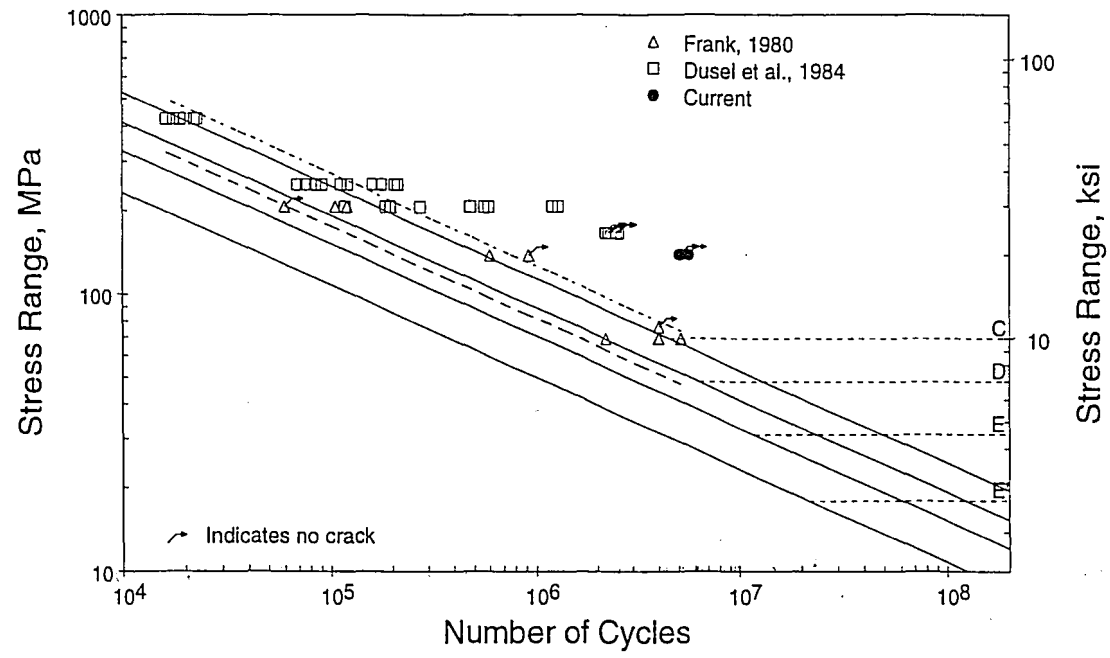

Figure 6.21 - S-N Curve Showing Previous Database of Fully-Tightened Anchor Bolt Fatigue Tests. Includes Only Those Data Obtained From Tests Conducted at Maximum Stresses Corresponding to Greater Than $0.6F_y$.

Chapter Seven

SUMMARY AND CONCLUSIONS

7.1 SUMMARY OF THE RESEARCH PROGRAM

The research reported herein forms the preliminary basis for the fatigue design of cantilevered support structures for galloping and vortex-induced vibrations. Aerodynamic and aeroelastic wind-tunnel tests were performed at the Massachusetts Institute of Technology to characterize the dynamic response of cantilevered sign and signal support structures to the galloping and vortex shedding phenomena. The aeroelastic wind-tunnel tests were simulated using dynamic finite-element analyses to determine the magnitude of the across-wind loads associated with galloping and vortex shedding. The results of the dynamic finite-element analyses were used to develop or evaluate existing equivalent static load models for galloping and vortex shedding. Fatigue-sensitive cantilevered support structure connection details were evaluated with respect to the AASHTO fatigue design guidelines [3]. One particular critical detail that is outside the scope of the AASHTO bridge specifications is the anchor bolts. The fatigue-test data in the literature on anchor bolts is insufficient to determine the constant-amplitude fatigue limit (CAFL). Therefore, fatigue tests were performed to determine the CAFL for snug- and fully-tightened anchor bolts. Finally, recommendations were developed for the design of cantilevered support structures for galloping- and vortex-induced fatigue.

7.2 FINDINGS

7.2.1 Aerodynamic Wind Tunnel Tests

The results of the aerodynamic wind tunnel tests indicate that cantilevered sign and signal support structures are potentially susceptible to galloping-induced vibrations resulting from the aerodynamic forces which act on the attachments to these structures. Specifically, the results of the aerodynamic wind tunnel tests indicate that rigidly-attached signal attachments are significantly more susceptible to galloping when configured with a backplate. The susceptibility of sign attachments to galloping was found to be independent of the aspect ratio of the attachment for the dimensions of the signs considered.

7.2.2 Aeroelastic Wind Tunnel Tests

The aeroelastic wind-tunnel tests revealed that the primary phenomenon involved in the vibration of cantilevered sign and signal support structures is galloping. Vortex shedding is only a significant factor when the horizontal mast-arms of cantilevered support structures are configured without attachments (e.g. during installation of the support structures). With regard to galloping, the results of the aeroelastic tests indicate that:

- Wind-tunnel testing of one-eighth scale models can reproduce the aeroelastic behavior of cantilevered support structures that were observed vibrating in the field.

- Galloping is highly sensitive to a variety of variables and was not easily repeatable even under essentially identical conditions in the wind tunnel.

- Galloping is induced by lift forces which act on the signal attachments and sign panels. The magnitude of these lift forces are approximately proportional to the area of the attachments projected on a vertical plane.

- The galloping response increases with wind velocity. As the wind velocity decreases, the galloping may persist under velocities that are much lower than the onset wind velocity.

With regards to vortex shedding, the results of the aeroelastic wind tunnel tests indicate that:

- Vortex-shedding vibrations are repeatable and the critical wind velocity associated with lock-in is well predicted by the Strouhal relation.

- The wind-tunnel tests confirm the observations made by previous researchers [29] that wind velocities less than 5 m/s generate pressures which cannot cause significant vortex-induced response.

- Member diameters typically used for mast-arms are such that the critical wind velocity for vortex-shedding lock-in is less than 5 m/s. Therefore, most cantilevered sign and signal support structures are not susceptible to vortex-induced vibrations.

- Models with large-diameter mast-arms which were susceptible to vortex shedding vibration did not vibrate (due to vortex shedding) when the attachments were in place.

- Cantilevered sign and signal support structures are not susceptible to vortex-induced vibrations resulting from the shedding of vortices from the attachments to these structures.

- Cantilevered sign and signal support structures are not susceptible to vortex-induced vibrations resulting from the shedding of vortices from the vertical support.

7.2.3 Finite-Element Analyses

The results of the finite-element analyses indicate that:

- The mass and stiffness of the prototype wind tunnel specimens was well represented by the wind-tunnel model specimens. The scaling of natural frequencies and displacements was reasonably consistent with the laws of similitude.

- The response of the wind-tunnel model that experienced vortex-induced vibration corresponds to an equivalent static pressure range of 4200 Pa which is reasonably consistent with provisions contained in the present AASHTO Standard Specifications for Structural Supports for Highway Signs, Luminaires, and Traffic Signals [4].

- The response of the wind-tunnel models that experienced galloping corresponds to an equivalent static pressure range between 840 and 1480 Pa.

- The response of the full-scale structures which were observed to gallop in the field corresponds to an equivalent static pressure range between 700 and 1060 Pa which is consistent with the above wind-tunnel results.

- Based on these results, an equivalent static pressure range equal to 1kPa represents a reasonable estimate of the across-wind pressure range at the onset of galloping in a wide range of cantilevered sign and signal support structures. Therefore, an equivalent static pressure range equal to 1kPa is recommended for use in design.

- The static pressure range computed from a static analysis is in good agreement with the equivalent static pressure range computed using the SDOF dynamic magnification factor. As a result, the equivalent static pressure approach is a reasonable method by which to design cantilevered support structures for galloping- and vortex-induced fatigue.

- The forces and displacements computed from a static analysis reasonably replicate the dynamic response of a structure to galloping and/or vortex shedding. As a result, the equivalent static pressure approach is a reasonable method by which to design cantilevered support structures for galloping and vortex shedding.

7.2.4 Anchor Bolt Fatigue Tests

The results of the anchor bolt fatigue tests indicate that:

- The AASHTO Category E´ design curve is a reasonable lower-bound estimate of the fatigue strength of axially-loaded, snug-tight anchor bolts in the regime of finite life (e.g. less than two million cycles).

- The AASHTO Category E design curve is a reasonable lower-bound estimate of the fatigue strength of axially-loaded, fully-tightened (i.e. tightened to one-third-of-a-turn beyond snug) anchor bolts in the regime of finite life.

- The constant amplitude fatigue limit corresponding to the AASHTO Category D design curve (i.e. 48 MPa) is a reasonable lower-bound estimate of the CAFL for axially-loaded, snug- and fully-tightened anchor bolts in the regime of infinite life.

- The bending stress range resulting from misalignments up to 1:40 need not be explicitly considered in the stress calculations when designing anchor bolts for infinite life provided that bevelled washers are utilized in the installation of the bolts. Prying forces resulting from localized distortion of the base-plate should be minimized in all anchor bolt installations (i.e. the base-plate should be designed sufficiently thick to resist localized distortion).

The above conclusions are based upon fatigue tests conducted under worst-case stress conditions (i.e. maximum stresses equal to the allowable static design strength). Therefore, the

effects of maximum stress, thread-forming method, and anchor bolt yield strength need not be explicitly considered in the design of anchor bolts for fatigue. In addition, the following qualitative observations concerning anchor bolt fatigue strength were made:

- The fatigue strength of anchor bolts is strongly influenced by the magnitude of the maximum stress. Therefore, anchor bolts which are subject to maximum stress levels less than the allowable static design strength will exhibit fatigue lives greater than those predicted by the above design recommendations.

- Under low levels of maximum stress, anchor bolts fabricated with rolled threads exhibit fatigue strengths slightly greater than anchor bolts fabricated with cut threads.

- At a maximum stress which is at a similar percentage of the yield strength, Grade 55 anchor bolts exhibit fatigue lives slightly greater than Grade 105 anchor bolts. As a result, it is imperative that Grade 105 anchor bolts be properly proportioned with respect to the above design recommendations.

7.3 RECOMMENDATIONS FOR DESIGN

7.3.1 Galloping

Cantilevered sign and signal support structures should be designed for galloping-induced fatigue using an equivalent static pressure range equal to 1 kPa. This pressure range is applied vertically to the projected area of any sign and/or signal attachments mounted to the horizontal mast-arm. The stress ranges resulting from this applied pressure range must be less than the constant amplitude fatigue limits for the various fatigue-sensitive details within the structure. The

constant amplitude fatigue limits corresponding to typical cantilevered support structure connection details are provided in the appendix to this report. The constant amplitude fatigue limit for anchor bolts is 48 MPa.

In addition, it is also recommended that the use of attachments known to be particularly susceptible to galloping be avoided. For example, signal attachments configured with backplates exhibit a greater susceptibility to galloping than signal attachments configured without backplates. As a result, the potential for galloping should be minimized by avoiding the use of backplates whenever possible.

7.3.2 Vortex Shedding

Cantilevered sign and signal support structures should be designed for vortex-induced fatigue when two criteria are satisfied: (1) sign/signal attachments are not immediately mounted to the horizontal mast-arm at the time of installation of the support structure and (2) the predicted critical wind velocity is greater than approximately 5 m/s. The following procedure should be used to determine the equivalent static pressure range to be used in the design:

The critical wind velocity associated with lock-in is calculated using the Strouhal relation:

$$V_{cr} = \frac{f_n D}{S} \tag{7.1}$$

where f_n is the natural frequency of the structure corresponding to the first mode of vibration in the vertical-plane, D is the diameter of the horizontal support, and S is the Strouhal number. For horizontal supports with circular cross-sections, the Strouhal number is to be taken as 0.18.

The equivalent static pressure range to which the structure is subjected during lock-in is taken as:

$$P_t = \frac{0.0473 V_{cr}^2 C_d C_h}{2\xi} \tag{7.2}$$

where C_d and C_h are the drag and height coefficients, respectively, determined in accordance with the provisions of the AASHTO Specifications [4], and ξ is the damping ratio. The damping ratio is to be conservatively estimated as 0.5%.

The equivalent static pressure range is to be applied vertically to the projected area of the horizontal support. The stress ranges resulting from this applied pressure range must be less than the constant amplitude fatigue limits for the various fatigue-sensitive details within the structure. The constant amplitude fatigue limits corresponding to typical cantilevered support structure connection details are provided in the appendix to this report. The constant amplitude fatigue limit for anchor bolts is 48 MPa.

7.3.3 Discussion of Design Recommendations

The recommendations outlined in Sections 7.3.1 and 7.3.2 are based upon prevention of fatigue crack growth (i.e. an infinite-life approach to fatigue design). It is proposed that cantilevered support structures be proportioned such that the maximum expected stress range resulting from the application of the equivalent static pressure range associated with either galloping or vortex shedding is less than the CAFL so that crack propagation will not occur. The infinite life approach is consistent with the intent of the current AASHTO LRFD Specifications [4]. Several points, however, are worthy of comment.

The design recommendations are intended to ensure that the stress ranges induced at critical connection details within a structure due to galloping and/or vortex shedding are less than the constant amplitude fatigue limits associated with those details. This requirement can be satisfied in one of two ways. First, the nominal dimensions of the support members can be

increased such that the nominal stress range at critical fatigue details is reduced below the fatigue limit. Second, critical connections within the structure can be carefully detailed (e.g. by the addition of stiffeners) such that the nominal stress range in the vicinity of the details is reduced below the fatigue limit. One disadvantage to the second method is that a localized reduction in the nominal stress range at the location of a detail will not significantly influence the global stiffness of the structure. As a result, a structure can be detailed in a manner which satisfies the design recommendations yet is still susceptible to large-amplitude, across-wind vibrations due to either the galloping and/or vortex shedding phenomena. Thus, both the fatigue and deflection limit states should be considered when proportioning cantilevered support structures for fatigue and vibration resistance.

In addition, it should be noted that the recommended equivalent static design pressure for galloping (1 kPa) is not intended to be representative of the maximum expected across-wind load to which a structure may be subjected during galloping-induced vibrations. Thus, the recommended fatigue design procedure for galloping-induced fatigue is not an infinite life approach with regards to the strict application of the definition of infinite life. Rather, the 1 kPa equivalent static pressure range represents a reasonable estimate of the magnitude of the across-wind pressure fluctuations to which a cantilevered support structure will be subjected under typical, steady-state wind conditions. It should be recognized, however, that unusually high steady-state wind velocities may occasionally occur. Thus, the possibility exists that cantilevered support structures may be subjected to equivalent across-wind pressures greater than 1 kPa in service. Generally, however, the number of occurrences of these extreme wind conditions can be expected to be reasonably small. Thus, for small numbers of occurrences, the performance of the structure with respect to fatigue will not be expected to be significantly influenced.

7.4 FUTURE RESEARCH

The discussion presented in Chapter Two showed that galloping-induced oscillations result when two conditions are satisfied: (1) the structure possess aerodynamic characteristics which are conducive to the generation of negative aerodynamic damping and (2) the structure is subjected to a minimum onset wind velocity at which the negative aerodynamic damping exceeds the positive mechanical damping possessed by the structure. The magnitude of the minimum onset wind velocity is dependent upon the dynamic characteristics of the structure (i.e. mass, damping, stiffness).

The research reported herein was oriented towards the determination of the applied pressure range (1 kPa) to which cantilevered support structures are subjected during galloping-induced vibrations. The implication in designing with this equivalent static pressure range is that cantilevered support structures will possess increased levels of mass and stiffness (provided, as per the discussion in Section 7.3.3, that the nominal member sizes are increased). Thus, the recommended design procedures for galloping implicitly mitigate the conditions under which galloping occur by increasing the magnitude of the onset wind velocity. Thus, areas for future research with respect to galloping include:

- Correlate the mass and stiffness properties of a cantilevered support structure to the magnitude of the onset wind velocity at which galloping-induced vibrations occur.

- Investigate the use of external damping devices to increase the mechanical damping possessed by cantilevered support structures. Increases in mechanical damping will mitigate galloping-induced vibrations.

- Develop cantilevered support structure sign and signal attachments which possess aerodynamic characteristics that provide positive aerodynamic damping. This would effectively eliminate the conditions under which galloping-induced vibrations occur.

- Investigate the effectiveness of external attachments to cantilevered support structures which provide aerodynamic damping. For example, McDonald et al. [32] found that mounting a damping plate to the horizontal mast-arm provided sufficient positive aerodynamic damping to mitigate galloping-induced vibrations.

With respect to vortex shedding:

- Further investigate the susceptibility of sign attachments to vortex shedding. Specifically, determine whether sign attachments possess three-dimensional characteristics which interfere with the shedding of vortices.

With respect to the fatigue strength of anchor bolts:

- Quantify potential benefits to using anchor bolts with rolled threads. Specifically, determine the level of maximum stress at which the beneficial effects of the rolled threads become apparent.

- Conduct additional tests to fully quantify the effects of yield strength on anchor bolt fatigue strength.

- Investigate the effects of prying in typical anchor bolt installations. Specifically, relate the anchor bolt pattern, bolt diameter, and base-plate thickness to the magnitude of the prying forces.

7.5 CONCLUSIONS

The following conclusions have been derived from the results of this research:

- The load model for vortex shedding of simple poles in the AASHTO Standard Specifications for Structural Supports for Highway Signs, Luminaires, and Traffic Signals [4] is adequate and applicable to the vortex-induced vibrations of cantilevered support structures configured without attachments.

- The present AASHTO Standard Specifications for Structural Supports for Highway Signs, Luminaires, and Traffic Signals [4] must be revised to include provisions for galloping of cantilevered sign and signal support structures. Cantilevered sign and signal support structures should be designed for galloping-induced loads using an equivalent static pressure range equal to 1 kPa. This pressure range is to be applied vertically to the projected area of any sign and/or signal attachments mounted to the horizontal mast-arm. The stress ranges resulting from this applied pressure range must be less than the constant amplitude fatigue limits for the various fatigue-sensitive details within the structure.

- The constant amplitude fatigue limits corresponding to most typical cantilevered support structure connection details are provided in AASHTO bridge specifications [3]. The constant amplitude fatigue limit for anchor bolts is 48 MPa.

REFERENCES

1. AASHTO-AGC-ARTBA Task Force 13, A Guide to Standardized Highway Lighting Pole Hardware, ARTBA Technical Bulletin No. 270, AGC Standard Form No. 133, 1980.

2. ABAQUS, Version 5.3, Hibbitt, Karlsson & Sorensen, Inc., Pawtucket, RI, 1993.

3. American Association of State Highway & Transportation Officials, AASHTO LRFD Bridge Design Specifications, SI Units, First Edition, AASHTO, 1994.

4. American Association of State Highway & Transportation Officials, Standard Specifications for Structural Supports for Highway Signs, Luminaires and Traffic Signals, AASHTO, 1985.

5. American Institute of Steel Construction, Manual of Steel Construction, LRFD, Second Edition, Volumes I & II, AISC, Chicago, IL, 1994.

6. American Welding Society, D1.1, Structural Welding Code, 1992.

7. Barsom, J.M., et al., Fracture & Fatigue Control in Structures, Second Edition, Prentice-Hall, Inc., Englewood-Cliffs, NJ, 1987.

8. Blevins, R.D., Flow-Induced Vibration, Second Edition, Van Nostrand Reinhold, New York, NY, 1990.

9. British Standards Institute, Code of Practice for Fatigue Design and Assessment of Steel Structures, BS7608, 1993.

10. Brockenbrough, R.L., Suggested Structural Design Criteria for Steel Lighting Standards, U.S. Steel Report 57 019-450(6), 1970.

11. Clough, R.W., et al., Dynamics of Structures, Second Edition, McGraw-Hill, Inc., New York, 1993.

12. Cook, S., Michigan Department of Transportation, Personal Communication, 1995.

13. Covert, E.E., et al., Static and Dynamic Wind Tunnel Tests on Selected Stoplight and Signs and Their Supports, Wright Brothers Facility Report 1306, Massachussets Institute of Technology, Cambridge, MA, 1995.

14. Davenport, A.G., et al., "Vibration of Structures Induced by Wind," Shock and Vibration Handbook, Third Edition (Harris, C.R. - Ed), McGraw-Hill, New York, NY.

15. Den Hartog, J.P., Mechanical Vibrations, Fourth Edition, McGraw-Hill, New York, NY, 1956.

16. Dusel, J.P., et al., Determination of Fatigue Characteristics of Hot-Dipped Galvanized A307 and A449 Anchor Bars and A325 Cap Screws, State of California, Department of Transportation, Division of Engineering Services, Sacramento, CA, 1984.

17. Edwards, J.A., et al., Deflection Criteria for Wind-Induced Vibrations in Cantilever Highway Sign Structures, Report 110-79-2, Center for Transportation Engineering Studies, North Carolina State University at Raleigh, Raleigh, NC, 1984.

18. European Prestandard, Eurocode 3: Design of Steel Structures, European Committee for Standardization, 1992.

19. Fisher, J.W., et al., Effect of Weldments on the Fatigue Strength of Steel Beams, National Cooperative Highway Research Program, NCHRP Report 102, Transportation Research Board, Washington, D.C., 1970.

20. Fisher, J.W., et al., Fatigue Strength of Steel Beams with Welded Stiffeners and Attachments, National Cooperative Highway Research Program, NCHRP Report 147, Transportation Research Board, Washington, D.C., 1974.

21. Fisher, J.W., et al., Fatigue Behavior of Steel Light Poles, Report No. FHWA/CA/SD-81/82, California Department of Transportation, Sacramento, CA, 1981.

22. Fisher, J.W., et al., Fatigue Cracking in Highway Sign Anchor Rods, Proceedings of the Ninth Structures Congress, Indianapolis, IN, 1991.

23. Fisher, J.W., et al., Structural Failure Modes of Advanced Double-Hull, Fatigue and Fracture Failure Modes, TDL 91-01, Vol. 3a, Lehigh University, Bethlehem, PA, 1992.

24. Frank, K.H., "Fatigue Strength of Anchor Bolts," Journal of the Structural Division, ASCE, Vol. 106, No. ST6, 1980.

25. Fung, Y.C., An Introduction to the Theory of Aeroelasticity, Dover Publications, Inc., Mineola, NY, 1993.

26. Havranek, D.D., Valmont Industries, Personal Communication to W. Henneberger of the Texas Department of Transportation, 1984.

27. Kaczinski, M.R., et al., Fatigue Resistant Design of Cantilevered Signal, Sign and Light Supports, National Cooperative Highway Research Program, Interim Report - NCHRP Project 10-38, Transportation Research Board, Washington, D.C., 1994.

28. Keating, P.B., et al., Evaluation of Fatigue Tests and Design Criteria on Welded Details, National Cooperative Highway Research Program, NCHRP Report 286, Transportation Research Board, Washington, D.C., 1986.

29. Kolousek, V., et al., Wind Effects on Civil Engineering Structures, Elsevier, New York, NY, 1984.

30. Kulak, G.L., et al., Guide to Design Criteria for Bolted and Riveted Joints, Second Edition, John Wiley & Sons, New York, 1987.

31. Liu, H., Wind Engineering - A Handbook for Structural Engineers, Prentice Hall, Englewood Cliffs, NJ, 1991.

32. McDonald, J.R., et al., Wind Load Effects on Signals, Luminaires and Traffic Signal Structures, Report 1303-1F, Wind Engineering Research Center, Texas Tech University, Lubbock, TX, 1995.

33. Novak, M., "Aeroelastic Galloping of Prismatic Bodies," Journal of the Engineering Mechanics Division, ASCE, Vol. 95, No. EM1, 1969.

34. Novak, M., "Galloping Oscillations of Prismatic Structures," Journal of the Engineering Mechanics Division, ASCE, Vol. 98, No. EM1, 1972.

35. Ontario Ministry of Transportation, Ontario Highway Bridge Design Code, Third Edition, Ontario Ministry of Transportation, 1992.

36. Parkinson, G.V., et al., "On the Aeroelastic Instability of Bluff Cylinders," Transactions ASME, Journal of Applied Mechanics, Vol. 83, 1961.

37. Research Council on Structural Connections (RCSC), Specification for Structural Joints Using ASTM A325 or A490 Bolts, RCSC, 1988.

38. Simiu E., et al., Wind Effects on Structures: An Introduction to Wind Engineering, John Wiley & Sons, NY, 1978.

39. Verma, K.K., et al., "High-Strength Bolts for Bridges," Engineering Journal, American Institute of Steel Construction, Vol. 29, No. 1, 1992.

APPENDIX:

FATIGUE CATEGORIZATION

OF

CANTILEVERED SUPPORT STRUCTURE

CONNECTION DETAILS

Appendix

FATIGUE CATEGORIZATION OF CANTILEVERED SUPPORT STRUCTURE CONNECTION DETAILS

A.1 INTRODUCTION

This appendix contains a categorization of fatigue-sensitive details which are commonly used in cantilevered sign, signal, and luminaire support structures. As was described in Chapter Five, identification of these details was based upon a review of:

- state department of transportation standard drawings of cantilevered sign, signal, and luminaire support structures,
- literature obtained from cantilevered support structure manufacturers, and
- literature developed by the AASHTO-AGC-ARTBA Task Force No. 13 [1].

The connection details are categorized according to the existing AASHTO [3] and/or AWS [6] fatigue design categories. As was discussed in Chapter Five, the categorization is based upon existing knowledge of the behavior of welded details under the application of repeated loading. A description of the format of the categorization is provided in Section A.2.

A.2 FORMAT

The general format of this categorization is similar to the format of the categorization of bridge details found in Reference 3. The categorization is divided into two sections. The first section consists of a tabular summary (Table A.1) of typical cantilevered support structure fatigue details and their corresponding AASHTO/AWS fatigue design categories. The AASHTO design S-N curves are shown in Figure A.15. The constant amplitude fatigue limits corresponding to the applicable AASHTO/AWS S-N curves are provided in Table A.2. The second section consists of illustrative drawings of the fatigue details described in the tabular summary. The illustrative drawings are included to aid in the interpretation of some of the details described in the table. The drawings are representative of actual cantilevered support structure connection details. As a result, several drawings contain more than one fatigue detail. Illustrative drawings are not provided for those details which are considered relatively self-explanatory.

The fatigue categorizations presented in Table A.1 are applicable to both steel and aluminum structures. Generally, the fatigue design category associated with a particular detail is the same for both steel and aluminum. The constant amplitude fatigue limits for aluminum, however, are approximately one-third those of steel (i.e. in the same ratio as the elastic modulii). The only detail for which a distinction in the fatigue category is made between steel and aluminum is indicated in the section of the table entitled "Mechanically-Fastened Connections."

Table A.1 - Fatigue Categorization of Cantilevered Support Structure Connection Details.

GENERAL CONDITION	SPECIFIC SITUATION	STRESS CATEGORY	APPLICATION	DETAIL	EXAMPLE
Mechanically Fastened Connections	1. Net section of tightened high-strength (ASTM A325, A490) bolted connections.	B	-	1	Fig. A.1
	2. Net section of other mechanically fastened connections:		-	2	Fig. A.2
	Steel:	D			
	Aluminum:	E			
	3. Anchor bolts; stress range based on the tensile stress area.	E	-	-	-
Holes and Cutouts	4. Net section of holes and cutouts.	D	Wire outlet holes. Drainage holes. Unreinforced handholes.	-	-
Groove-Welded Connections	5. Tubes with continuous full- or partial-penetration groove welds parallel to the direction of the applied stress.	B´	Longitudinal seam welds.	-	-
	6. Full-penetration groove-welded splices (backing ring not removed) with welds ground to provide a smooth transition between members.	D	Column or mast-arm butt-splices.	3	Fig. A.3

Table A.1 - (continued)

GENERAL CONDITION	SPECIFIC SITUATION	STRESS CATEGORY	APPLICATION	DETAIL	EXAMPLE
	7. Full-penetration groove-welded splices (backing ring not removed) with weld reinforcement not removed.	E	Column or mast-arm butt-splices.	3	Fig. A.3
	8. Full-penetration groove-welded tube-to-transverse plate connections (backing ring not removed).	E′	Column-to-base-plate connections. Mast-arm-to-flange-plate connections.	4	Fig. A.4
Fillet-Welded Connections	9. Fillet-welded lap splices.	E	Column or mast-arm lap splices	5	Fig. A.2
	10. Axially loaded members with fillet-welded end connections without notches perpendicular to the applied stress. Welds distributed around the axis of the member so as to balance weld stresses.	E	Angle-to-gusset connections. Slotted tube-to-gusset connections with coped holes.	6	Fig. A.1, Fig. A.5
	11. Axially loaded members with fillet-welded end connections with notches perpendicular to the applied stress. Welds distributed around the axis of the member so as to balance weld stresses.	E′	Slotted tube-to-gusset connections without coped holes.	7	Fig. A.5

GENERAL CONDITION	SPECIFIC SITUATION	STRESS CATEGORY	APPLICATION	DETAIL	EXAMPLE
	12. Fillet-welded tube-to-transverse plate connections.	E′	Column-to-base-plate or mast-arm-to-flange-plate socket connections.	8	Fig. A.6, Fig. A.7, Fig. A.8
	13. Fillet-welded connections with one-sided welds normal to the direction of the applied stress.	E′	Built-up box mast-arm-to-column connections.	9	Fig. A.8
	14. Fillet-welded mast-arm-to-column pas's-through connections.	E′	Mast-arm-to-column pass-through connections.	10	Fig A.9
	15. Fillet welded T-, Y-, K-, and L-tube-to-tube connections.	see a	Chord-to-vertical or chord-to-diagonal truss connections. Mast-arm directly welded to column.	11	Fig. A.10
	16. Fillet-welded T-, Y-, and K-angle-to-tube connections.	see b	Chord-to-vertical or chord-to-diagonal truss connections.	-	-

Table A.1 - (continued)

Table A.1 - (continued)

GENERAL CONDITION	SPECIFIC SITUATION	STRESS CATEGORY	APPLICATION	DETAIL	EXAMPLE
Attachments	17. Non-load bearing longitudinal attachments with partial- or full-penetration groove welds, or fillet welds, in which the main member is subjected to longitudinal loading:		Longitudinal stiffeners. Reinforcement at handholes.	12	Fig. A.11, Fig. A.12
	$L \leq 51$ mm:	C			
	51 mm $< L \leq 12t$ or 102 mm:	D			
	$L > 12t$ or 102 mm when $t \leq 25$ mm:	E			
	18. Non-load bearing longitudinal attachments with $L > 102$ mm in which the main member is subjected to longitudinal loading and the weld termination embodies a transition radius with the weld termination ground smooth:		Weld terminations at ends of longitudinal stiffeners.	12	Fig. A.13
	$R > 51$ mm:	D			
	$R \leq 51$ mm:	E			
	19. Transverse load-bearing fillet-welded longitudinal attachments in which the main member is subjected to minimal axial and/or flexural loads.	C	Longitudinal stiffeners.	13	Fig A.11, Fig. A.13

Table A.1 - (continued)

GENERAL CONDITION	SPECIFIC SITUATION	STRESS CATEGORY	APPLICATION	DETAIL	EXAMPLE
	20. Transverse load-bearing longitudinal attachments with partial-or full-penetration groove welds or fillet welds, in which the main member is subjected to longitudinal loading and the weld termination embodies a transition radius which is ground smooth:		Gusset-plate-to-chord attachments.	14	Fig. A.14
	$R > 51$ mm:	D			
	$R \leq 51$ mm:	E			
	Note that transverse load-bearing longitudinal attachments must first be checked with respect to the longitudinal stress range in the main member per the requirements for non-load bearing longitudinal attachments. The attachment must then be separately checked with respect to the transverse stress range in the attachment per the requirements for transverse load-bearing longitudinal attachments.				

Notes:

a) Category ET with respect to stress in branching member. Category E with respect to stress in chord.
b) Category E′ with respect to stress in branching member. Category E with respect to stress in chord.

Detail Category	Constant Amplitude Fatigue Limit (MPa)
B	110
B′	83
C	69
D	48
E	31
E′	18
ET*	8

*AWS [6] fatigue design category for tubular joints.

Table A.2 - Constant Amplitude Fatigue Limits for Steel Structures. For Aluminum Structures, Reduce the Indicated Fatigue Limits by One-Third.

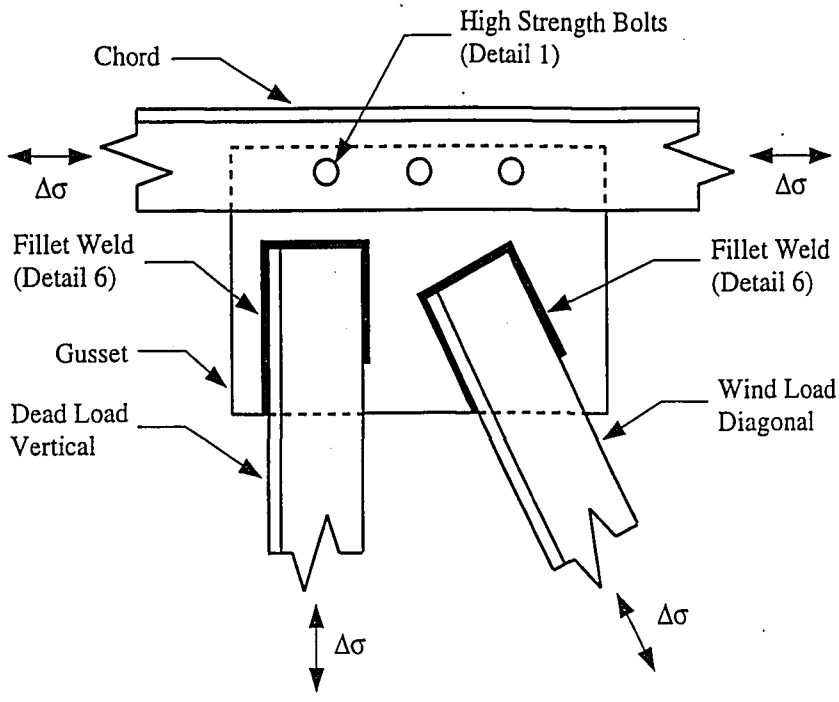

Figure A.1 - Double-Angle Truss Gusset.

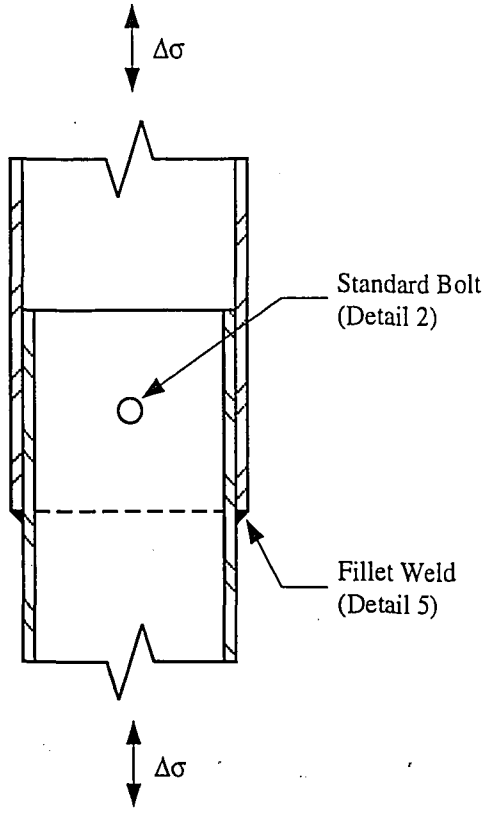

Figure A.2 - Fillet-Welded Lap-Splice.

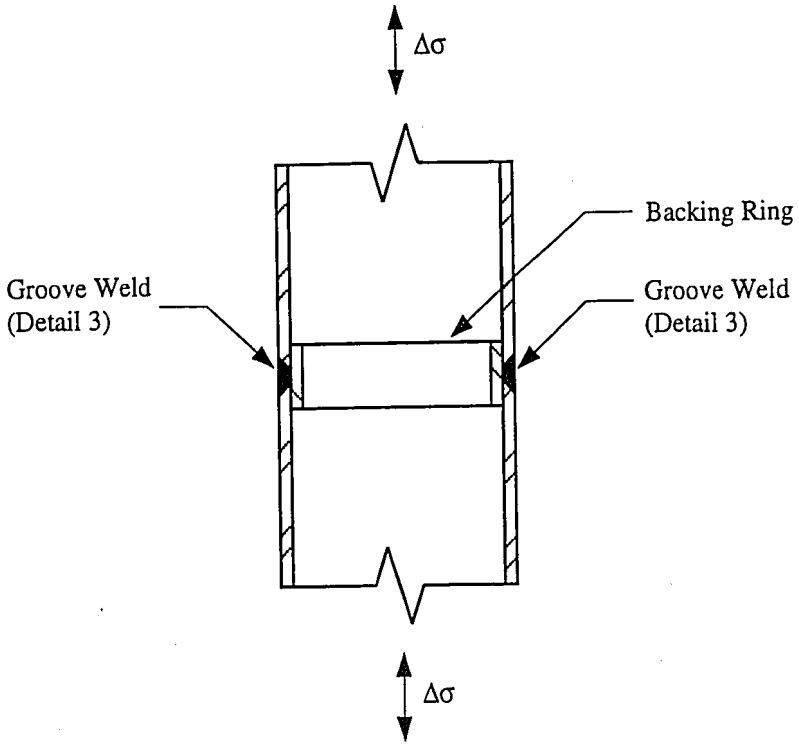

Figure A.3 - Groove-Welded Butt-Splice.

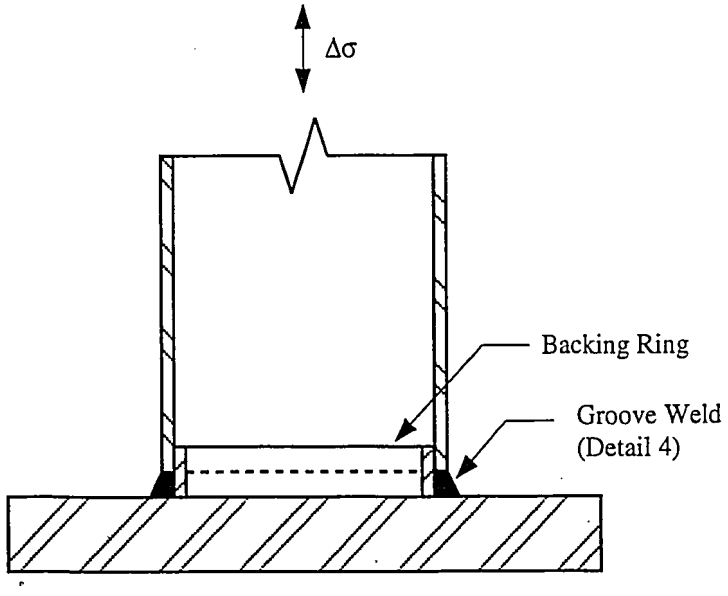

Figure A.4 - Groove-Welded Tube-to-Transverse Plate Connection.

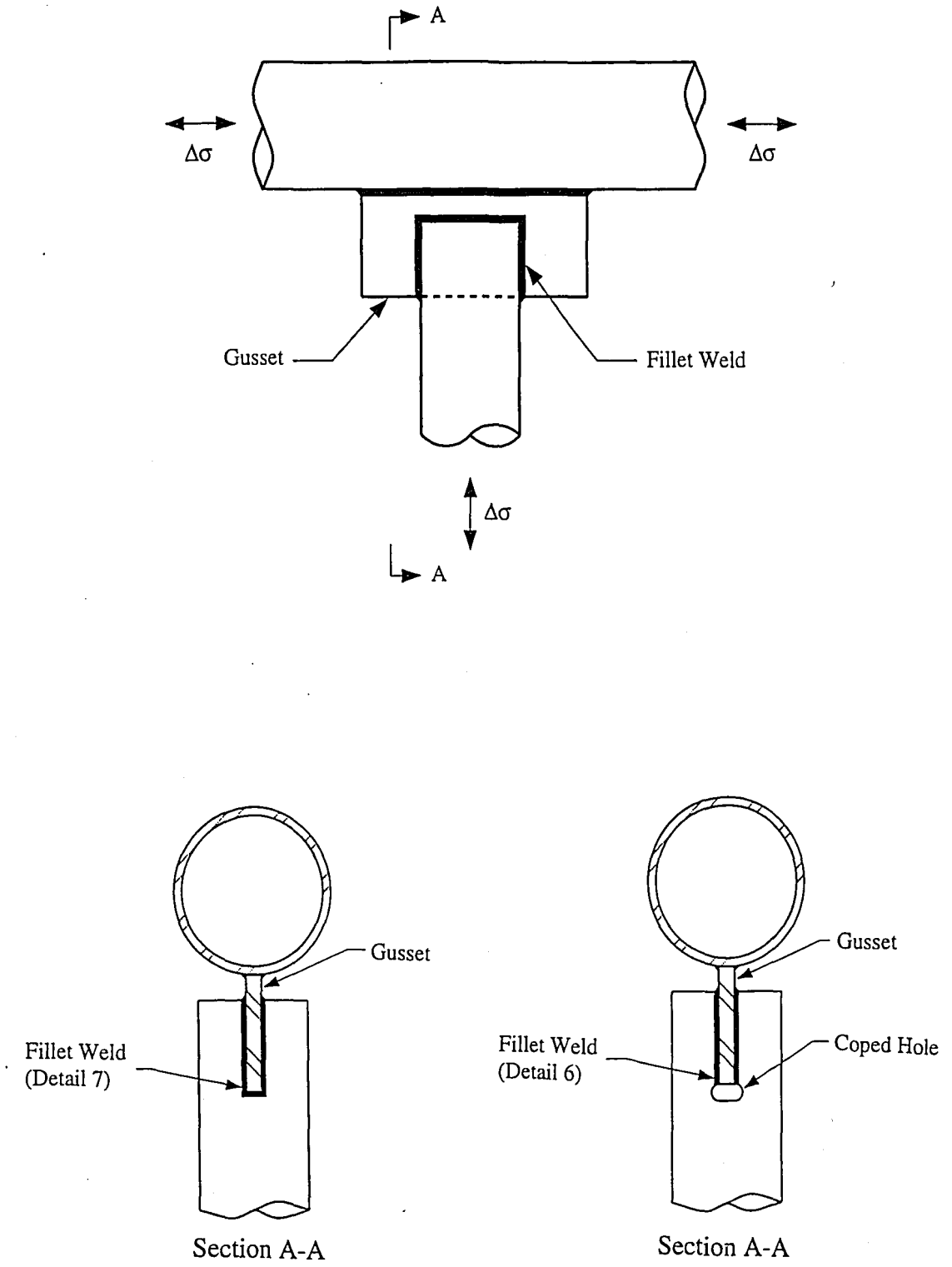

Figure A.5 - Slotted Tube-to-Gusset Connection.

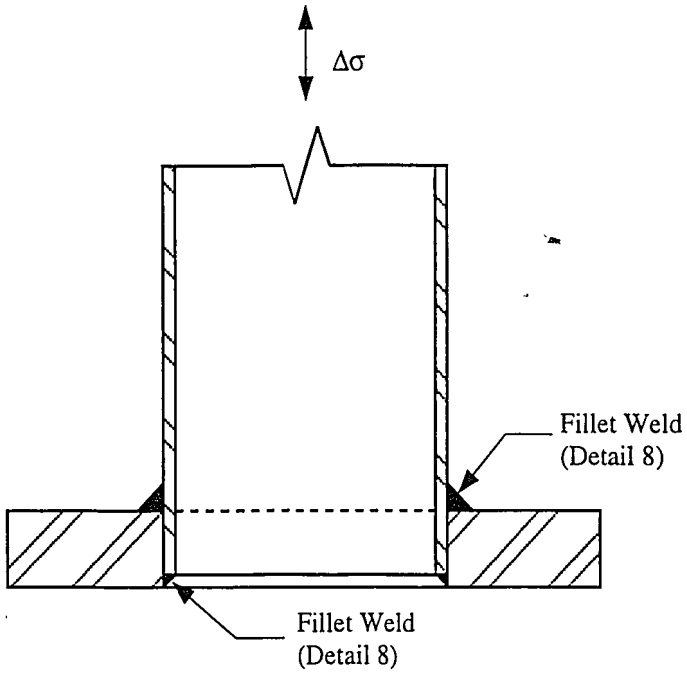

Figure A.6 - Fillet-Welded Socket Connection.

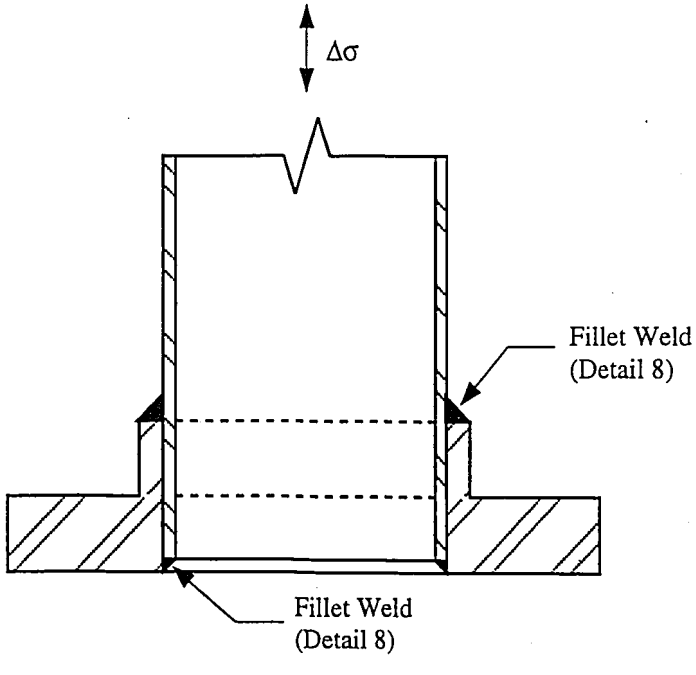

Figure A.7 - Fillet-Welded Socket Connection.

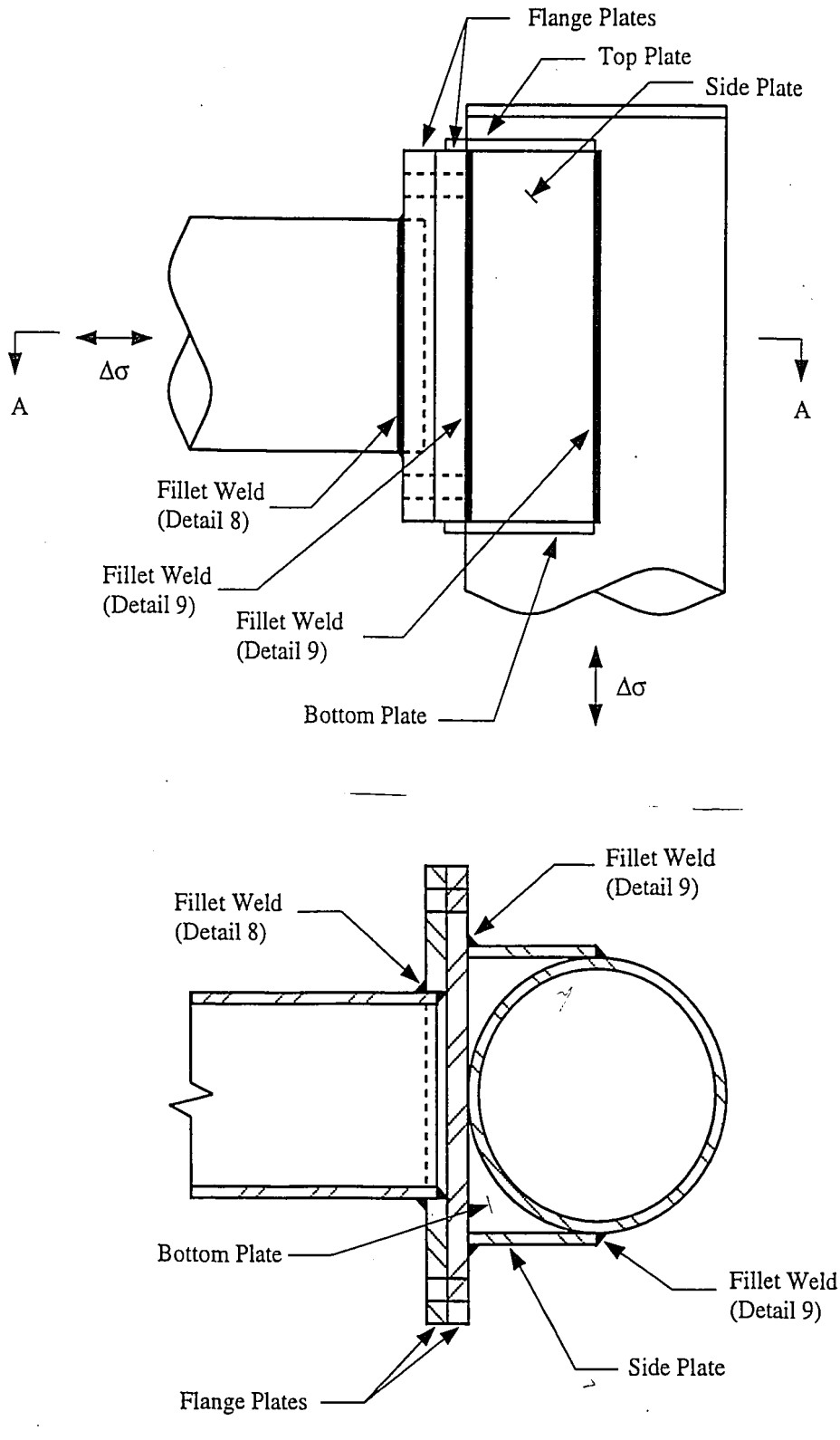

Figure A.8 - Fillet-Welded Mast-Arm-to-Column Connection (Built-up Box).

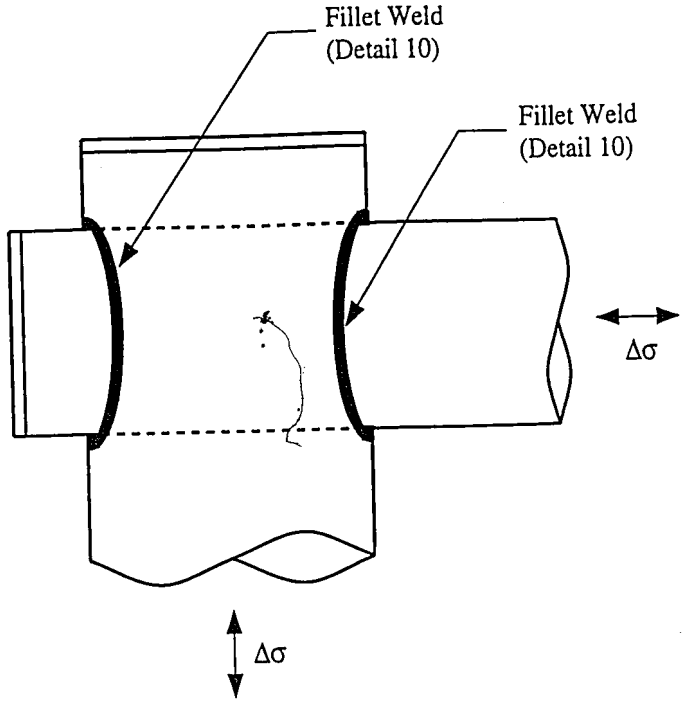

Figure A.9 - Fillet-Welded Tube-to-Tube Column Pass-Through Connection.

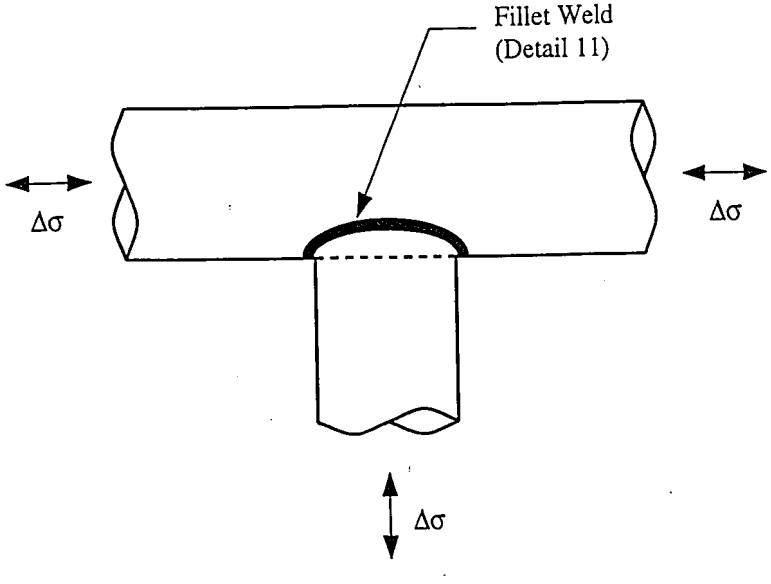

Figure A.10 - Fillet-Welded Tube-to-Tube Connection.

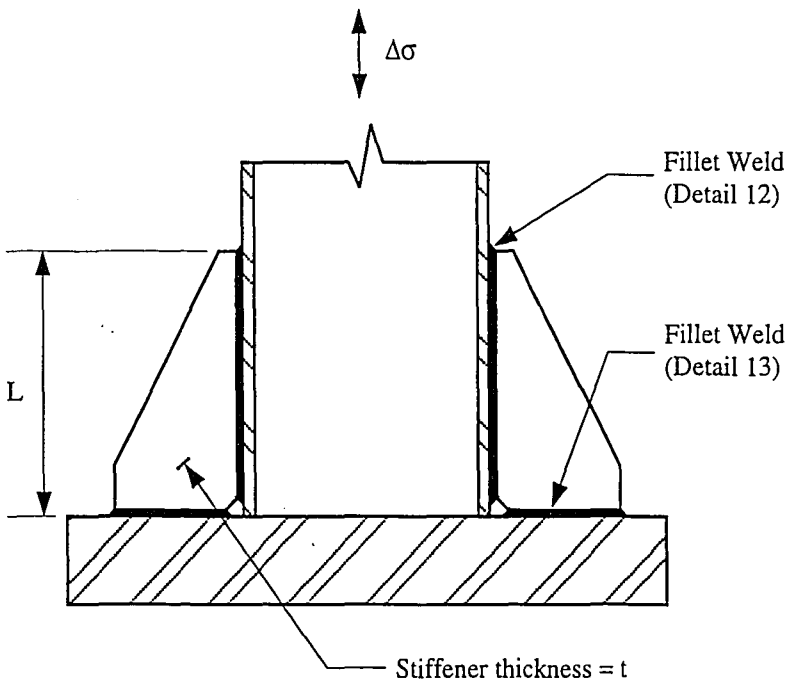

Figure A.11 - Non-Load Bearing Longitudinal Attachment.

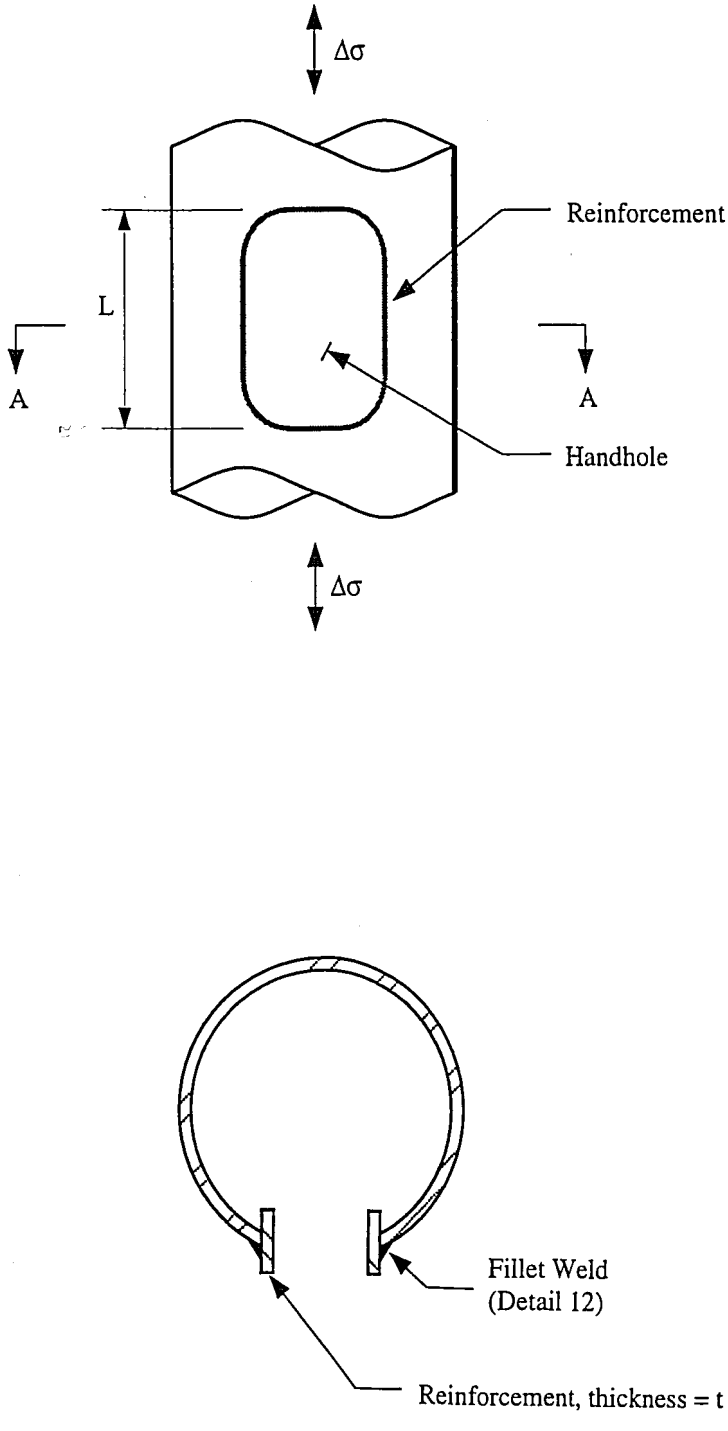

Figure A.12 - Reinforced Handhole.

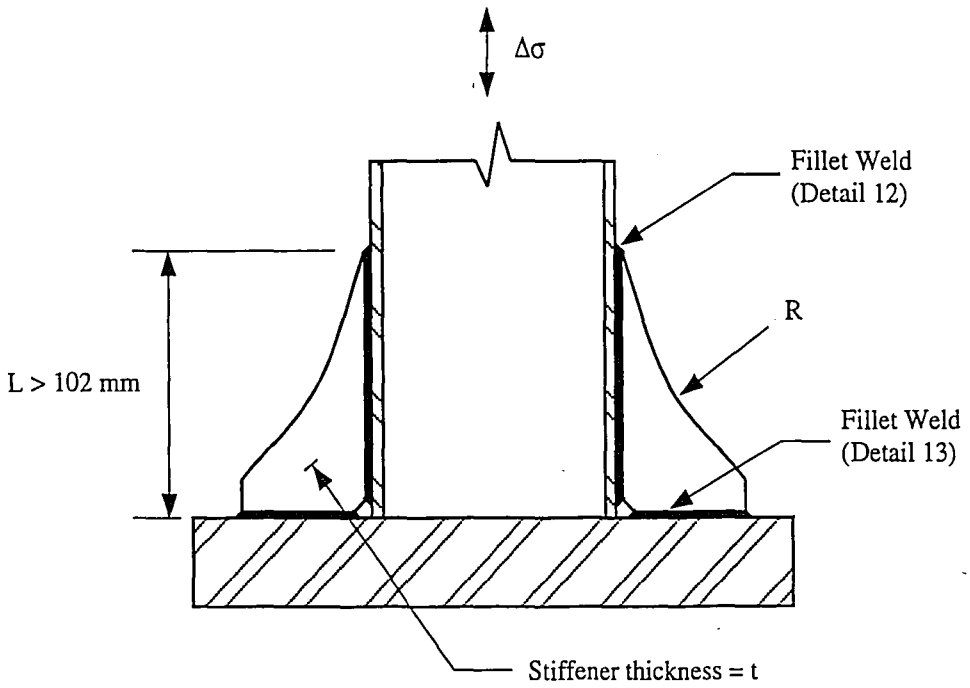

Figure A.13 - Non-Load Bearing Longitudinal Attachment.

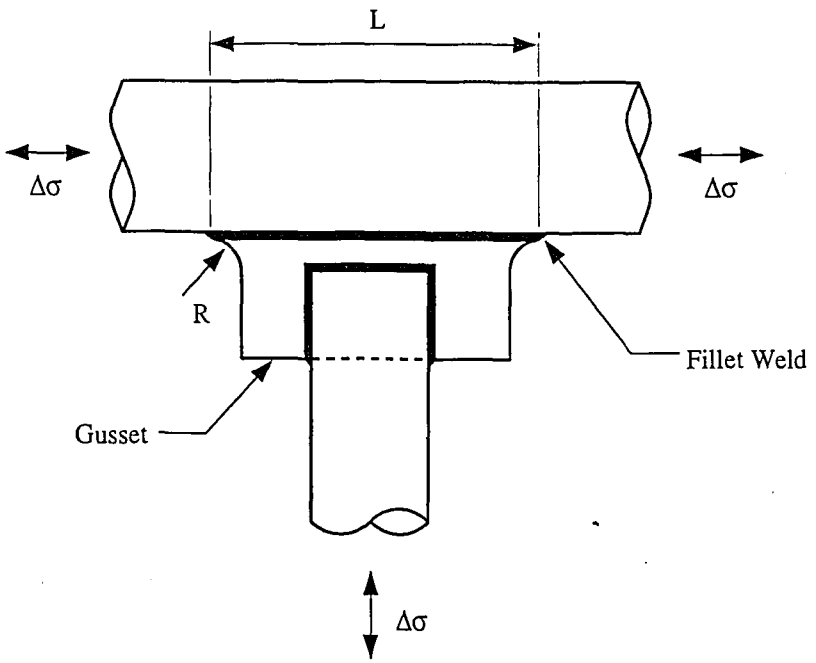

Figure A.14 - Transverse Load-Bearing Longitudinal Attachment.

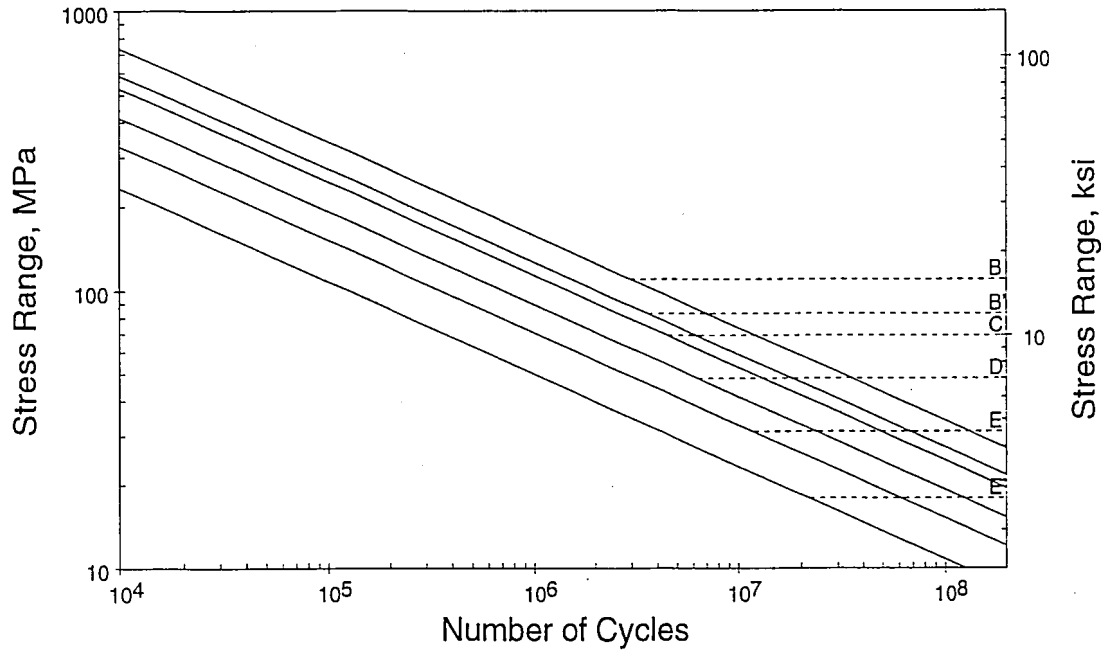

Figure A.15 - AASHTO Fatigue Design S-N Curves (Category A Not Shown).

VITA

James P. Van Dien was born in Clifton, New Jersey on January 2, 1971 and raised in Fords, New Jersey. He is the first of two children born to Peter and Kathleen Van Dien. After graduating from Woodbridge High School in Woodbridge, New Jersey in June 1989, he attended Lehigh University in Bethlehem, Pennsylvania. The author earned the degree of Bachelor of Science in Civil Engineering from Lehigh University in May 1993. In September of that year he entered graduate school at Lehigh University to pursue the degree of Master of Science in Civil Engineering. While in graduate school, the author worked as a full-time research assistant at the Center for Advanced Technology for Large Structural Systems (ATLSS) at Lehigh University.

END OF TITLE